EFFECTS OF TEMPERATURE AND SHOT-PEENING INTENSITY ON FRETTING FATIGUE BEHAVIOR OF TITANIUM ALLOY TI-6AL-4V

THESIS

Salman Albinali, 1LT, RBAF

AFIT/GAE/ENY/05-M25

DEPARTMENT OF THE AIR FORCE
AIR UNIVERSITY

AIR FORCE INSTITUTE OF TECHNOLOGY

Wright-Patterson Air Force Base, Ohio

AFIT/GAE/ENY/05-M25

EFFECTS OF TEMPERATURE AND SHOT-PEENING INTENSITY ON FRETTING FATIGUE BEHAVIOR OF TITANIUM ALLOY TI-6AL-4V

THESIS

Presented to the Faculty

Department of Aeronautics and Astronautics

Graduate School of Engineering and Management

Air Force Institute of Technology

Air University

Air Education and Training Command

In Partial Fulfillment of the Requirements for the

Degree of Master of Science in Aeronautical Engineering

Salman Albinali

1LT, RBAF

March 2005

AFIT/GAE/ENY/05-M25

EFFECTS OF TEMPERATURE AND SHOT-PEENING INTENSITY ON FRETTING FATIGUE BEHAVIOR OF TITANIUM ALLOY TI-6AL-4V

Salman Albinali, BS
1LT, RBAF

Approved:

_____/signed/_____	_03/03/05_
Shankar Mall (Chairman)	date
_____/signed/_____	_03/03/05_
Vinod K. Jain (Member)	date
_____/signed/_____	_03/03/05_
Theodore Nicholas (Member)	date

Abstract

Effects of temperature and shot-peening intensity on fretting fatigue behavior of Ti-6Al-4A were investigated in this study. S-N curves were obtained for both room and elevated temperatures (260 °C) for two different shot-peened intensities (4A and 10A). Stress relaxation behavior under both fretting fatigue at elevated temperature and temperature exposure only were also investigated after their measurements were calculated using X-ray diffraction method. The crack initiation location and the crack angle orientation along the surface were determined using optical and scanning electron microscopy (SEM). Cracks initiated near the trailing edge of the tested specimens. Cracks initiated on the contact surface for both specimens with 4A and 10A shot-peened intensities tested at elevated temperature. Finite element analysis was preformed by commercially available software, ABAQUS, to obtain contact region state variables such as stress, strain and displacement. Those state variables were needed for the computation of fretting fatigue parameters. Fatigue parameters, such as stress range, effective stress and modified shear stress range (MSSR), were analyzed. It was found that there was relaxation of residual compressive stress during fretting fatigue at room and elevated temperature, greater stress relaxation occurred when higher temperature was applied. Also, both 4A and 10A specimens had the same percentage of residual stress relaxation due to temperature exposure only. Further, elevated temperature conditions negate the effect of shot-peening, thereby providing no improvement in fatigue life. On the other hand shot-peening at room temperature conditions improved fatigue life due to shot-peening. Both shot-peening intensities at room temperature provided an improvement to

fatigue life with the 10A intensity providing the greatest extension to fatigue life. Also, the (MSSR) parameter was effective in characterizing the fretting fatigue behavior in terms of fatigue life, crack initiation location and orientation.

Acknowledgments

I would like to express my sincere appreciation to my thesis advisor Dr. Shankar Mall for his guidance, patience and support throughout this thesis project.

I would also like to thank Dr. Sathish Shamachary, Dr. Hyukjae Lee and Taiwan Army Captain Chia-hwa Lee who gave me all the technical support needed for conducting this project. Also, the financial support of Dr. Mark Blodgett, Air Force Research Laboratory (AFRL/MLLP) is gratefully acknowledged. In addition, I would like to thank Mrs. Annette Robb, Director, International Programs Directorate for her effort in making living in the U.S. a great experience.

Finally, I would like to express my gratitude to the Royal Bahraini Air Force and Bahrain Defense Force HQ who believed in me and gave me the opportunity and honor to complete my Master of Science degree in Aeronautical Engineering in AFIT, USA.

Salman Albinali

Table of Contents

Page

Page

List of Figures

Figure Page

Page

Page

List of Tables

Table Page

List of Symbols

ET	elevated temperature
RT	room temperature
4A	shot-peening intensity 4 Almen
7A	shot-peening intensity 7 Almen
10A	shot-peening intensity 10 Almen
RS	residual stress
a	contact half-width
$a_{analytical}$	contact half-width carried out from analytical solution
$a_{Exp,\ max}$	maximum contact half-width measured from experiments
$a_{Ruiz,\ max}$	contact half-width at maximum load conditions from Ruiz program
A	a specimen's cross section area
b	a specimen's half thickness
c	stick zone boundary
d	specimen thickness
E	modulus of elasticity
f	coefficient of friction
f_{FEA}	coefficient of friction used in FEA
FEA	finite element analysis
h	depth of penetration
L	specimen overall length
MSSR	modified shear stress range fatigue predictive parameter
N_f	numbers of fatigue cycles to break a specimen into two pieces

N_i	numbers of fatigue cycles to crack initiation
p	contact pressure distribution in the contact zone
P	applied contact loads
p_0	maximum contact pressure or Hertzian Peak Pressure
q	surface shear stress distribution
Q	tangential loads
Q_{max}	maximum tangential loads
Q_{min}	minimum tangential loads
r	fretting pad radius
R	stress ratio
R_1	radius of fretting pad
R_2	radius of fretting specimens
R_σ	stress ratio of axial stress
SEM	scanning electronic microscopy
σ_{xx}	normal stress along x-direction
σ_{xy}	shear stress on x-y plane
σ_{yy}	normal stress along y-direction
u	displacement
w	specimen width
ε_a	total strain amplitude
ν	Poisson's ratio
θ	direction of stress in a material, observed angle of orientation
$\Delta\sigma$	axial stress range

$\Delta\tau$	shear stress range
σ	normal stresses at a given point with a specific orientation
$\sigma_{1,2}$	principal normal stresses
σ_{axial}	applied axial stress
$\sigma_c(y)$	residual compressive stress along y-direction
σ_{eff}	effective axial stress
$\sigma_t(y)$	residual tensile stress along y-direction
σ_{Freq}	frequency of the applied axial stress
σ_{max}	maximum applied axial stress
σ_{min}	minimum applied axial stress
σ_{xx}	normal stress along x-direction
$(\sigma_{xx})_{axial}$	x-direction normal stress contributed from axial load
$(\sigma_{xx})_{contact}$	x-direction normal stress contributed from contact load
$(\sigma_{xx})_{tangential}$	x-direction normal stress contributed from tangential load
σ_{xy}	shear stress on x-y plane
σ_{yy}	normal stress along y-direction
τ	shear stress at a given point with a specific orientation
τ_{max}	maximum shear stress at a given point

EFFECTS OF TEMPERATURE AND SHOT-PEENING INTENSITY ON FRETTING FATIGUE BEHAVIOR OF TITANIUM ALLOY TI-6AL-4V

I. Introduction

1.1. Fretting Fatigue

Fretting fatigue is a phenomenon that causes damage in components under vibratory load due to their localized relative motion. This motion leads to premature crack initiation and failure, causing reduction in fatigue life. Fretting fatigue is the cause of high cycle fatigue failure which is common in turbine engines; therefore it is of a great interest for the United States Air Force. Fretting fatigue can occurs at the interface of components such as the disk slot and blade attachment (Figure 1) in the fan, compressor or turbine section of a turbine engine and could reduces the service life of components and if not detected could lead to a catastrophic failure. In order to prevent such failures severe reduction in service life of components had to be implemented to insure safe operation. This resulted in high maintenance cost and reduced operation hours. Research in the fretting fatigue area could provide a better understanding on the crack initiation mechanism that will help to develop techniques that will be able to decrease maintenance cost and increase operating hours for newly designed components. Many studies have been conducted on different areas of fretting fatigue in an effort to better understand this phenomenon and provide solutions. Researchers formulated different fatigue parameters

to investigate and predict crack initiation mechanism. In Chapter II formulation and parameters effecting fretting fatigue will be discussed.

1.2. Shot-peening

One of the most common cold working processes used to enhance the plain fatigue and fretting fatigue performance is shot-peening. This process involves the bombardment of the material surface with small, hard steel balls. This action causes a biaxial yielding, which creates a residual compressive stress and grain distortion near the shot-peened surface. At the same time a compensatory tensile stress within the interior is also created. The residual compressive stress plays a critical role in fretting fatigue crack initiation and crack propagation retardation [1]. There are several factors/variables in shot-peening process which can have considerable effect on the fatigue performance. One of them is the shot-peening intensity. It was observed the higher the intensity from 4A to 10A leads to higher level of tensile stress and moves the boundary between negative and positive stress to a larger depth. It was also observed that an increase in intensity practically did not affect the maximum value of residual compressive stress on the contact surface. Moreover, it has been reported that the residual stress is subject to relaxation during fretting fatigue cycles [2]. Original residual stress along with stress relaxation phenomenon modifies contact stress profiles and causes different operating performance in fretting fatigue life.

1.3. Elevated Temperature

In many applications, mechanical components have to function at elevated temperatures. One such important example is blade/disk dovetail joints in a gas turbine engine as shown in Figure 1. Unlike certain alloys Ti-6Al-4V showed no significant

change in the coefficient of friction and wear rate at elevated temperature [3,4,5]. When unpeened components were subjected to fretting fatigue at room temperature and elevated temperature 260°C no change in fatigue life was observed [6]. When shot-peening components are subjected to fretting fatigue at elevated temperature, thermal and/or thermomechanical stress relaxation can occur. Thermal relaxation action is essentially a thermal recovery process in which elevated temperature foster annihilation of crystalline defects, and thermomechanical relaxation is a mechanism, which couples thermal and mechanical effects [2]. It was reported that relaxation of residual compressive stress occurred during fretting fatigue at room and elevated temperatures, which in turn manifested in reduction of fretting fatigue life, and stress relaxation due to elevated temperature and mechanical load (i.e. fretting fatigue) were independent processes [7].

1.4. Purpose and Objectives

As mentioned earlier fretting fatigue life is significantly reduced when compared to plain fatigue enforcing a high cost for operation and maintenance inspections and repairs. In order to reduce this cost and improve performance of components undergoing fretting fatigue extensive studies have been conducted to analyze different variables such as environmental corrosion, elevated temperature, shot-peening process, fretting pad geometry, axial load frequency, and contact load frequency [8,9,2,7,10,11,1,12]. Most of the previous studies focused more or less on one of the previously mentioned variables. In real life application a number of variables could be coupled at the same time. This study is focused in that direction where the effect of different shot-peening intensity combined with the effect of elevated temperature was investigated. This investigation

was conducted to help engineers better understand the relation between shot-peening intensity and elevated temperature.

The primary purpose of this study is to investigate the fretting fatigue behavior of titanium alloy Ti-6Al-4V at elevated temperature (260 ºC) subjected to different shot-peened intensities (4A and 10A). The elevated temperature was chosen to be (260 ºC) due to the fact that titanium alloy Ti-6Al-4V is a material commonly used in turbine engine components and its maximum usage temperature is about 275 ºC. Constant amplitude fretting fatigue tests were conducted over a wide rang of maximum applied axial stresses σ_{max} = 333 to 666 MPa with stress ratio of R = 0.1. A cylindrical-end shape with 50.8 mm radius was chosen as the fretting pad geometry which was pressed against the specimen surface with a constant normal load of 1335 N. In addition, experiments were conducted at both room and elevated temperature 260 °C so that comprehensive comparisons could be made based on different shot-peening intensities at two temperatures. Also, shot-peening intensity effects on the crack initiation location, and crack propagation behavior will be investigated in this study. Three magnitudes of shot-peening intensity (Almen) were investigated in this study (4A, 7A and 10A) all with 100% surface coverage of the specimens. All data for the 7A shot-peened intensity at both room and elevated temperatures were obtained in previous studies by Yuskel [1] and Lee [2]. Some of the data for the 4A and 10A shot-peening intensity at room temperature was obtained from a previous study by Martinez [10] and Sabelkin [11]. In this study S-N curves at room temperature for the 4A and 10A shot-peened intensity were completed and full S-N curves at elevated temperature for the 4A and 10A specimens were developed.

The emphasis of this study was laid down on the correlation between elevated temperature, shot-peening intensity and fretting fatigue mechanisms in terms of fatigue life, crack initiation location, and crack initiation orientation. Fretting fatigue mechanisms at elevated temperature were also compared with those at room temperature. In addition, effects of shot-peening intensity were also investigated at room and elevated temperature conditions. Effects of thermal load on stress relaxation were also investigated using temperature exposure only tests. Shot-peening induced residual stress profiles were determined with different stress relaxation rates to investigate the modified shear stress range (MSSR) fatigue predictive parameter for its effectiveness in predicting fretting fatigue behavior in terms of fatigue life, crack initiation location, and crack initiation orientation.

1.5. Methodology

The complexity introduced by real component geometry and load bearing condition of turbine engines might make replicating the exact configuration as a turbine engine a complex, time consuming and an expensive task. Therefore, a simplified cylinder-on-flat model Figure 2 was adopted as the experimental setup in this study for the sake of investigating fretting fatigue behavior. A uni-axial servo-hydraulic machine was used to apply desired load conditions and record experimental results. Two heaters, placed at the front and back of the specimen, were used to heat and maintain the temperature in the gage section of the specimen at (260 ºC) for the elevated temperature part of the study. The fatigue life diagrams, i.e. S-N curves were developed to investigate the effect introduced by elevated temperature and shot-peening intensity. A furnace was used to conduct temperature exposure only tests at 260 °C. Optical and scanning electron

microscopy (SEM) was used to examine the fracture surface, contact half-width, crack initiation location, crack initiation orientation. Finite element analysis (FEA) was conducted to compute local fretting variables such as stress, strain, and displacement. The X-ray diffraction technique was applied to measure the shot-peening induced residual stress on the surface, which accompanied with stress relaxation which was superimposed into FEA stress solutions for the development of fatigue predictive parameters. X-ray diffraction technique was also used to measured residual stress after fretting and temperature exposure only tests. The stress evolution, stress concentration, contact half-width, and other variables were also analyzed.

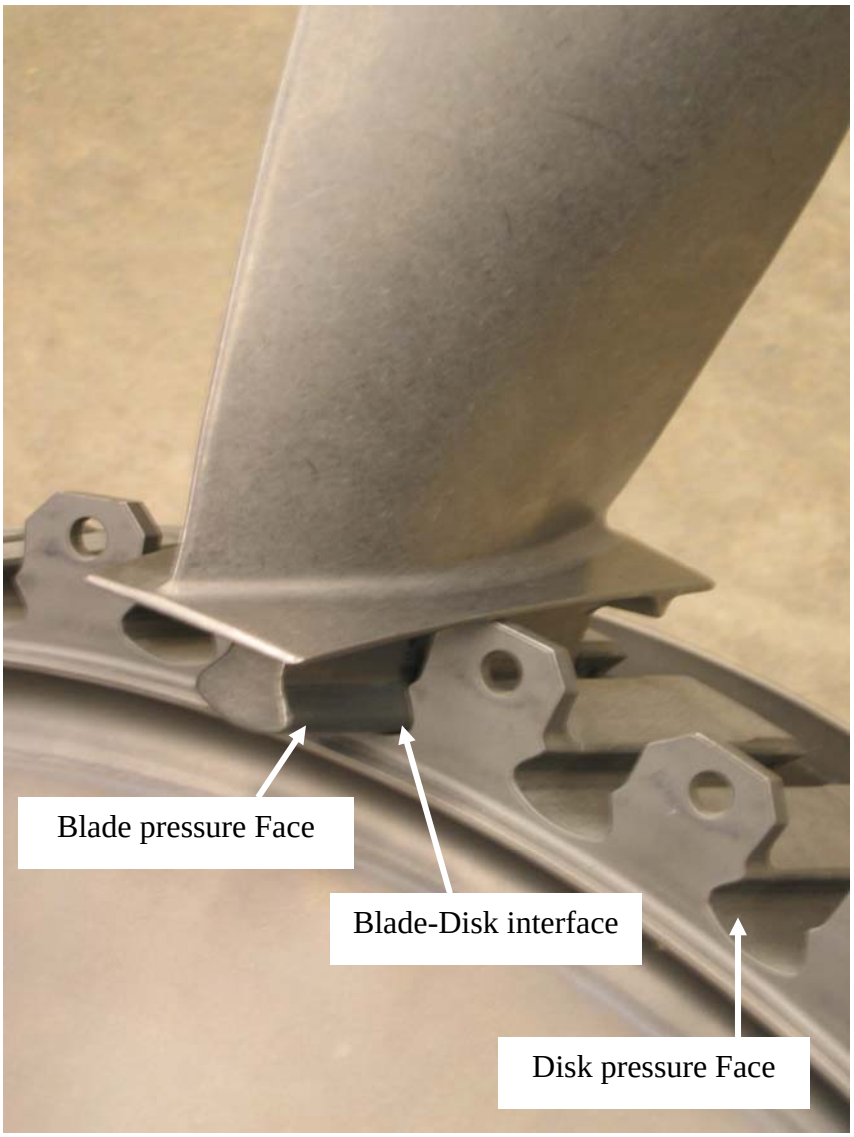

Figure 1. Blade/Disc Dovetail Joint in a Turbine Engine.

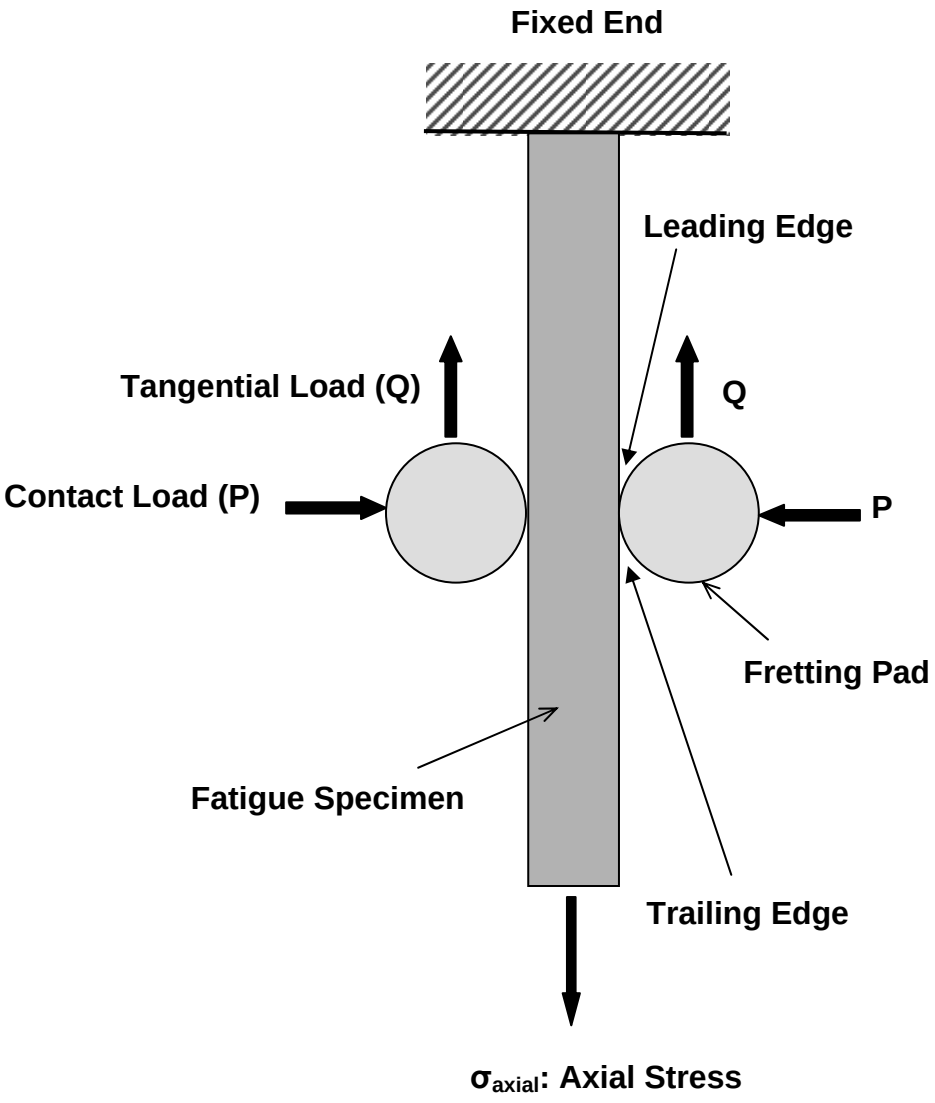

Figure 2: Simplified Fretting Fatigue Configuration

II. Background

Many studies have been conducted to understand the mechanism of fretting fatigue. This chapter is devoted to the analyses of contact mechanics in terms of contact width, Hertzian peak pressure, etc. The effect of shot-peening process and intensity is also covered. Also, elevated temperature as a factor contributing in fretting fatigue will be discussed. Stress relaxation behavior of shot-peened specimens under fretting fatigue is discussed as well. Fatigue parameters are also presented and summarized in this chapter.

2.1. Typical Fretting Fatigue Configuration

Pervious studies have developed a general and simple test scheme as shown in Figure 5 to improve the understanding of the fretting fatigue phenomenon and isolate its controlling variables which would lead to a simplification in analysis. In this general fretting fatigue configuration, fretting specimen and pads are presented as two mechanical components in contact with each other. Axial stress, σ_{axial}, is typically applied by a hydraulic test machine at one end of a specimen that is gripped at the other end. The applied axial load can be controlled to produce fatigue loads with different frequency, waveform, magnitude and stress ratio to simulate the load conditions of interest. At the same time the fretting pads are pressed against the specimen by a constant contact load P in the direction perpendicular to an applied axial load.

A tangential load known as shear load (Q) is induced along the contact surface when an axial load and a contact load are applied. This tangential load forces pads and specimens to move relative to each other in a partial slip condition. The tangential load is defined as half of the difference between the applied axial load and the load measured at

the gripped end of specimens. A contact region along the contact surface of a pad and specimen is created by fretting fatigue. The edge of the contact region near the fixed end is called the leading edge and the edge of the contact region near the applied axial loads is defined as the trailing edge. Contact half-width (a) incorporates both stick-zone (c) and partial slip zones and the center of contact width is defined as the origin of x-direction see Figure 3 and Figure 4. In this study a similar fretting fatigue configuration were cylindrical-end pads in contact with a flat specimen was used.

2.2. Shot-peening Surface Treatment

2.2.1. Introduction to Shot-peening

Surface treatment such as shot-peening is widely known to improve material strength under fatigue conditions and is commonly used in aerospace industries where most of the main structural components are subjected to cyclic loading. Fretting fatigue can damage microstructure on the highly stressed contact surface which fosters crack nucleation. In a shot-peening process a high velocity spherical projectiles called shot such as iron, glass or ceramic beads are used to bombard material surface, creating plastically deformed surface layer constrained by un-deformed interior underneath as seen in Figure 6. This action introduces a biaxial residual stress profile on the peened material, which is compressive near the peened surface and tensile away from the peened surface as shown in Figure 7.

The shot-peening induced compressive stress plays a critical role in crack initiation and propagation retardation mechanism under plain and fretting fatigue conditions. This residual compressive stress can close a pre-existing crack tip at the early stage of fatigue life and can reduce crack propagation rate by compensating detrimental

tensile stress applied by global loads [13]. In order to optimize shot-peening induced fatigue strength, shot-peening controlling parameters should be manipulated carefully including shot-peening media, shot velocity or pressure, angle of impingement, shot hardness and shape and intensity. In this study, 4A and 10A shot-peened specimens were used to investigate elevated temperature and shot peening intensity effect on fretting fatigue behavior. Also, shot-peening induced residual stress was superimposed into results from finite element analysis in order to evaluate the effectiveness of fatigue predictive parameters.

2.2.2. Shot-peening Intensity

The shot-peening intensity, known as Almen intensity, is a measurement of shot-peening stream energy and is directly related to the induced residual stress magnification and distribution. Using larger beads and/or increasing shot velocity of shot stream can increase Almen intensity. Martinez [10] and Sabelkin et al. [11] investigated fretting fatigue behavior under shot-peening specification 4, 7, and 10 Almen intensity. They showed that the residual stress on a peened surface was not significantly different under different Almen. On the other hand underneath the peened surface, a significant difference in the residual stress profile was observed. Also, the greater the peening intensity the greater the compressive depth and magnitude were for specimens under different Almen intensity. It was also shown that the crack initiation location occurred on the peened surface under 4A and 7A, but in the interior under 10A due to the greater residual tensile stress magnitude induced by the 10A shot-peening process. In this study all shot-peened specimens were peened under 4 and 10 Almen intensity to investigate the

effects of elevated temperature and shot-peening intensity under fretting fatigue configuration.

2.2.3. Residual Stress Relaxation Behavior

Relaxation behavior has been reported to be a resultant of the cyclic loading conditions. This relaxation effect reduced the improvement on material fatigue strength under fretting fatigue conditions [2,10,14]. Martinez et al [10,14] used specimens peened with specification of 7A±1 under 100% surface coverage to investigate the contribution of fretting fatigue on residual stress relaxation behavior. It was shown that before a specimen failed due to fretting fatigue cycles, residual stress profile became non-uniform and anisotropic within a fretting scar on the contact surface. Moreover, stress relaxation increased with the increase of fretting fatigue cycles until a specimen failed. After failure occurred, full relaxation of residual stress was measured at crack location, accompanied with no relaxation far away from the contact region. As a fretting region was approached, residual stress was observed under some degree of relaxation on the contact surface. Lee et al. [2,7] showed that, under fretting fatigue at laboratory temperature, the same percentage of stress relaxation was measured to occur from the contact surface throughout different depths of peened specimens. Also, stress relaxations due to elevated temperature and mechanical load were found to be independent processes.

In other researches [1,2,15,16] it was found that residual stress relaxation due to fretting fatigue cycles affected fatigue life and crack initiation location significantly. Larger relaxation caused more fatigue life reduction and might shift crack initiation location from the interior of specimens to the contact surface.

2.2.4. Shot-peening Effect on Fretting Fatigue Life

Due to the introduction of residual compressive stress induced by shot-peening process in the substrate specimens, both plain and fretting fatigue strength under laboratory environment was improved for shot-peened Ti-6Al-4V specimens when compared with un-peened ones [1,2,10,14,15]. In addition, crack initiation locations for shot-peened specimens may occur either on the contact surface or far away from contact surface at a depth of 200-300 microns. These initiation locations were close to the location where maximum tensile residual stress which also depends on the residual stress profile gradient, the depth of compressive residual stress, microstructure crack on the contact surface and specimen thickness. In order to get the most beneficial effects from residual compressive stresses the depth of the compressive regime must be greater than the depth where cracks may initiate such that pre-existing crack tips could be closed and crack initiation and propagation can be retarded.

2.3. Temperature Effect

An investigation by Sahan [6] of un-peened Ti-6Al-4V specimens under room and elevated temperature 260˚ C showed no life retardation due to temperature. Another investigation of shot-peened specimens tested at room temperature, 100˚C, and 260˚C was conducted by Lee et al. [2,7]. No beneficial effect from shot-peening was observed at 260˚C and in all the tests multiple-crack initiation pattern was observed and cracks always initiated at the trailing edge on the contact surface. In their study most of the scar surface was basically covered by debris/oxides and no noticeable effect of debris/oxides on the coefficient of friction was observed.

Stress relaxation phenomenon was also observed away from the contact region for all specimens that failed at room temperature, 100˚C and 260˚C. In addition, higher temperature as well as longer exposure time induced larger stress relaxation. Approximately 38% residual stress relaxation was observed a little bit away from the contact region and 69% relaxation was measured for specimens under fretting tests at 260˚C. In addition, stress relaxation in the interior of specimens was determined using X-ray diffraction to be almost the same with relaxation rate measured on the surface for both room temperature and 260˚C conditions. Lee [2] postulated that approximately 30% of residual stress relaxation occurred due to the fretting mechanistic mechanism at room temperature, and an additional 30% relaxation was due to exposing shot-peened specimens to elevated temperature. Furthermore, stress relaxation due to elevated temperature and fretting loads could be treated as independent processes, and total stress relaxation could be linearly superimposed from fretting mechanistic effect and elevated temperature effect respectively. Lee [2] also showed that microscopic damage on contact surface and residual stress relaxation caused cracks to initiate on the contact surface instead of within the interior of specimens.

2.4. Fatigue Parameters

Crack initiation models and predictive parameters are developed on the basis of stress or strain history of the plain fatigue configuration. These techniques can be extended to fretting fatigue data. Attention has been drawn to the use of multiaxial fatigue parameters such as a critical plane approach to describe fretting fatigue behavior. Critical plane fatigue parameters were generated based on the maximum damage plane which is formulated during fatigue.

Fatigue life of mechanical components under fretting fatigue conditions has been demonstrated to be significantly reduced as compared to fatigue life under plain fatigue conditions [1,17,18]. A fretting fatigue condition is associated with high cycle fatigue HCF, where a large fraction of fatigue life is spent in crack nucleation and growth to a detectable size while only a small fraction of life is spent in the crack propagation from detectable size to a critical size. Therefore, unlike using damage tolerant approach for predicting fatigue life under low cycle fatigue regime an alternative approach is needed to predict HCF crack initiation behavior.

2.4.1. Stress Range and Effective Stress

Fretting fatigue conditions is effected by local interfacial mechanistic parameters such as peak contact pressure, local cyclic bulk stress, local cyclic shear stress, and slip amplitude and contact semi-width [19]. However, predictive parameters based on global boundary conditions, i.e. contact load, tangential load, and far field stresses are still favored in some fields because global boundary conditions are more readily controlled in experiments and are the most obvious variables in a practical situation. Consequently, predictive models relating global mechanistic variables are most desirable in terms of applicability and two such parameters are stress range and effective stress.

Stress range for applied axial load can be described as:

$$\Delta\sigma = \sigma_{\max} - \sigma_{\min} \tag{1}$$

Equation (1) doesn't include the effect from mean stress or stress ratio, which were well documented in fatigue literature to be relevant to fatigue strength. Walker [20] proposed an alternative method using effective stress to account for the effects from stress ratio as follows:

$$\sigma_{eff} = \sigma_{\max}(1-R)^{m} \quad (2)$$

where σ_{eff} is the effective stress taking into account the effect from stress ratio and residual stress, and m was found to be 0.45 by Lykins [17]. Equation (2) takes the stress ratio and mean stress effects into account when compared to Equation (1).

When evaluating effectiveness of Equation (2) for un-peened Ti-6Al-4V specimens in fatigue life prediction under fretting fatigue conditions, Mall et al. [21,22] found this equation could only collapse fretting fatigue life data into a single curve well under specific pad geometries. Lee et al. [2] noticed Equation (2) worked well in fretting fatigue life prediction under elevated temperature up to 260˚ C.

In order to fit the experimental data on a curve, the applied stress range can be described as

$$\Delta\sigma = C_1 (N_f)^{C2} + C_3 (N_f)^{C4} \quad (3)$$

where C_1, C_2, C_3, C_4 can be found using a curve fitting technique with Kaleidagraph for each curve. Also, effective stress can be described as

$$\sigma_{eff} = C_1 (N_f)^{C2} + C_3 (N_f)^{C4} \quad (4)$$

Different C_1, C_2, C_3, C_4 coefficients can also be found for effective stress values.

Equation (1) and (2) worked well in correlating fatigue life with global load conditions under certain circumstances. Nevertheless, it should be noted that these equations only provide a simplistic nature on a mechanic basis. They do not include the stress concentration effect occurring at the trailing edge of contact region and multiaxial loading conditions induced by fretting fatigue. This explains why critical plane-based predictive parameters formulated on local stress distribution are needed.

2.4.2. Critical Plane Based Fatigue Approach

The maximum or minimum in-plane principal stresses acting at a specific point can be expressed as:

$$\sigma_{1,2} = \frac{\sigma_{xx} - \sigma_{yy}}{2} \pm \sqrt{(\frac{\sigma_{xx} - \sigma_{yy}}{2})^2 + \tau_{xy}^2} \tag{5}$$

$$\tau_{\max} = \sqrt{(\frac{\sigma_{xx} - \sigma_{yy}}{2})^2 + \tau_{xy}^2} \tag{6}$$

where σ_1 and σ_2 are principal normal stresses and the planes on which they act are called principal planes. σ_{xx}, σ_{yy}, τ_{xy} are stress components at a local point. τ_{max} is the maximum shear stress at a given point, and it always acts on a plane with 45^o from the orientation of principal planes.

The critical plane is defined as the plane where a fatigue parameter has its maximum value. In order to evaluate critical plane-based fatigue parameters, local normal and shear stresses are computed as follows

$$\sigma = \frac{\sigma_{xx} + \sigma_{yy}}{2} + \frac{\sigma_{xx} - \sigma_{yy}}{2}\cos(2\theta) + \tau_{xy}\cos(2\theta) \tag{7}$$

$$\tau = -\frac{\sigma_{xx} - \sigma_{yy}}{2}\sin(2\theta) + \tau_{xy}\cos(2\theta) \tag{8}$$

where θ is evaluated from -90^o to $+90^o$. A good critical plane fatigue parameter formulated from Equations (7) and (8) should be able to predict fatigue life, crack initiation location, and crack initiation orientation. These requirements will be adopted to examine the validity of fatigue parameters.

2.4.3. Smith-Watson-Topper Parameter (SWT)

The Smith-Watson-Toper [23] proposed a fatigue parameter as follows

$$SWT = \frac{\left(\sigma_f^{'}\right)^2}{E} * \left(2N_i\right)^{2b'} + \sigma_f^{'} \varepsilon_f^{'} \left(2N_i\right)^{b'+c'} \tag{9}$$

where $\sigma_f^{'}$ is fatigue strength coefficient, b_f' is fatigue strength exponent, ε_f' is fatigue ductility coefficient, c' is fatigue ductility exponent, E is the elasticity modulus, and N_i is cycles to crack initiation. This equation is widely known as Smith-Watson-Topper (SWT) parameter.

Szolwinski and Farris [24] made modifications to SWT parameter using critical plane approach as follows:

$$SWT = \sigma_{\max} \varepsilon_a \quad or \quad \max(\sigma_{\max} \varepsilon_a) \tag{10}$$

where σ_{max} is the stress normal to a critical plane, and ε_a is the normal strain amplitude to a critical plane. This parameter asserts crack initiation occurs on the plane where the product of σ_{max} and ε_a is maximal. Using the computed local stress and strain from finite element analysis of the fretting fatigue experiments, this parameter was calculated at all planes ranging from $-90^o \leq \theta \leq +90^o$, which provided this parameter's maximum value.

The SWT parameter, for un-peened specimens, was found effective in predicting the number of cycles to crack initiation and crack initiation location with strong dependence on pad geometry [21,22,24,25]. However, it didn't provide good agreement with crack initiation orientation. Also, the maximum shear strain amplitude did not coincide with crack initiation location under fretting fatigue conditions for un-peened specimens as it showed under plain fatigue tests as mentioned by Neu et al. [25]. For

shot-peened specimens, Yuksel [1] found this parameter was effective in crack initiation location prediction but failed in predicting either fatigue life or crack initiation orientation.

2.4.4. Shear Stress Range Parameter (SSR)

SSR parameter considers only maximum and minimum shear stress on the critical plane. To compute this parameter, the shear stress was calculated at all points along all planes ranging from $-90^o \leq \theta \leq 90^o$ from the state of stress (σ_{xx}, σ_{yy}, τ_{xy}) computed from FEA by applying the following equation:

$$\tau = -\frac{\sigma_{xx} - \sigma_{yy}}{2} \sin 2\theta + \tau_{xy} \cos 2\theta \tag{11}$$

Then SSR, $\Delta\tau = \tau_{max} - \tau_{min}$ was computed at all planes and at all points in the contact region, where $\tau_{max} - \tau_{min}$ are shear stresses due to the applied maximum and minimum axial load, respectively. Since the mean stress or stress ratio also affect fretting fatigue behavior, this effect on the critical plane was accounted by incorporating a technique proposed by Walker [26]. Thus SSR parameter is expressed as:

$$(SSR = \Delta\tau_{crit}) = \tau_{max}(1 - R_\tau)^m \tag{12}$$

where τ_{max} and R_τ are the maximum shear stress and the shear stress ratio (τ_{min} / τ_{max}) at the critical plane, respectively, and m is a fitting parameter determined as 0.45 from a previous study [27].

It was shown that the SSR, for un-peened specimens with different pad geometry, was useful in conjunction fretting fatigue life with plain fatigue life [21,22]. In addition, this parameter can also correlate crack initiation location and orientation with experimental observations. On the other hand, for shot-peened specimens, Yuksel [1] showed that under fretting fatigue conditions, this parameter is only effective in crack

initiation orientation prediction but failed in predicting both fatigue life and crack initiation location.

2.4.5. Findley Parameter (FP)

Crack initiation mechanism in multiaxial loading fatigue conditions should be influenced by both normal and shear stresses. Since SSR only accounts for the effect from shear stress, another multiaxial fatigue parameter involved the effect from normal stress on a critical plane in addition to shear stress amplitude can be found in Findley's study as follows [28]

$$FP = \tau_a + k\sigma_{\max} \tag{13}$$

where k is an influence factor determined to be 0.35 from plain fatigue data [22], and τ_a is stress amplitude defined as $\tau_a = (\tau_{max} - \tau_{min})/2$. FP was calculated at all planes ranging from $-90^o \leq \theta \leq +90^o$ from computed stresses and strains obtained from finite element analysis. These calculations provided the critical plane, where this parameter is the maximum.

For un-peened specimens with different geometry pads under fretting fatigue conditions, FP could predict crack initiation location well but was not able to predict fretting fatigue life from plain fatigue data. In addition, the predicted crack orientations were different from experimental observations as was found by Mall et al [22,25]. For shot-peened specimens under fretting fatigue conditions it was found that this parameter was most effective in crack initiation location prediction but failed to predict fatigue life and crack initiation orientation [1].

2.4.6. Modified Shear Stress Range Parameter (MSSR)

This parameter is formed by combing maximum normal stress, which generally aids in opening the crack surface, on a critical plane of maximum SSR into the original SSR as follows

$$MSSR = A\Delta\tau_{crit}^{B} + C\sigma_{\max}^{D} \tag{14}$$

where $\Delta\tau_{crit}$ is same as Equation (12) and σ_{max} is the maximum normal stress on the critical plane of the SSR parameter. A, B, C, D are fitting constants determined by curve fitting approach. These constants are determined empirically as A=0.75, B=0.5, C=0.75, and D =0.5 [22]. MSSR was calculated at all planes ranging from $-90^{o} \leq \theta \leq +90^{o}$ from computed stresses and strains obtained from finite element analysis. These calculations provided the critical plane, where this parameter is the maximum.

MSSR was the only critical plane-based parameter available in predicting fatigue life, crack initiation location, and crack initiation orientation along with their experimental counterparts for both shot-peened and un-peened Ti-6Al-4V specimens with little dependency on pad geometry under fretting fatigue conditions [1,21,22]. Therefore, MSSR parameter was determined to be an appropriate fatigue predictive parameter while investigating crack initiation behavior of both shot-peened and un-peened Ti-6Al-4V under fretting fatigue phenomenon.

MSSR was also able to satisfactorily characterized fretting crack initiation orientation and location independent of contact geometry for two values of coefficient of friction, 0.5 and 0.8 [29]. Lee et al. [2] observed that MSSR was effective in fretting fatigue life prediction for shot-peened specimens under elevated temperature from room temperature up to 260˚C when residual stress was imposed with stress relaxation

phenomenon. Sabelkin et al. [16] showed that MSSR could predict fretting fatigue life as well as crack initiation location in agreement with experimental counterparts for specimens shot-peened under 4A, 7A, and 10A specification with 100% surface coverage.

In this study, MSSR was adopted as the fatigue parameter to be investigated in fretting fatigue behavior prediction.

2.5. Contact Mechanics

A cylindrical-end body in contact with a flat body setup is adopted as the fretting fatigue configuration and is incorporated in this study. Contact mechanics and analytical solutions associated with this configuration are discussed in detail in this section. A diagram of two bodies in contact under fretting fatigue loads is shown in Figure 3. Here, A represents the cross sectional area of the fretting specimen, σ_{axial} represents the applied axial stress, P is the applied contact load, Q is the reacted tangential load, d is the thickness of a specimen, b indicates half thickness of a specimen, and a represents the contact half width. The constant radius of fretting pads in the cross sectional plane is r, and the radius of the fretting fatigue specimen is infinite in the cross sectional plane, that is, a flat surface of specimens is used in this study. For analytical solutions, an assumption was made at the beginning that these two contact bodies have infinite boundaries, and analytical equations were formulated based on the displacement relationships of the two contact bodies.

Assume that given points in the contact zone are displaced in the y-direction by $v_1(x)$-$v_2(x)$ and invoke the displacement relationship developed by Hills and Nowell [30]; the relationships in the contact region was obtained:

$$\frac{1}{A^*}\frac{\delta h(x)}{\delta x} = \frac{1}{\pi}\int \frac{p(\xi)}{x-\xi} d\xi - \beta q(x) \tag{15}$$

where $h(x)=v_1(x)-v_2(x)$ is the amount of overlap that will occur if the contacting bodies could penetrate each other freely, p is the pressure in the contact zone and q is the surface shear stress. The other parameters of equation (15) are:

$$A^* = 2\{\frac{1-\nu_1^2}{E_1} - \frac{1-\nu_2^2}{E_2}\} \tag{16}$$

$$\beta = \frac{1}{2A^*}\{\frac{1-2\nu_1}{E_1} - \frac{1-2\nu_2}{E_2}\} \tag{17}$$

where E is modulus of elasticity and ν is Poisson's ratio for the contact bodies, respectively.

Assuming that the tangential displacement can be defined by $g(x) = u_1(x)-u_2(x)$, a similar equation can be formulated as follows:

$$\frac{1}{A^*}\frac{\delta g(x)}{\delta x} = \frac{1}{\pi}\int \frac{q(\xi)}{x-\xi} d\xi - \beta p(x) \tag{18}$$

In this study, since the contact bodies are made of the same material, hence β=0, and equations (15) and (18) can be further simplified.

When fretting bodies are brought into contact with each other by applying a contact load, the displacement of adjoining points on the contact surface within the stick zone will be the same. Furthermore, a pressure distribution p(x,y) will be introduced by the contact load. The solution of the pressure distribution from the contact load is usually termed Hertz solution. In order to solve the pressure distribution, two primary assumptions are made. First, the radii of both bodies are large in comparison to the contact dimension. Second, the contacting bodies have infinite boundaries. The infinite

boundary assumption is commonly referred to as the half space assumption. A half space exists if one half of the specimen thickness (b= d/2) matches the requirement b/a > 10. Fellows et al. [31] found the violation of the infinite half space assumption will introduce significant deviation into analytical solutions when compared to solutions from finite element analysis.

If one idealizes the profile of contact surfaces as a parabola, a weight function can then be achieved as:

$$w(x) = \sqrt{a^2 - x^2} \tag{19}$$

where a is the contact half-width. Solving equations (18) and (19) yields:

$$p(x) = -\frac{k}{a}\sqrt{a^2 - x^2} \tag{20}$$

where k is termed the radius of curvature, $k=1/R_1+1/R_2$, where R_1 and R_2 are the radii of fretting pad and specimen, respectively. Equilibrium in the contact surface between the applied contact load and the pressure distribution can then be defined as

$$P = -\int_{-a}^{a} P(\xi)d\xi = \frac{\pi k a^2}{2A^*} \tag{21}$$

From equations (20) and (21), one can write with the following:

$$p(x) = -P_0\sqrt{1-(\frac{x}{a})^2} \tag{22}$$

where P_0 is maximum pressure (Hertzian Peak Pressure) defined as:

$$p_0 = \frac{2P}{\pi a} \tag{23}$$

Contact half-width, a, can be found from equation (21) as follows:

$$a^2 = \frac{2PA^*}{\pi k} \tag{24}$$

In this study, since the fretting specimen has a flat surface ($R_1=\infty$), equation (24) can be simplified as:

$$a = \sqrt{\frac{8PR_1}{\pi}\frac{1-\nu^2}{E}} \tag{25}$$

The axial stress resulting from the applied contact load P can be expressed in Cartesian coordinates as:

$$(\sigma_{xx})_{contact} = -p_0\{\frac{\sqrt{a^2-x^2}}{a}\} \tag{26}$$

As shown in Figure 4, after applying a contact load (P) and the accompanying tangential load (Q), there will be a stick zone in the middle portion of the contact surface and slip zones at both sides. The portion between –c and c defines stick zones whereas the portions between –a and -c as well as c and a present the slip zones. The stick zone is a portion where the adjoining contact points of the fretting bodies, the specimen and the pad, move together. On the other hand, the adjoining contact points can move freely with each other within the slip zones. The stick zone in fretting fatigue configuration is determined simplistically by the contact geometry, contact pressure and coefficient of friction. The formation of the stick zone leads to an amplification of remotely applied stresses in the vicinity of contact surface and premature crack initiation.

Shear stress distribution along the contact surface can be expressed as:

$$q(x) = \frac{C}{\sqrt{a^2-x^2}} \tag{27}$$

where $C=Q/\pi$, Q is the total shear stress along the contact length which is obtained by integrating the shear stress distribution as:

$$Q = \frac{fp_0\pi}{2a}(a^2 - c^2) \tag{28}$$

where f is the coefficient of friction and the stick zone size is described as:

$$\frac{c}{a} = \sqrt{1 - |\frac{Q}{fP}|} \tag{29}$$

The stress distribution cased by the tangential load in the X-direction is found as:

$$(\sigma_{xx})_{\tan gential} = 2fp_0 - \frac{2}{\pi}\int_{-a}^{a}\frac{q'(x)}{x+a}dx \tag{30}$$

where

$$q'(x) = -\frac{fp_0 c}{a}\sqrt{1 - (\frac{x-e}{c})^2} \tag{31}$$

and

$$e = \frac{\sigma a}{4fp_0} \tag{32}$$

$$\sigma = \frac{E\varepsilon_{xx}}{1-\nu^2} \tag{33}$$

where ε_{xx} is the corresponding strain induced by the axial tensile stress (σ_{axial}) under plane strain.

Total axial stress along the contact surface between the fretting specimen and the fretting pad can then be expressed as:

$$\sigma_{xx} = (\sigma_{xx})\text{contact} + (\sigma_{xx})\text{tangential} + (\sigma_{xx})\text{axial} \tag{34}$$

Chan and Lee [32] wrote a FORTRAN program named “Ruiz program” to calculate the numerical solutions required by analytical analyses for variables such as Hertzian Peak Pressure in Equation (23), contact half-width in Equation (25), σ_{xx} in Equation (34), and so forth. These solutions from both analytical equations and Ruiz

program are computed to verify the finite element model used in this study and then was compared to experimental results.

2.6. Summary

The review of fretting fatigue literature can be summarized in the following. Fretting fatigue occurs between two contact components under relative motion and reduces fatigue life when compared with plain fatigue. Shot-peening, on the other hand, improves material fatigue strength. In order to better understand fretting fatigue mechanisms, analytical solutions have been developed and comprehensive researches have been conducted to analyze different contributing variables, such as shot-peening process and elevated temperature. Predictive parameters using both plain fatigue technique and critical plane-based approach were also investigated for the effectiveness in fretting fatigue mechanism predictions. Most of the previous studies focused on the effect of varying one contributing factor to fretting fatigue. No study is available which investigates the effect of elevated temperature on shot-peening intensity. Due to that and for the sake of better understanding the fretting fatigue phenomenon in a real life application, the primary object of this study was to investigate the effect of elevated temperature on shot-peening intensity in fretting fatigue.

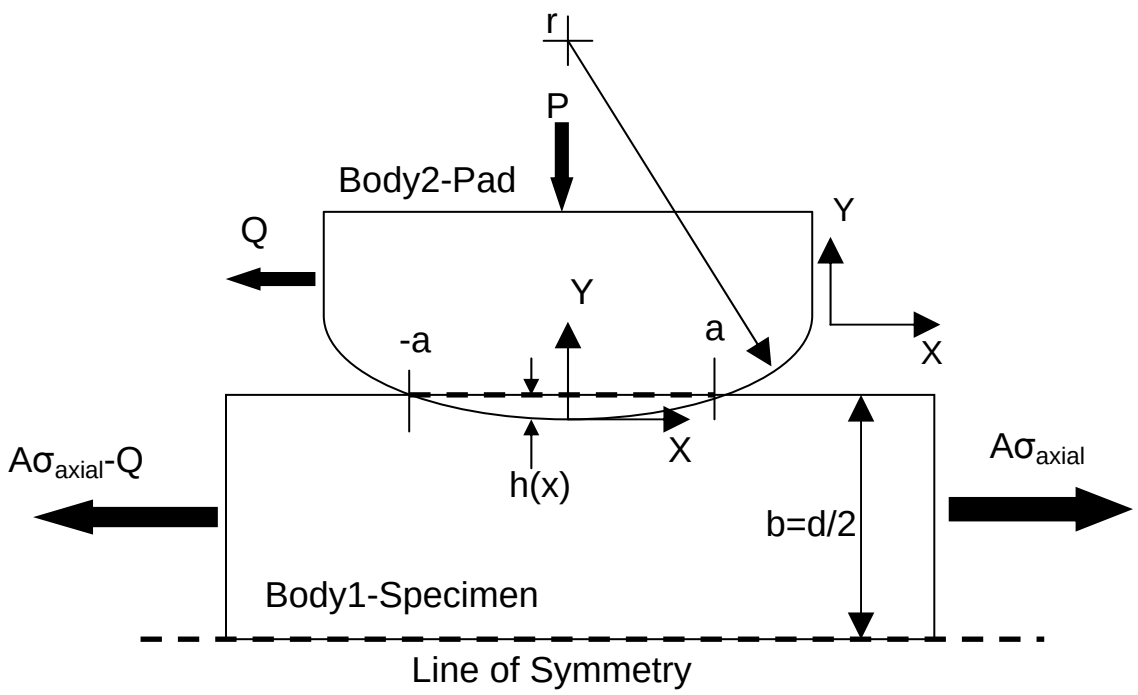

Figure 3. Free Body Diagram of Two Bodies under Fretting Fatigue Loads

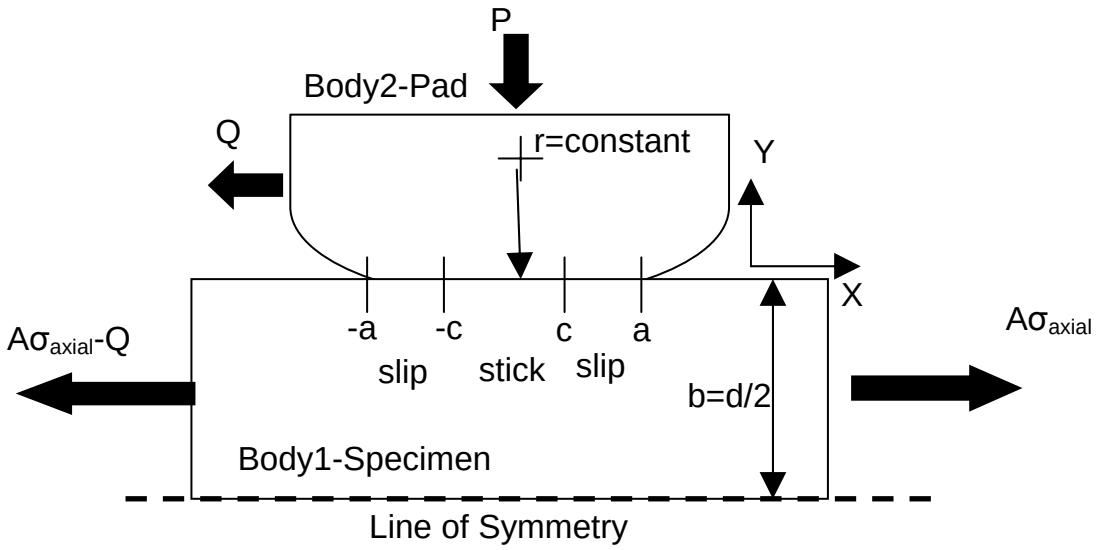

Figure 4. Partial Slip Condition for Deformed Bodies

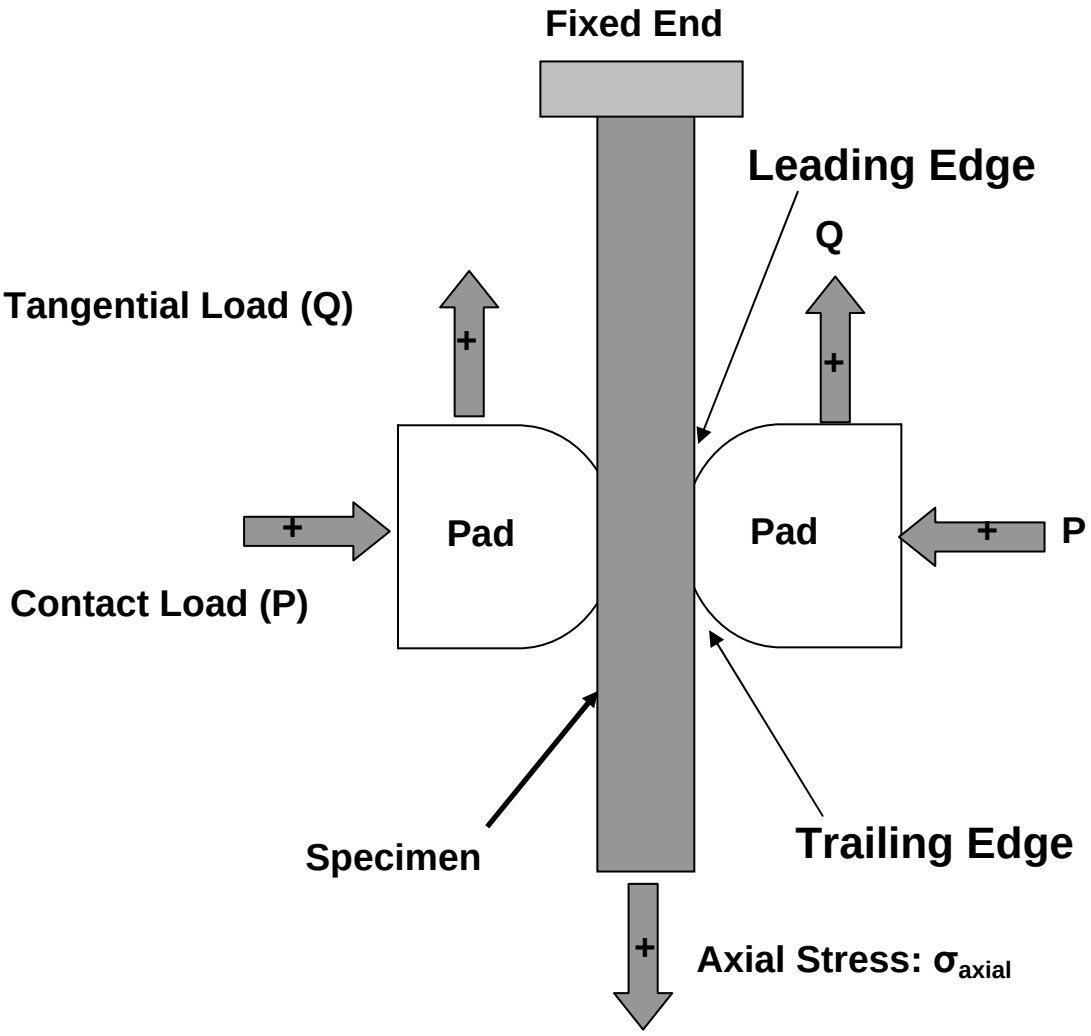

Figure 5. Typical Fretting Fatigue Configuration

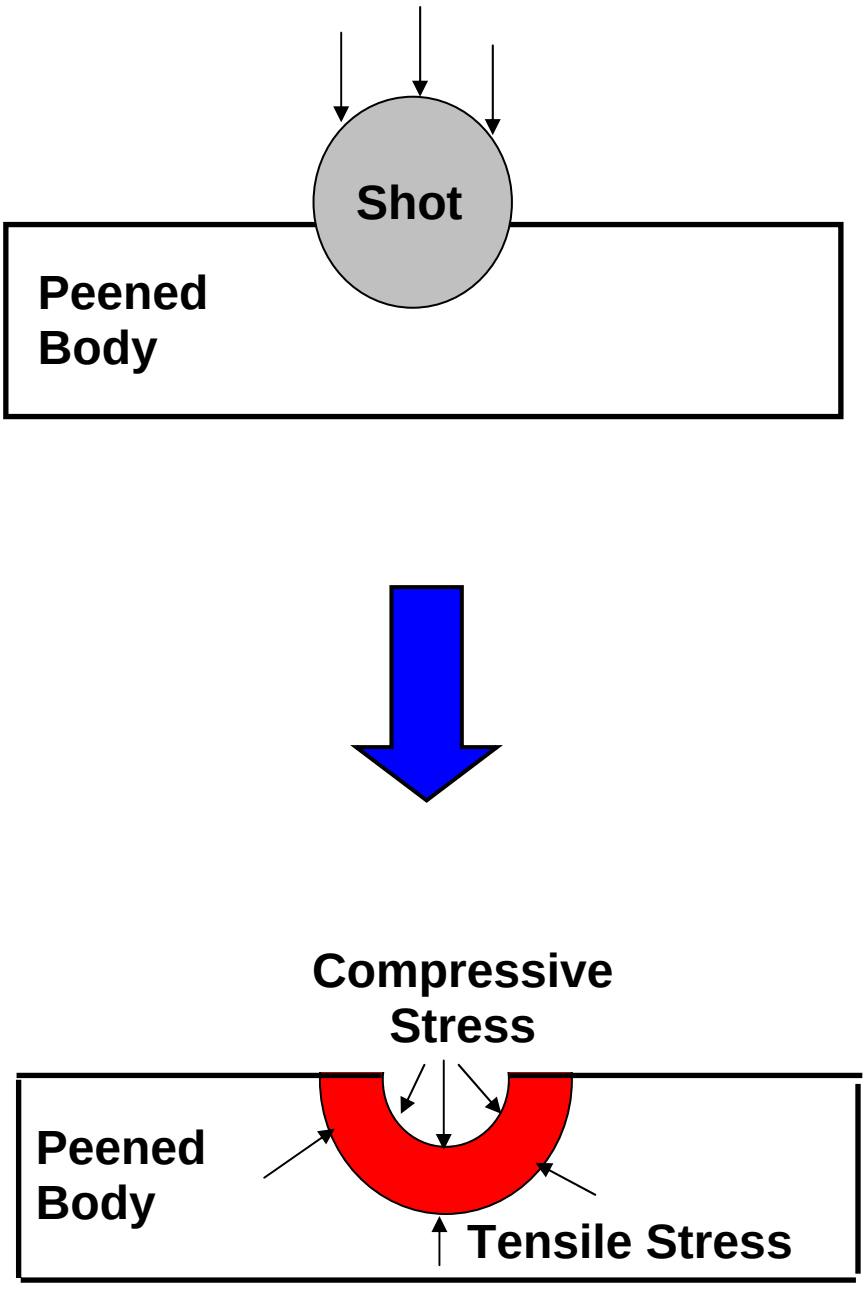

Figure 6. Schematics of Shot-peening Process

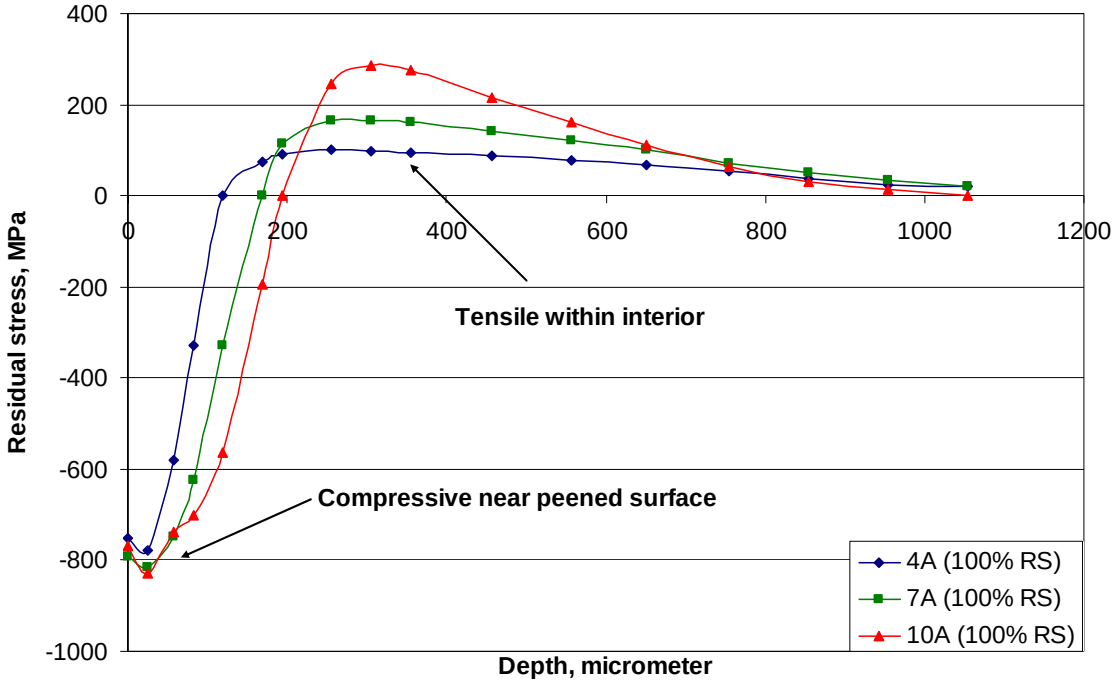

Figure 7. Typical Residual Stress Profile Induced by Shot-peening ($\sigma_{xx}=\sigma_{yy}$, $\tau_{xy}=0$) for 4A, 7A and 10A specimens [11]

III. Experimental Configuration

This chapter documents the experimental configuration used in this study to investigate the effect of elevated temperature and shot-peening intensity on the fretting fatigue behavior of Ti-6Al-4V. The procedure used to study the effects of temperature exposure is also covered. Experimental test details such as test apparatus, specimen and pad geometry, material property, load determination, and test procedure are covered in this chapter.

3.1. Test Apparatus

The experimental setup in this study incorporated a 22.2 kN servo-hydraulic uniaxial test machine at room and elevated temperature. A photograph showing the complete test machine is presented in Figure 8. This test machine, as demonstrated schematically in Figure 9, has a fretting fixture capable of keeping the normal load constant via lateral springs through out the test. The axial load can be varied with the help of the 22.2 kN servohydraulic load frame. The axial load variation that the test specimen experiences during the fatigue test were controlled by load cells attached to the servohydraulic load frame. This actuator was controlled by Multi-Purpose Test Software (MPT) which allowed users to vary the magnitude, frequency, and waveform of the axial load. When a cycle load is applied to the specimen, the contact pads move relative to the specimen and cause fretting fatigue action on the face of the specimen. Due to this alignment becomes a big concern, therefore testing and alignment should be checked before every test.

3.2. Specimen and Pad Geometry

The dimensions of the dog-bone specimens are illustrated in Figure 10. Both shot-peened intensities (4A and 10A) specimens have the same dimensions. The thickness (2b) of the gauge section is 6.35 mm, and width (w) is 6.35 mm, having a gauge cross sectional area (A) 40.3225 mm^2, and overall length (L) 60 mm. The geometry of the fretting pads is also displayed in Figure 10. These cylindrical-end pads are not shot-peened and they have an equivalent radius (r) of 50.8 mm at one end with flat-end at the other side. The thickness of pads is 9.525 mm, and width is 9.525 mm.

3.3. Material Property

Both shot-peened intensities specimens and the pads used in this study were made up of the forged titanium alloy, Ti-6Al-4V, for this alloy is commonly used to fabricate turbine engine disks and blades. The alloy was preheated and solution treated at 935˚C for 105 minutes, cooled in air, then vacuum annealed at 705˚C for 2 hours, and cooled again in argon. The resulting micro structure showed 60% by volume of α (HCP) phase (platelets) and 40% by volume of β (BCC) phase (matrix). The measured grain size was about 10 μm. The material had a modulus of elasticity of 126 GPa, yield strength of 930 MPa, Poisson's ratio of 0.3, and Brinell hardness number of 302.

Dog-bone specimens were machined by the wire electrical discharged method. In addition, the shot-peened specimens were shot-peened per SAE Aerospace Material Specification (AMS) 2432 standard, using computer controlled equipment with 4 and 10 Almen intensity. The process was accomplished with ASR 110 cast steel shot with 100% surface coverage in the gage section.

Residual stress on the surface for the shot-peened specimen was measured via X-ray diffraction technique before fretting fatigue cycles were applied in the Air Force Research lab (AFRL/MLLP), and its value was determined as about -750 MPa for 4A specimens and -770 MPa for 10A specimens. These were very close to a previous study by Martinez [10]. Therefore, the residual stress profile measured from Martinez study for 4A and 10A shot-peened specimens was adopted as one of the input variables for finite element analysis (FEA) and Modified Shear Stress Range (MSSR) parameter calculation in this study. X-ray diffraction technique was used in this study to measure residual stress on the surface of the shot-peened specimens after fretting tests and temperature exposure tests. The X-ray diffraction measurements of residual stress were conducted using a two-angle sine-squared technique, in accordance with SAE J784a, employing Cu kα radiation from (213) planes of the HCP structure of the Ti-6Al-4V. The surface area irradiated in these measurements was 0.5mm × 5mm.

The coefficient of friction has to be determined for use in finite element analysis covered in Chapter IV. In previous studies [32] it was shown that after cycling the specimen, the coefficient of friction increases. Due to that the coefficient of friction in this study is measured after the cycling of the specimen reach a constant value approximately 10,000 cycles as observed by Sahan [6]. In this study the coefficient of friction ranged from 0.53 to 0.96. Also the difference in coefficients of friction between 4A and 10A shot-peened specimens was not significant. Therefore, a constant value of 1.0 was designated as the static coefficient of friction for all tests at elevated temperature except for those cases where Q/P measured from experimental results exceeded 1.0. For

these exceptions, a maximum value of Q/P from experimental records was assigned instead to prevent gross slip condition, see Table 1.

3.4. Determination of Applied Load

The main goal of this study is to investigate the effects of elevated temperature and shot-peening intensity on the fretting fatigue behavior. For both fretting test at room and elevated temperatures an axial stress, σ_{axial} ranging from 333 to 666 MPa was applied at a frequency of 10 Hz with stress ratio, R of 0.1 to produce tension-tension condition. A constant contact load of 1335 N was applied via lateral springs, followed by maximum σ_{axial} as the second step. After maximum normal and axial loads were applied at Step 2, subsequent load steps were then applied as a sinusoidal function, using peak/valley load and frequency until specimens broke into two pieces.

3.5. Test Procedure

One pair of fretting pads was mounted individually into the holding blocks that were affixed to a fixture frame. The pads were aligned to ensure the contact surfaces of pads were orthogonal to specimen and perpendicular to the applied axial load. This was insured from the pressure sensitive tape, which was put between specimen and pad. Afterwards, specimens were then taken out from hydraulic machine, and a warm-up procedure programmed in MPT was executed to warm up the test machine for at least 30 minutes. This warm-up procedure was programmed using the displacement control for the axial load actuator. K-type thermocouples attached on the specimen and pads using high temperature ceramic glue were used to measure and control the temperature at 260 °C. It was observed that once the fretting test at elevated temperature starts the thermocouple which is attached to the specimen detach instantly but the ones attached to

the pads stays in contact.. Next, a test specimen was mounted and clamped into test machine by the upper and the lower grips. Thermocouple from the specimen was connected to a monitor and thermocouples from the pad were connected to both monitors and controllers. Contact loads were then applied manually as Step 1 with an increment of 222.4 N to each side of the pads until a maximum value of 1335 N was reached. Two heaters, placed at the front and back of specimen, were used to heat and maintain the temperature at 260 °C over a 10 mm long gage section surrounding the contact region Figure 11. Heaters were connected to the thermocouples from the pads and controlled through a closed-loop controlled system with two separated silicon controlled rectifiers (SCR). During fretting fatigue test, temperature in the gage section of specimen was maintained within ±3 °C of the desired temperature. The heaters are then started and temperature is raised gradually until the desired temperature is reached. Once the desired temperature is reached it is left for an hour to stabilize and minor corrections were preformed accordingly. Axial loads followed as Step 2 in increments until a maximum load was met. After Step 2, the applied loads were then imposed using a sinusoidal function with maximum/minimum load and frequency until specimens broke into two pieces.

During the tests, peak-valley compensator (PVC) was activated for axial loads to reduce variation between command and feedback signals sensed by the test machine. The induced tangential load was determined by half of the difference between the lower axial load and upper axial load after tests were executed for 10,000 fretting fatigue cycles. Axial loads and tangential loads were monitored and recorded continuously during tests until an experiment was ended due to specimen failure. After a specimen failed, the

fretting fatigue cycles were recorded as its fretting fatigue life. These previously mentioned fretting variables were then used as the load inputs for FEA modeling and MSSR prediction to be discussed in latter chapters. In addition, specimens were exposed to elevated temperature in a box furnace at 260° C for either 2 or 24 hrs to investigate the stress relaxation behavior due to temperature exposure only Figure 12.

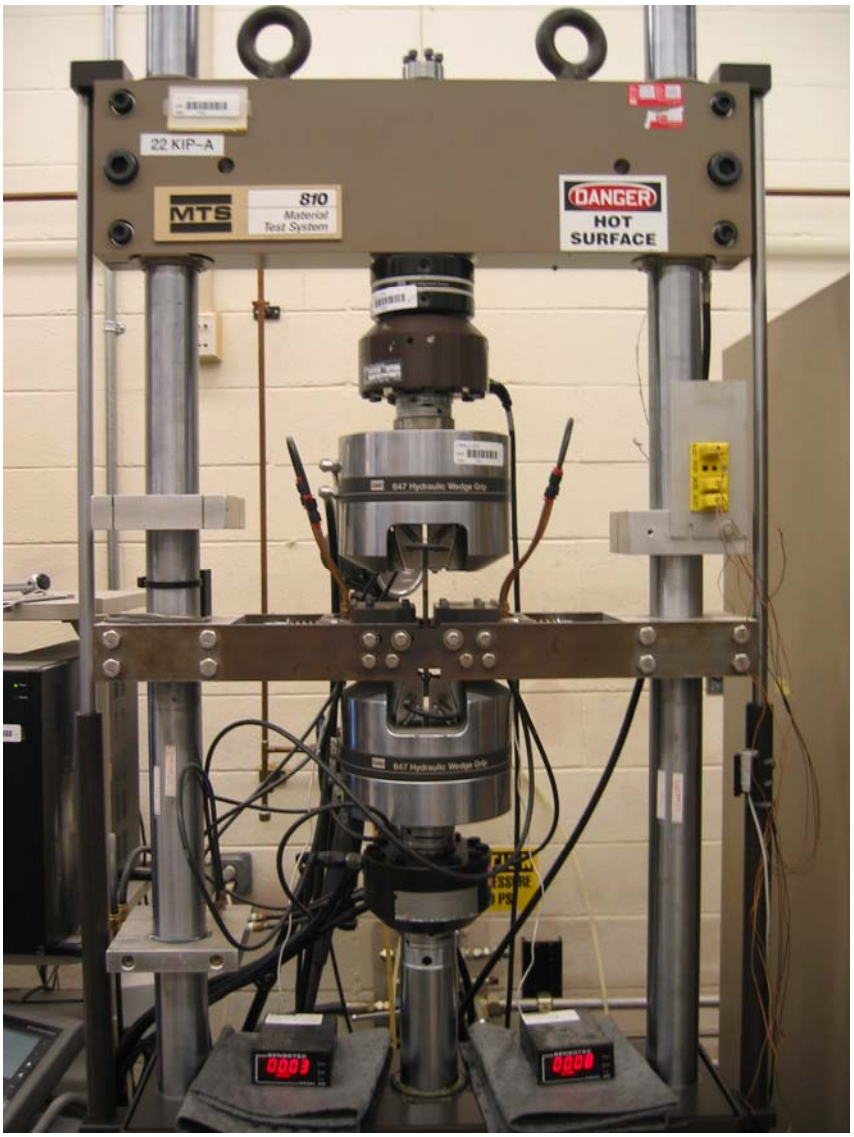

Figure 8. Uni-axial Servo-Hydraulic Material Test Machine with fretting fixture

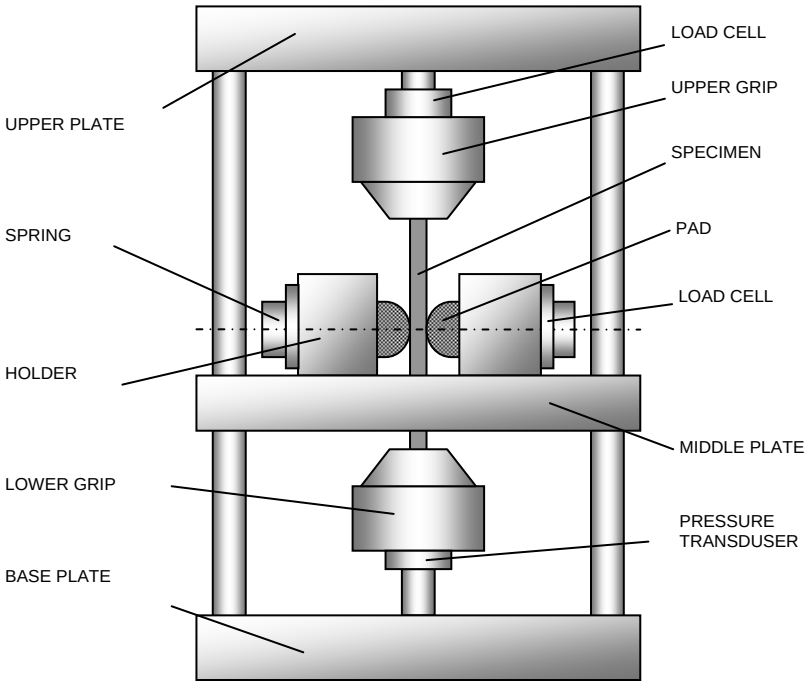

Figure 9. Schematic of Uni-axial Fretting Fatigue Set-up Configuration

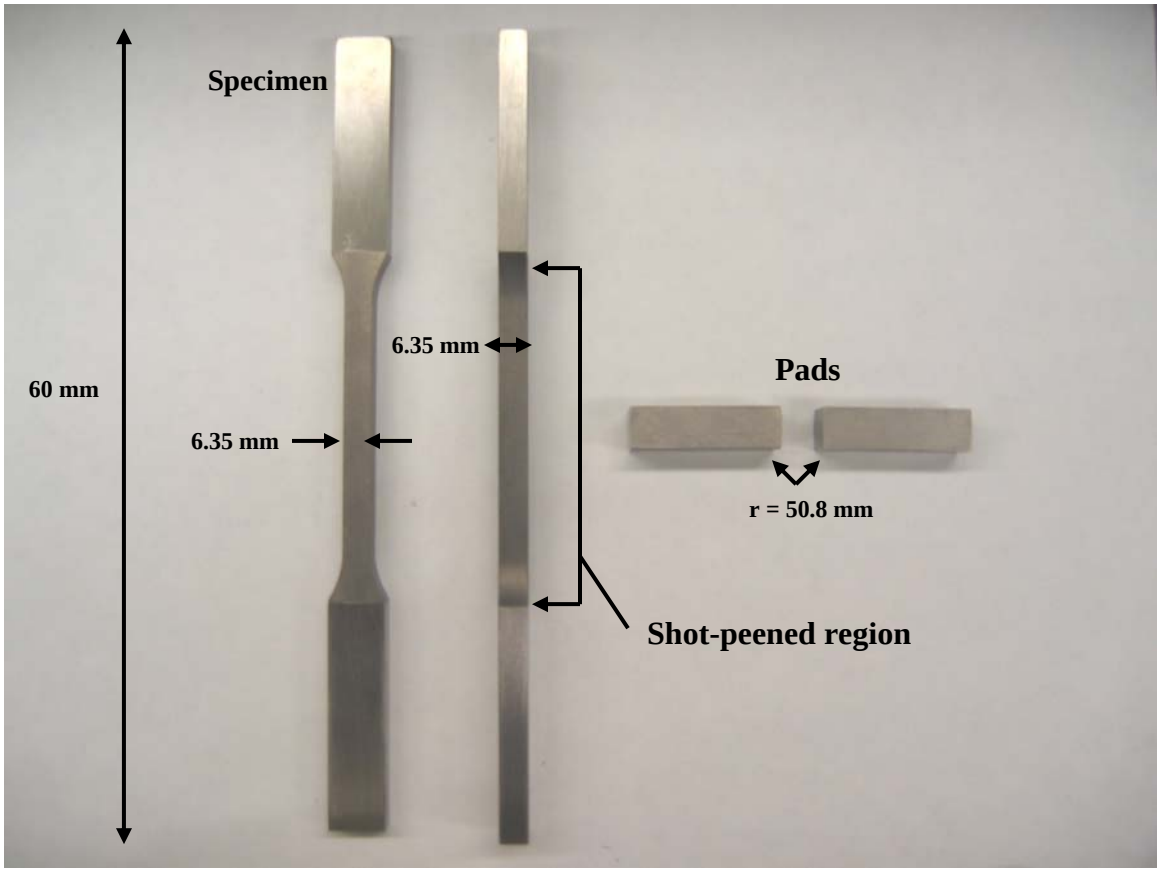

Figure 10. Specimen and Pad Geometry

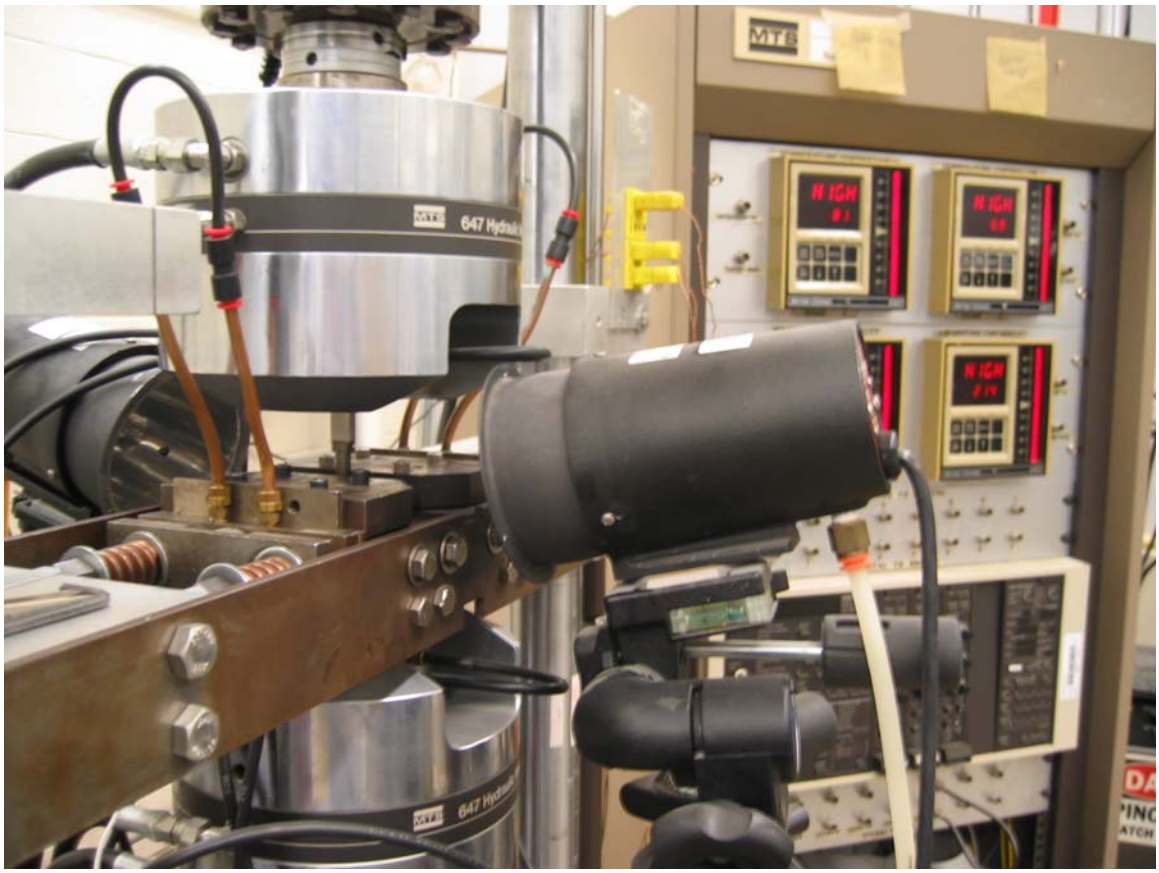

Figure 11. Spot Heaters and Temperature Control Unit in Test Configuration

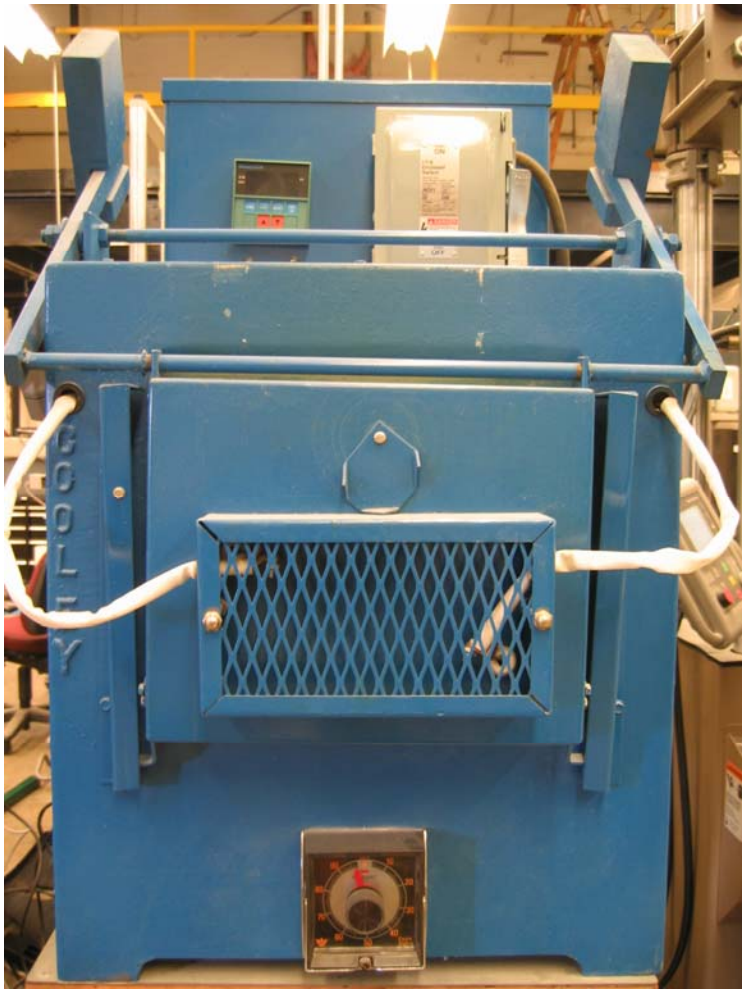

Figure 12. Box Furnace used for Temperature Exposure Tests.

IV. Finite Element Analysis

In this chapter the reason why finite element analysis (FEA) was needed for conducting analysis of fretting fatigue tests will be discussed. FEA analysis such as model development, load inputs, coefficient of friction, model validation and cyclic load effects will also be addressed.

4.1. Requirement for Finite Element Analysis

Finite element analysis segregates a continuum body into a finite number of elements. The basic premise is to formulate the governing equations at the discrete points, the nodes, which make up the elements, and then solve the equations as well as unknowns simultaneously to obtain the solution.

An infinite half-space assumption in fretting fatigue analysis is defined as half specimen thickness (b)/ contact half-width (a) >10. Finite specimen half-thickness can affect substrate compliance, and the stress components may differ for specimens with finite half-thickness. There is significant discrepancy between finite specimen half-thickness models and infinite half-space cases with respect to stress distribution within contact zone [33,34]. The infinite half-space assumption is a requirement for a FEA result to match an analytical solution obtained from a FORTRAN based “Ruiz” program. As mentioned in Section 2.6, analytical solutions were developed based on infinite half-space assumption. However, throughout this study, b/a was 6.26 for elevated temperature case and 7.24 for room temperature case, therefore the infinite half-space assumption was violated. This explains why finite element analysis, a numerical analysis technique that doesn’t require an infinite half-space assumption to be met, is necessary for conducting quantitative analysis in this study. In addition, FEA can be used to determine the

governing variables of fretting fatigue, such as contact stress, strain and displacement. These variables along with residual stress profiles and stress relaxation phenomenon can then be adopted to develop fretting fatigue predictive parameters which are addressed in Chapter V and VI.

4.2. Finite Element Model

A commercially available software, ABAQUS, was used for modeling the fretting fatigue configuration in this study as shown in Figure 13. In this study, four node, plain strain quadrilateral elements were used instead of eight node elements in order to eliminate the oscillation in the stress state along the contact interface introduced by the mid-side node of the eight node element. The contact condition was developed by using "master-slave" interfacial algorithm for modeling the finite element model of both shot-peened and un-peened experimental configuration. The model consisted of three parts: rigid body constraint, fretting pad, and fretting specimen. The fretting pad was constrained in the x and y direction by the rigid body constraint. Multi-point constraint (MPC) was applied to the pad and specimen to keep it from rotating due to the application of loads as presented in Figure 13. Only one half of the fretting specimen was used in FEA model due to the symmetric nature to increase the computational efficiency of the analyses and to save memory resources. The half space of fretting specimen was constrained in the x and y direction along its boundary. The stiffness of the rigid body constraint was chosen to be very low for improved convergence of the finite element analysis. Moreover, very little load was transmitted from rigid body constraint to fretting pad. The main purpose of this rigid body constraint was to restrict the rotation of fretting pad in the x and y-direction before the load steps were applied to FEA model. The

contact load was applied at the top of the pad, the tangential load was applied on the left hand side of the fretting pad, and the axial stress was applied to the right hand side of half space of the specimen. A small sliding contact condition was used between the fretting specimen and fretting pad.

The mesh of the pad and the specimen were refined incrementally from the center of contact surface by changing certain geometric coordinates in the ABAQUS input file. The mesh near contact surface was refined to increase the accuracy of the stress, strain, and displacement distribution profile. On the other hand, coarse mesh far away from contact surface was designed for saving computing time and system resources. Half specimen thickness was equal to 1.59 mm for all specimens. The material property of both the fretting pad and specimen was 95 GPa and 126 GPa as modulus of elasticity for elevated temperature and room temperature respectively. Poisson's ratio was 0.3 and a value of 1.0 was assigned to be the static coefficient of friction (f) for all models except for cases where $Q/P > 1.0$ from experimental result was violated. For these exceptions, $(Q/P)_{max}$ from experimental records was applied to avoid gross slip conditions between a pair of fretting pad and specimen. A summary of coefficients of friction used as the inputs for FEA is listed Table 1, Chapter VI.

4.3. Load Inputs

For all FEA analysis, a maximum contact load was always applied as Step 1 and then kept constant until Step 2 to avoid gross slip condition. The maximum axial and tangential loads then followed as the second step. Among all tests, the frequency of axial load was held at 10 Hz while changing stress range and stress ratio to achieve tension-tension configuration. After Step 2, applied loads were simulated as a sinusoidal function

with predetermined peak/valley values for axial, contact, and measured tangential loads as documented in Table 1. A detailed explanation for the applied load sequence is illustrated in Figure 14.

4.4. Coefficient of Friction

As mentioned in earlier, the difference among coefficients of friction was not significant for specimens at elevated or room temperatures. In addition, Iyer [35] showed that increasing friction from 0.37 to 0.5 (25% increase) caused no effect on contact half-width, 7% elevation on peak local cyclic stress range, and 15% raise in peak local cyclic shear stress range. Lykins [17] also observed increasing the coefficient of friction from 0.45 to 0.7 (66% increase) caused 20% increase in strain amplitude. Lee [12] showed that increasing coefficients of friction from 0.4 to 1.0 (250% increase) only produced, at most, 27% variation in σ_{xx} stress profile and 16% elevation in MSSR parameter. Among these studies, a slight difference in a coefficient of friction didn't generate much deviation in stress profile, contact half-width, and so forth. Previous studies also found that the experimentally stabilized static coefficient of friction ranged between 0.37~0.46 for un-peened Ti-6Al-4V specimens [32] and 0.33~0.46 for shot-peened Ti-6Al-4V specimens [1,15]. From these measurements, the shot-peening process didn't modify the coefficient of friction significantly, and the value of a static coefficient of friction could be treated as the same for both shot-peened and un-peened specimens.

For this study, a constant value, 1.0 was used as the static coefficient of friction for all tests except for those cases in which $Q/P < 1.0$ from experimental results was violated. For these exceptions, $(Q/P)_{max}$ from test conditions was assigned as the

coefficient of friction for FEA modeling. The detailed values for coefficients of friction used in FEA are listed in Table 1, Chapter VI.

4.5. Model Validation

Although the "Ruiz" FORTRAN program was developed on the basis of infinite half-space assumption under static applied contact and axial loads, and the half-space assumption was violated in this study, it is still a useful tool for quick check of FEA model by comparing their outputs. For this check, results from FEA at Step 2 of Test 13 were chosen to compare with their counterparts calculated from Ruiz Program under the same load conditions. This check was conducted by checking the contact half-width, the stress profile, Hertzian peak pressure, and nominal stress.

4.5.1. Contact Half-Width

Contact half-width can be solved analytically using Equation (25). Using this equation, contact half-width ($a_{analytical}$) was calculated to be 0.507 mm for elevated temperature and 0.439 mm for room temperature condition, identical to the value from Ruiz program. From discussions above, contact half-width calculated from Equation (25) and the Ruiz program was identical to each other. Therefore only the ($a_{Ruiz,max}$) contact half width was chosen in the rest of this study.

4.5.2. Stress State and Hertzian Peak Pressure

Since the Ruiz program is based upon the conditions that both contact and axial loads are applied statically, and the infinite half space criterion is met. In order to obtain these aforementioned conditions, Step 2 of Test 13 along the contact surface was chosen to validate stress profiles from FEA. Figure 15 demonstrates that the stress curves from FEA approach are close to those from the Ruiz program. The maximum values of σ_{xx}

from FEA was determined as 818 MPa at x/ $a_{Ruiz,max}$ =0.952. In comparison with the outputs from the Ruiz program, the variation was calculated as 0.2 % in magnitude and 9 % in location along x-direction. Hertzian peak pressure (P_0) from FEA, shown in Figure 16, was determined as 264 MPa at x/ $a_{Ruiz,max}$ = 0.01. On comparison with values from the Ruiz program, the variation was 0.4% in magnitude and 0.01% in location along x-direction.

4.5.3. Applied Nominal Stress

The final criterion to validate FEA model is the nominal stress σ_{xx} far away the contact zone along x-direction. In principle, σ_{xx} from FEA analysis far away the contact region should be consistent with the applied axial stress. Figure 17 presents that at the location where x/$a_{Ruiz,max}$ = 18.8, the value of σ_{xx} from FEA calculation reached 390 MPa. On comparison with the applied axial stress of 390 MPa, no deviation was found.

4.6. Cyclic Load Effect and Steady State

Since the FEA axial loads in this study were applied cyclically, it is crucial to judge what the effect is from this alternating load condition and whether or not the FEA solutions can converge to a steady state. Test 13 was selected to investigate cyclically applied load effect and the corresponding steady state phenomenon. Figure 18 demonstrates that when a cyclic load was introduced into the FEA model, an unsteady period occurred in stress profile. However, this unsteady phenomenon reached a steady state just after one load cycle was completed. It can also be seen from Figure 18 (a) and (c) that σ_{xy} was subjected to more deviation during transition from unsteady to steady state than σ_{xx}. That means σ_{xy} was more susceptible to the alternating load effect. Under

variable load conditions, σ_{yy} stress profile was not varied at all, suggesting that σ_{yy} stress profile was independent on the effect introduced by cyclic axial loads.

Figure 18 also shows that the Ruiz solution could only approach FEA stress solution at Step 2 very well just as expected since this step indicates a quasi-static situation. Much more deviation was found after FEA solution reached a steady state after Step 4, i.e. after one load cycle. This observation indicated that the Ruiz program and analytic solution are much more effective in describing a fretting fatigue configuration under static applied axial and contact loads. On the other hand, FEA is necessary for fretting fatigue analysis under cyclic axial loads configuration.

4.7. Maximum and Minimum Load Conditions

As illustrated in Figure 14, axial loads and tangential loads were subjected to continuously changing magnitude during fretting fatigue cycles. Therefore, clarifying and defining maximum and minimum load conditions are helpful to improve the readability and comprehension for the subsequent discussions. The maximum load condition is defined as a load step at which the maximum axial and tangential loads occur simultaneously under a variable loading condition. Also, the minimum load condition means a load step at which minimum axial and tangential loads happen at the same time under a variable loading condition. The contact load stays constant through the test.

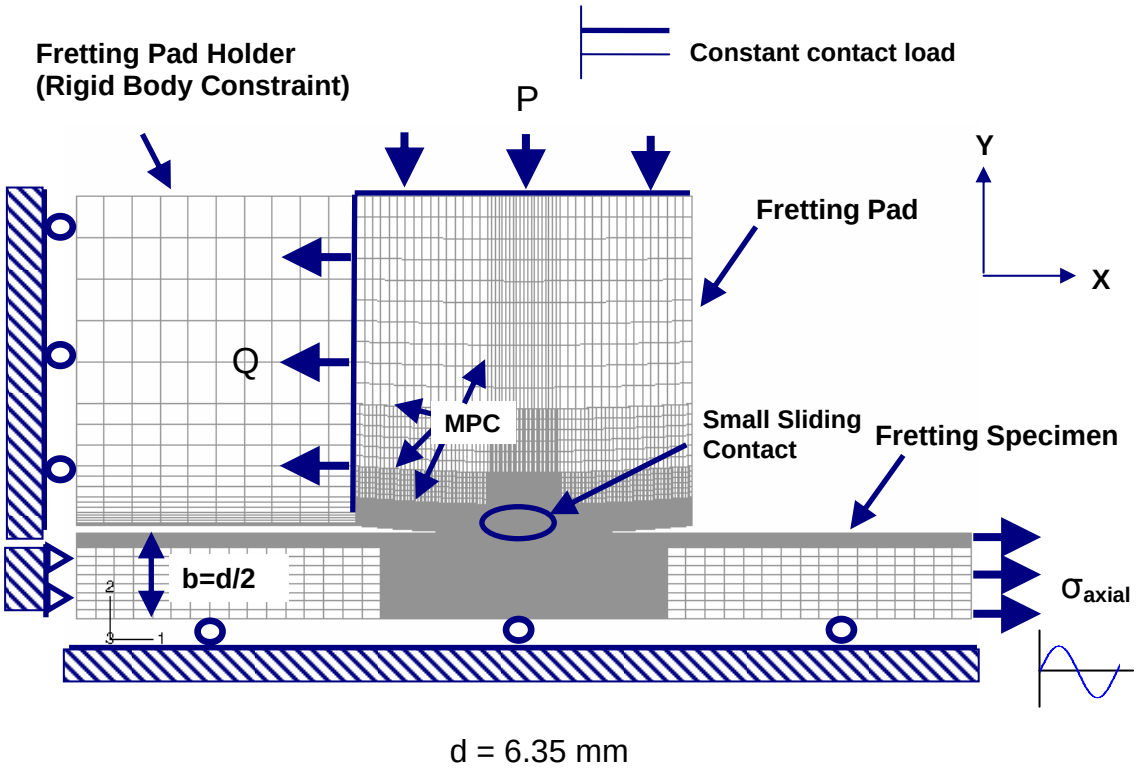

Figure 13. FEA Model with Load and Boundary Conditions

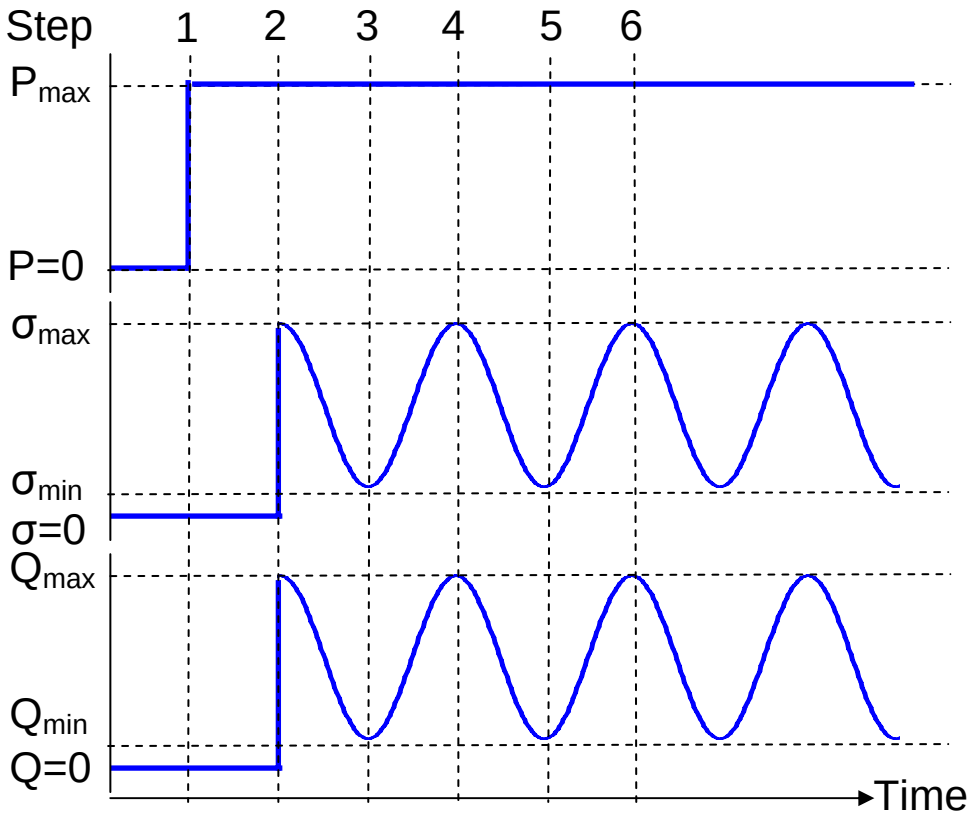

Figure 14. Load Configuration and Sequence

Note:
The experimental measured tangential loads are recorded in Table 1 in Chapter VI.

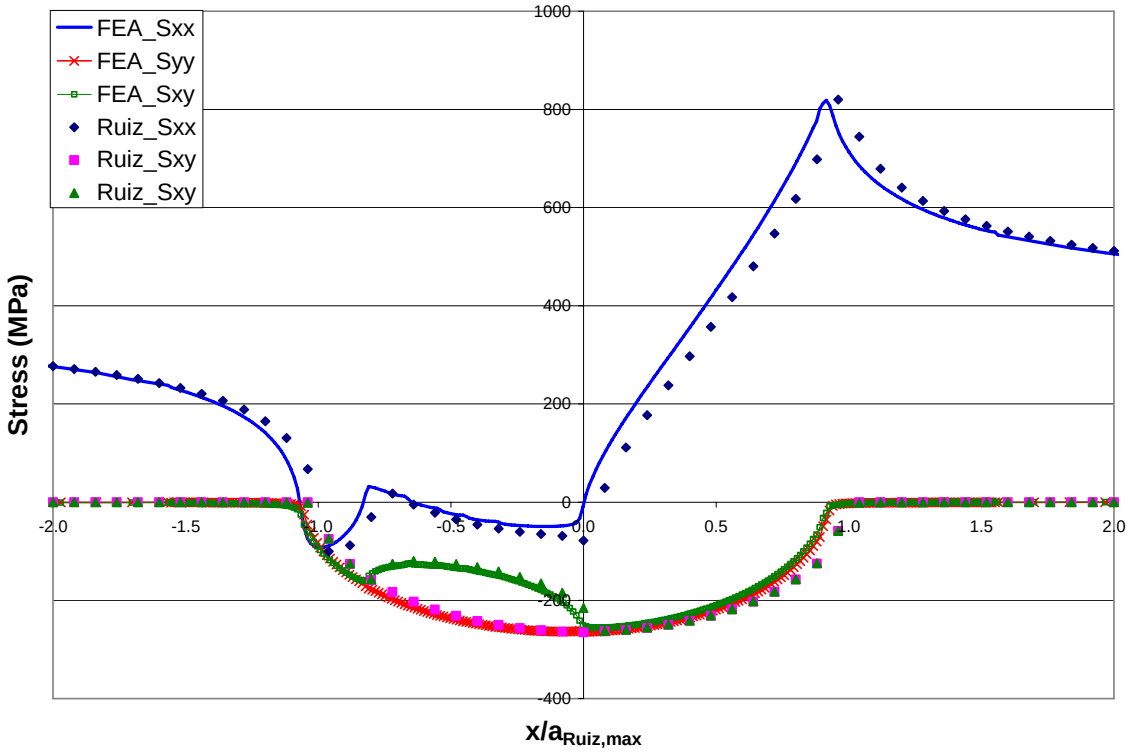

Figure 15. Stress Profile Calculated from FEA and Ruiz Program along Contact Surface at Step 2, Test 13

Note:

Load Condition: σ_{max} =390 MPa, σ_{min} =39 MPa

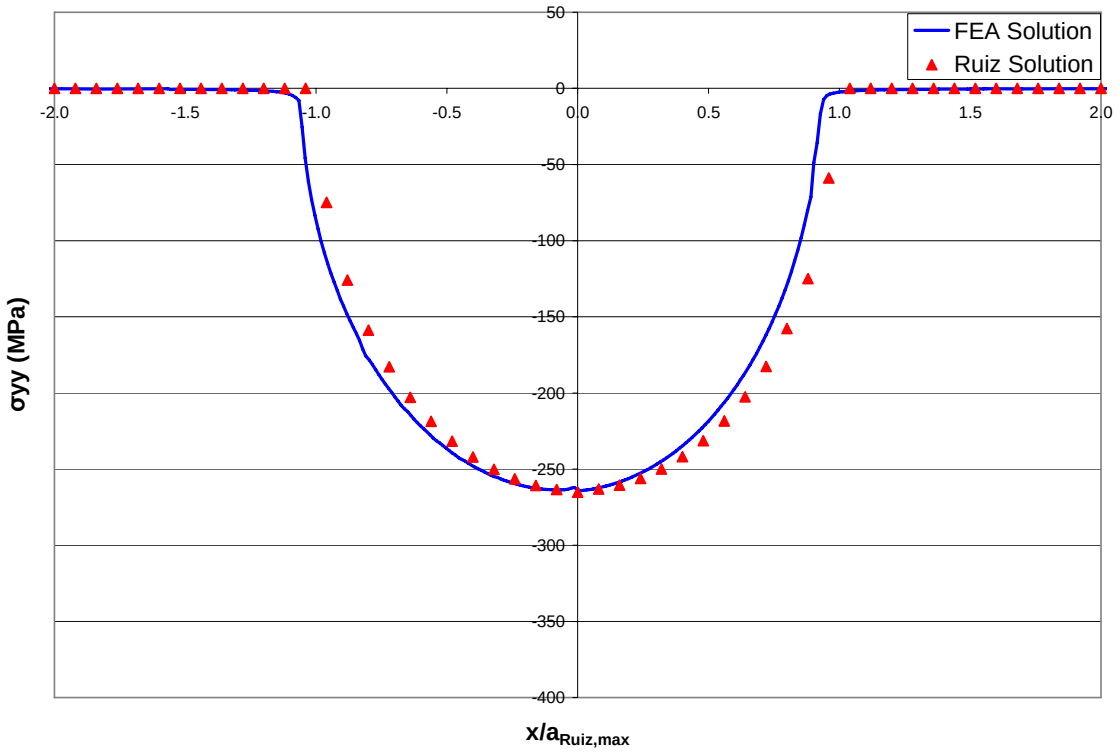

Figure 16. Stress Profile Calculated from FEA and Ruiz Program along Contact Surface at Step 2, Test 13 for Hertzian Peak Pressure

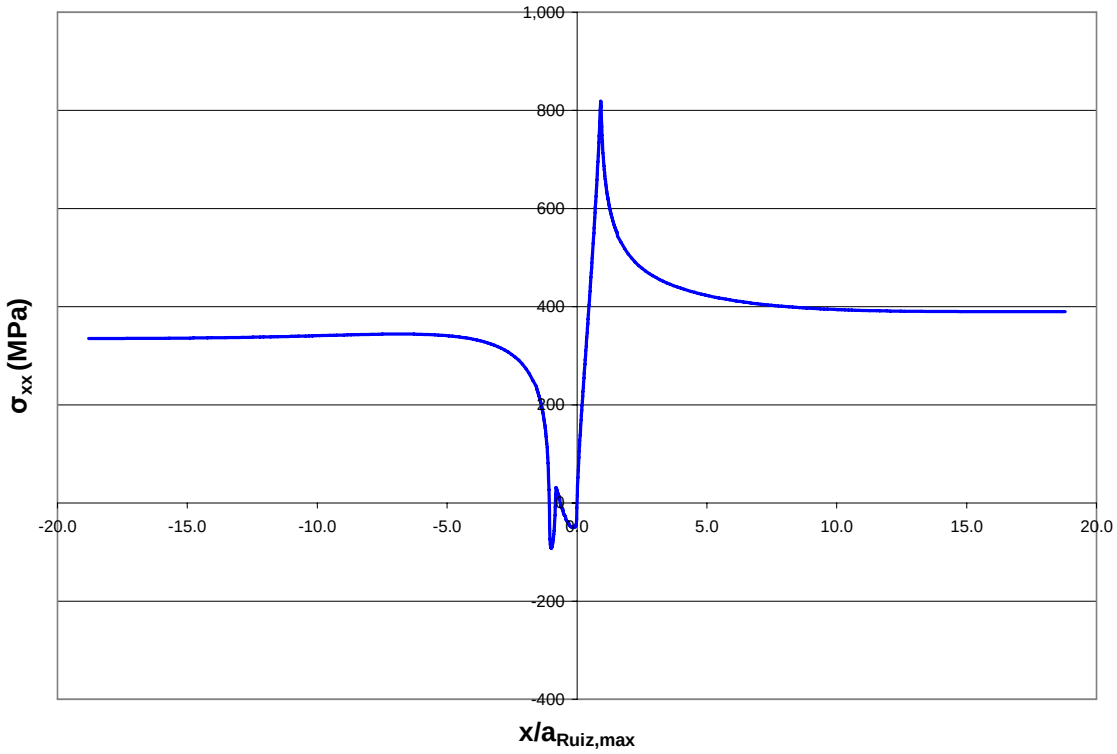

Figure 17. Stress Profile Calculated from FEA for σ_{xx} far away from the Contact Region at Step 2 of Test 13

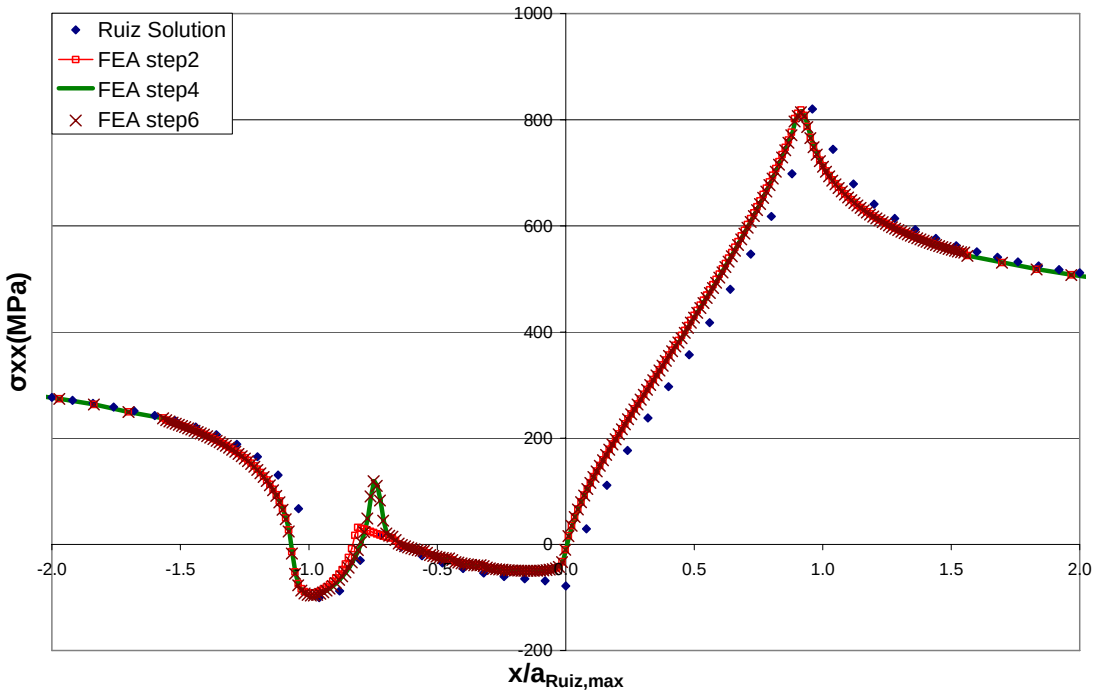

(a) Comparison of σ_{xx} Distribution along Contact Surface from Test 13 at Different Steps

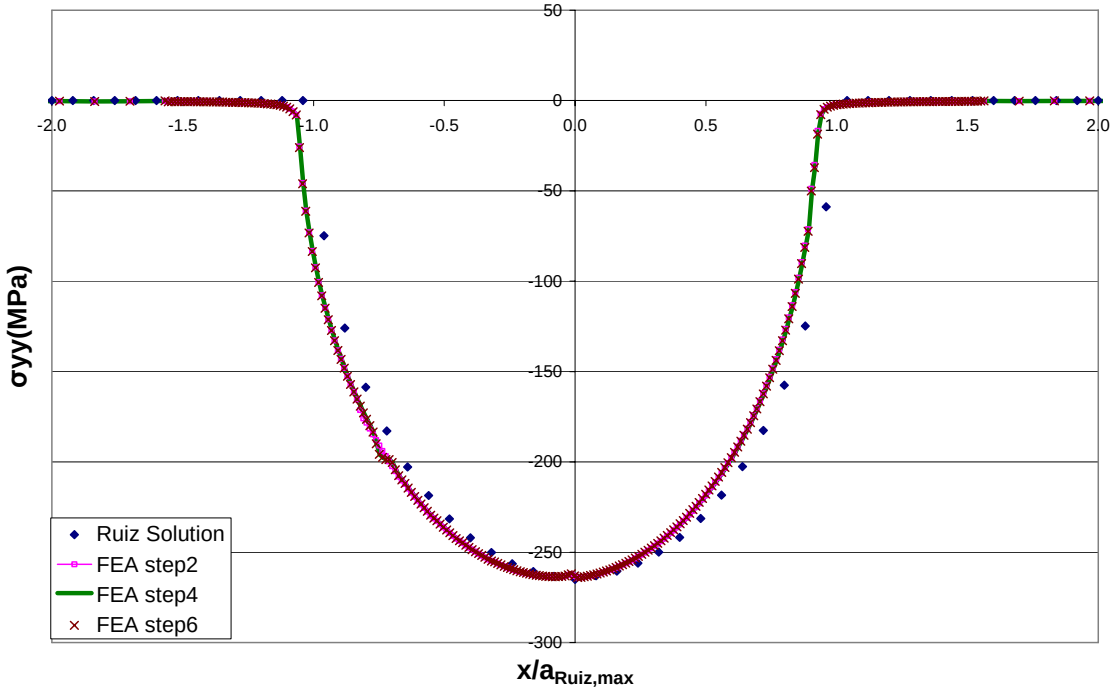

(b) Comparison of σ_{yy} Distribution along Contact Surface from Test 13 at Different Steps

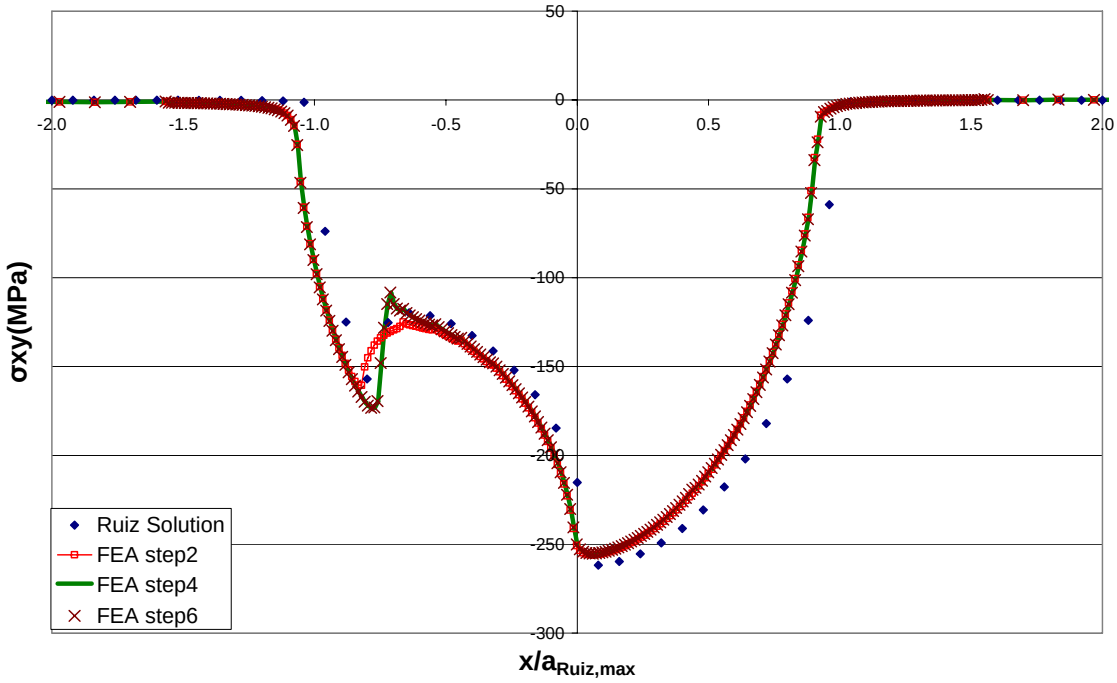

(c) Comparison of σ_{xy} Distribution along Contact Surface from Test 13 at Different Steps

Figure 18. Comparison of Stress Distribution along Contact Surface from Test 13 at Different steps

Note:

Load Condition: σ_{max} =390 MPa, σ_{min} =39 MPa

10A specimen tested at 260 ºC

V. MSSR Analysis

This chapter addresses the MSSR calculation procedure under fretting fatigue configuration. Additionally, the method used in this study to account for shot-peening induced residual stress along with stress relaxation on the MSSR determination for shot-peened specimens is also elaborated.

5.1. MSSR Parameter

Based on the discussion mentioned in Section 2.4.6, the MSSR parameter was the only critical plane-based parameter which was more effective in predicting fretting fatigue life, crack initiation location, and crack initiation orientation simultaneously. Moreover, MSSR can also take into consideration the effects from multiaxial loading and stress concentration at the trailing edge as it should be the case under a fretting fatigue condition. Based on these observations, the MSSR parameter was adopted in this study as the only critical plane-based parameter to be used for predicting fretting fatigue behavior.

The formula defining the fatigue predictive parameter, MSSR, was explained in detail in Section 2.4.6, and it is expressed as Equation (14). In this study, comprehensive MSSR calculation was conducted using FEA stress outputs superimposed with the corresponding residual stress along all planes ranging from $-90^{o} \leq \theta \leq +90^{o}$ in 0.1° increment throughout the whole specimen, where θ is the orientation at which stress state in material is observed. Since two load steps are needed for the determination of MSSR, these two steps among several steps were first computed at the peak and valley of axial loads within the test as illustrated in Figure 14. It was observed that step 4-5 and step 6-7 were almost identical showing a stable condition unlike step 2-3. Therefore the author chose step 4-5 to be analyzed for all tests. After all MSSR between steps 4-5 in a test was

determined it was then analyzed in latter sections by its location, orientation, and correlation with fretting fatigue life under cyclic axial load conditions.

5.2. Residual Stress

For shot-peened specimens, the determination of shot-peening induced residual stress is crucial because this residual stress must be superimposed to FEA stress solutions to carry out the MSSR parameter. Residual stress is considered as a bi-axial stress tensor, that is, $\sigma_{xx} = \sigma_{yy}$ and $\sigma_{xy} = 0$, except at the surface. In addition, residual stress profile can be distinguished into two portions, compressive stress near the peened surface and tensile stress in the interior of specimens after a specific depth. The compressive residual stress profile may be susceptible to shot-peening specifications. Readers can refer to Section 2.2 for a comprehensive discussion on shot-peening process and the nature of the induced residual stress.

In this study with shot-peened specimens, the original compressive stress along the specimen surface was chosen to be -750 MPa for the 4A specimens and -770 MPa for the 10A specimens which is identical to the value obtained from a previous study [11] using X-ray diffraction technique.

5.3. Stress Relaxation

From Martinez study [10], after specimens failed due to fretting fatigue cycles, residual stress within the contact zone was subjected to a complete (100%) relaxation. Additionally, Lee et al. [2,7] found that for specimens shot-peened under 7A100 specification, residual stress relaxation occurred evenly at different depths of specimens. Martinez [10] also observed that for specimens that were shot-peened under 4A100 and 10A100 specifications, these specimens, before failure occurred, were subjected to 20%

and 40% stress relaxation within the contact region after 25,000 and 2 millions fretting fatigue cycles, respectively.

In summary, residual stress within the contact zone relaxed with the increasing fretting fatigue cycles, and the relaxation increased from (0%) relaxation before applying fretting fatigue cycles until a complete (100%) relaxation happened at specimen failure. This relaxation phenomenon occurred evenly at locations with the same depth in a specimen [2]. However, the exact correlation between fretting fatigue cycles and residual stress relaxation rate is still unclear.

In order to investigate the effects from residual stress and stress relaxation on the MSSR parameter, this study used the initial residual stress profile as presented in Figure 19 and assumed stress relaxation occurred uniformly at different depths of specimens. Further, 0%, 50% and 100% stress relaxation were applied during the computation of MSSR, which will be discussed in Chapter VI.

This aforementioned assumption accompanied with uniform relaxation rate at different depths was used to determine the residual stress profile, which was then superimposed to FEA stress solution for MSSR determination. The MSSR calculation results under stress relaxation are discussed in depth in Chapter VI.

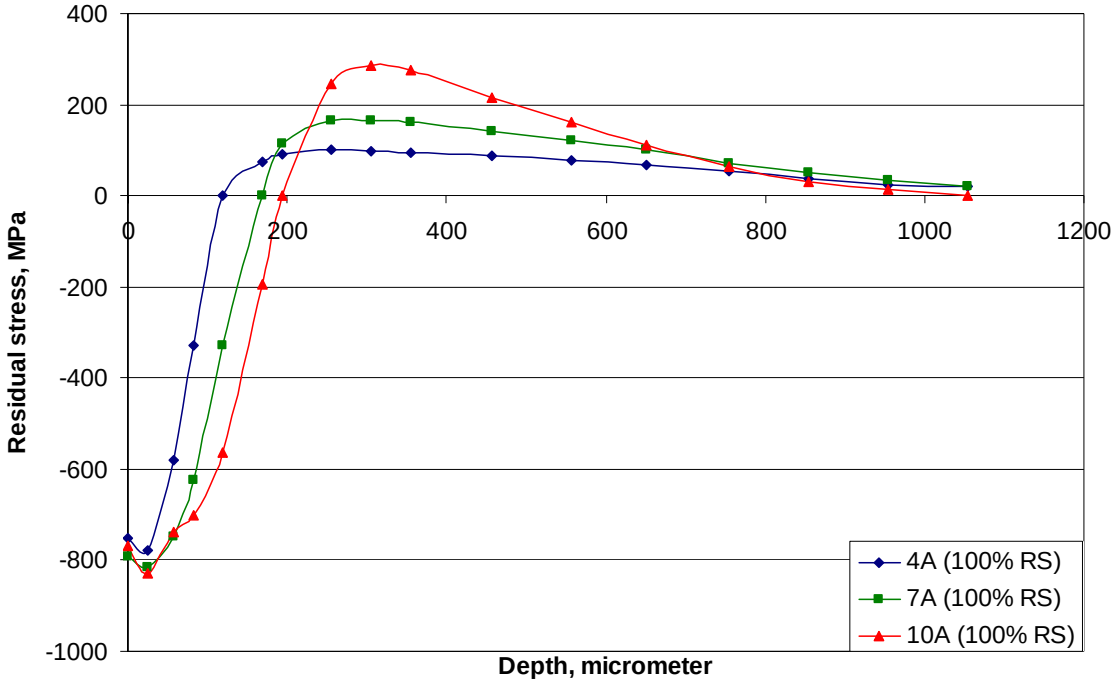

Figure 19. Residual Stress Profile Used in this Study for Shot-peened Specimen [11]

VI. Results and Discussion

This chapter addresses the results from experimental tests, finite element analysis (FEA), and analysis of fatigue life data using a critical plane based fatigue parameter (MSSR). The analysis of fracture surface, crack initiation mechanism, fatigue life, stress solutions from FEA, MSSR prediction, elevated temperature effects, effects of exposure to only and shot-peening intensity effects are also summarized and discussed in this chapter.

6.1. Experimental Tests

Fifteen fretting fatigue tests and four temperature exposure tests were accomplished in this study, and the experimental results for the fretting fatigue tests are summarized in Table 1. It should be mentioned that Table 1 also includes results from earlier studies [1,2,10] for comparison. Among the fretting fatigue tests, nine tests were conducted at elevated temperature 260 ºC and six tests at room temperature conditions.

6.1.1. Determination of Fretting Fatigue Condition

Fretting fatigue conditions were determined using hysteresis loop between a tangential load and an axial load as shown in Figure 20. This figure shows clearly that partial slip fretting condition was met just after a few hundreds of fretting fatigue cycles. Figure 21 shows that after a steady fretting fatigue configuration was fulfilled, tangential loads remained stabilized from the beginning to the very end of a test. Combining Figure 20 and 21 together, it was obvious that for this study, partial slip fretting fatigue condition was met in a few hundreds of fretting fatigue cycles and this was the case until the very end stage of experiments. In other words, steady state fretting fatigue

configuration was quickly met among all tests after relatively few fretting fatigue cycles, and, after that, all fretting variables including coefficient of friction, contact load, tangential load and axial load remained in a stable condition through out the majority of fatigue life until the specimen broke into two pieces.

6.1.2. Q/P Ratio

The Q/P ratio was determined by dividing the tangential load (Q), by the contact load (P). The maximum Q/P, $(Q/P)_{max}$, ratio is considered as the lower boundary of the static coefficient of friction between a fretting specimen and pads in order to prevent gross slip condition. The maximum Q/P ratio for most test was less than 1.0 therefore this value was used as a constant for the finite element model f_{FEA} as shown in Table 1. For some cases where the Q/P exceeded 1.0 a larger value was used to avoid the gross slip condition in the finite element model. Figure 22 illustrates that under fretting fatigue phenomenon, Q/P was proportional to axial load is subjected to variation in value over time. In other words, Q/P was changing dynamically all the time under fretting fatigue tests, but $(Q/P)_{max}$ presented much smaller variation among different tests.

6.1.3. Characteristics of Tangential Load

Typical characteristics of tangential load were presented in Figure 23. The tangential loads always demonstrated as a sinusoidal wave in phase with the corresponding axial load. Also, the frequency of tangential load was always identical to that from axial loads. Contact loads only played a role in affecting the magnitude of tangential loads but had no effect on their waveform, frequency, and phase lag. Figure 23 is also useful in demonstrating the interactions between tangential loads, contact loads, and axial loads. This plot also provided the information about how to

discretize a continuous load condition from experimental tests into discrete load steps for FEA modeling as mentioned before in Figure 14. Comparison between Figure 14 and Figure 23, shows that they both have the same pattern and features in terms of load conditions, and hence the load inputs for FEA model was verified by these experimental outputs.

6.1.4. Fracture Surface

Fracture surfaces of specimens were examined with optical and scanning electron microscopes. The observed fracture topographies presented four distinguishable regions as shown in Figure 24(a); there were debris in Region 1, fine striations in Region 2, large dimples in Region 3, and catastrophic fracture in Region 4. Figure 24(b) explains the pattern observed from region 1, where crack initiated and grew at the early stage. This region is characterized by cleavage facets and oxidized debris which was very obvious due to elevated temperature effect. Region 2, illustrated in Figure 24(c), shows fine striations with grain boundary and was the main region for crack propagation. Large dimples with grain boundary definition were found in Region 3 as presented in Figure 24(d). In Region 4 final unstable crack growth occurred which was characterized by the ductile tearing and shear lip, resulting in catastrophic failure. As seen in Figure 24(a) it was noticed that some small pieces of the material had chipped-off near the contact surface especially in high temperature tests. The author postulates that the reason for that was that the small plastic deformation introduced to the surface by shot-peeing combined by the effect of elevated temperature made the fretting action capable of chipping some small parts of the material off at the crack location.

6.1.5. Fatigue Life, Stress Range and Effective Stress

In order to determine fatigue life for both specimens tested at 260 °C and at room temperature S-N curves were developed using both stress range, Equation (12) and effective stress, Equation (13). Figure 25 was plotted using stress range and Figure 25(a) shows that shot-peening with 4A intensity provides a better life at room temperature than 260 °C. Figure 25(b) shows the same trend as the previous graph for the 7A specimen which was taken from a previous study [2]. Figure 25(c) shows the effect of 10A intensity which also follows the trend of the previous two cases. It is interesting to note that elevated temperature 260 °C significantly reduced fatigue life for all three different shot-peening intensities i.e. 4A, 7A and 10A. Figures 26(a) to (c) was plotted using effective stress and shows the same trend as Figure 25. Figure 27(a) was plotted to examine the effect of elevated temperature 260 °C alone on all three shot-peening intensities. It was clear that all the data fell within a scatter band. The author concluded that elevated temperature negated the effect of shot-peening. The reason for this behavior was the stress relaxation phenomenon which will be discussed in later sections. Figure 27(b) compares fatigue life N_f for all three shot-peening intensities at 260 °C at different stress levels $\Delta\sigma$. It's interesting to note that fatigue life at stress range higher than 400 MPa falls within a scatter band and fatigue life under stress range of 400 MPa had a trend but the difference between data points was within a factor of two which is common scatter in fretting fatigue. Figure 27(c) compares fatigue life N_f for all three shot-peening intensities at 260 °C to data from previous studies [1,6] for unpeened specimens at room and elevated temperature 260 °C. It was noticed that elevated temperature lead to shot-peened specimens to behave in a similar way to unpeened specimens at both room and

elevated temperatures. Figure 27(d) compares the effect of different shot-peening intensity specimens 4A, 7A and 10A to their fatigue life N_f at room temperature. The 10A specimen provided the longest fatigue life. In comparing all three cases at room temperature it was noticed that even though 10A provided the longest fatigue life, all three cases fell with a scatter band all extended the fatigue life when compared to the unpeened case Figure 27 (e). Further the 7A specimen seemed to be close or even provided a slightly lower fatigue life that the 4A specimen. The author postulates that the reason for that was that 7A specimens' data were taken from a previous study [2] which reported the maximum residual stress at the surface to be about -600 MPa which was relatively lower than the values -750 MP and -770 MPa for the 4A and 10A specimens used in this study respectively. In summary, experimental data at room temperature for different shot-peening intensity 4A, 7A and 10A show no clear distinction between fatigue life and shot-peening intensity level. All three shot-peening intensities 4A, 7A and 10A provided extension to fatigue life. It was also noticed that the amount of residual stress at the surface was the main factor contributing to fatigue life which was about the same for all three shot-peeing intensities. On the other hand the amount and location of the compensatory tensile stress which was different in all the three shot-peening cases had no noticeable effect on fatigue life at elevated temperature, since the crack initiated at the contact surface in all cases.

6.1.6. Contact Half-Width

A typical scar pattern is illustrated in Figure 28. This photograph shows clearly a stick zone with partial slip regions aside just as the deformed contact model demonstrated in Figure 4. A contact region, termed as $2a_{Exp,max}$ was defined by incorporating both the

stick zone and partial slip regions. Contact half-widths from the Ruiz program and experimental measurements had a good agreement for example from Test 2 $2a_{Exp,max}$ = 8.42E-4 m and $2a_{Ruiz,max}$ = 10.14E-4 with 17% difference between them. These measurements also confirmed that contact half-widths were only affected by the magnitude of the constant contact load and independent upon the axial load conditions as predicted by equation (35).

6.1.7. Crack Initiation Location and Pattern

In general, crack initiation location in all tests, as shown in Figure 29, always occurred at the trailing edge, at a location where $x/a_{Exp,max} \approx +1$ along x-direction. For both specimens 4A and 10A at elevated temperature, the crack always initiated at the contact surface as demonstrated in Figure 30 and Figure 31. In Lee's study [2] of the 7A specimen tested at elevated temperatures, it was found that the crack always initiated at the surface as well. In room temperature 4A and 7A specimens had cracks initiated at the contact surface and the 10A specimens cracks initiated away from the surface [1,10].

6.1.8. Crack orientation

In a previous study [1] of a 7A shot-peened specimen tested at room temperature, the orientation of crack initiation ranged from -37° to -54° and was reported that crack orientation for shot-peened specimens could fall within the angle 45°± 15°. The author in this study was interested in determining crack orientation for shot-peened specimens tested under elevated temperature conditions. Crack initiated in the surface of both 4A and 10A shot-peened specimens and the 10A specimen was selected to investigate crack initiation orientation. Photographs from scanning electron microscopy presented in Figure 32 shows that crack initiation orientation was at -55˚ for the 10A specimen tested

at elevated temperature 260° C. Comparing these observations to previous results, elevated temperature and shot-peening intensity didn't make a difference in crack initiation orientation.

6.1.9. Stress relaxation due to temperature exposure only

Figure 33 shows the effect of temperature on residual stress at the contact surface of 4A, 7A and 10A specimens which were exposed to a temperature of 260° C for 2 and 24 hrs in ambient atmosphere. These tests were run to isolate the effect of temperature exposure only from that of fretting fatigue. Data for the 7A specimens are taken from an earlier study [7]. The magnitude of surface residual stress is expressed as a percent value of the initial residual stress from untested specimens. It was observed that different shot-peened intensities 4A, 7A and 10A behaved almost the same way under temperature exposure. Further, about 30% of residual stress was relaxed in the first 2 hrs and slightly more than that after 24 hrs. Thus, it can be concluded that residual stress of the 4A, 7A and 10A specimens all relaxed with the same amount due to thermal exposure at 260 °C.

6.1.10. Residual stress relaxation along contact surface

Percentage of residual stress normalized by initial residual stress (i.e. before fretting test) profile along the contact surface of the one half of a failed 4A specimen fatigued at elevated 260 °C is shown in Figure 34. The applied stress range was 400 MPa and failure occurred at 108,065 cycles. Measurements of residual stress were taken near the center of the specimen ±5 mm of the fretting region. The one half of the failed specimen with the scar clearly observes see Figures 28 and 29 was measured using X-ray diffraction method. The maximum stress relaxation occurred at the contact surface and was about 55% of initial residual stress. It was also noticed that regions away from the

scar relaxed and the relaxation was about 25-30%. The contact region experienced both mechanical and thermal effects that influenced the residual stress relaxation. On the other hand regions away from the contact surface i.e. 1.5 mm and further were mainly affected by thermal relaxation. This is in close agreement with results found in Section 6.1.9 and with results found by Lee [2,7].

Figure 35 shows a comparison of residual stress relaxation behavior on the contact surface at room temperature for 4A, 7A and 10A [11] and elevated temperature 260° C from this study, which is expressed in the terms of the normalized residual stress as a function of normalized fretting fatigue cycle. The normalization is done here by an initial value of the measured residual stress i.e. before applying the fretting fatigue and by the fatigue life N_f. Tests were run at one location to different percentages of their expected life. Then the test was stopped and run again at a different location till failure accrued and the specimen split in to two parts. Examining Figure 35 it is noticed that the data points developed for the 4A and 10A specimens tested at elevated temperature lie within a scatter band with the 4A, 7A and 10A data tested at room temperature. It was also observed that by the specimens reaching 50% of their expected fatigue life 50 to 60% of initial residual stress relaxed. Thus, it could be concluded that mechanical loads i.e. fretting fatigue caused residual stress relaxation, the higher the loads applied the grater amount of relaxation could occur. Thermal loads at 260 °C caused residual stress relaxation and at longer exposure time a greater amount of relaxation will occur. At failure, crack location experience full relaxation, where the scar will have some residual stress remaining.

6.2. Finite Element Analyses

With load details discussed in Section 4.3, the measured experimental load values shown in Table 1 were applied to FEA model to compute stress, strain, and displacement distribution within a whole specimen. The issues addressed in this section include modulus of elasticity effect on FEA solutions, σ_{xx} stress concentration, asymmetric distribution of σ_{yy}, evolution of stress state at different depths within the specimen, and the influence of residual stress on stress profile.

6.2.1. Variation of σ_{xx}, σ_{yy} and σ_{xy}

In a previous study investigation of temperature effects in experiments showed no difference between the FEA model run at room temperature and 260 °C [6]. The reason for that was the fact that specimens were heated first before applying any load required to conduct fretting fatigue tests and all loads, used in analysis, were measured after the specimen achieved the test temperature of 260 °C. Due to that, all FEA computations were conducted without applying temperature to the model except for material properties at 260 °C. Figure 35 shows the variation of $\sigma_{xx,}$ σ_{yy} and σ_{xy} of specimens at room temperature (using 125 GPA of elastic modulus) and at 260 °C (using 95 GPa of elastic modulus) along the contact surface in the x-direction. The maximum value of σ_{xx} can be found at the trailing edge, around 0.4-0.47 mm of x in both cases. These increased stresses from the applied stress, 390 MPa, at the trailing edge contributed to the reduction of fatigue life during fretting fatigue. The specimen tested at room temperature showed a slightly higher maximum value of σ_{xx} about 879 MPa at the trailing edge versus 816 for the 260 °C condition but the difference was not significant. For σ_{yy} the specimen tested at

room temperature showed a slight higher maximum value of σ_{yy} about -302 MPa versus -263 MPa for the 260 °C condition and the value for σ_{xy} for the specimen tested at room temperature also showed a slight higher maximum value of σ_{xy} about -288 MPa versus -252 MPa for the 260 °C condition but the differences were not significant.

6.2.2. Stress Profile with Residual stress

In the following and rest of the text residual stress of untested specimen with 100% residual stress (i.e. no relaxation) will be referred to as (100%RS), specimen with half of their residual stress relaxed will be referred to a (50%RS) and specimen with their residual stress fully relaxed will be referred to as (0%RS).

Figure 37 presents stress profiles at different depths for a shot-peened specimen at Step 4 of Test 2 with 0%RS, which is identical to a case of an unpeened specimen. Figure 36(a) shows variation of σ_{xx} at 260 °C for five different depths from the contact surface. As depth increased, σ_{xx} at the trailing edge decreased and the σ_{xx} profile became flattened. The corresponding distribution for σ_{yy} and σ_{xy} are shown in From Figure 36(b) and 36(c). To investigate the effect of residual stress on stress state in the contact region during fretting, residual stress profiles in Figure 18 were superimposed on the calculated stress from FEA.

The influence on stress profiles from stress relaxation on contact surface at Step 4 of Test 2 is illustrated in Figure 38. This Figure show maximum σ_{xx} decreased from 976 MPa at $x/a_{Ruiz,max} = 0.93$ under 0%RS, to 611 MPa at the same $x/a_{Ruiz,max}$ location under 50%RS, to 236 MPa at the same $x/a_{Ruiz,max}$ location under 100%RS. Hertzian peak pressure was also lowered from -265 MPa at $x/a_{Ruiz,max} = -0.048$ under 0%RS, to -640 MPa at the same $x/a_{Ruiz,max}$ location under 50%RS, to -1015 MPa at the same $x/a_{Ruiz,max}$

location under 100%RS. No effect on σ_{xy} stress distribution from stress relaxations was found as expected since residual stress was assumed as bi-axial distribution, $\sigma_{xx} = \sigma_{yy}$ and $\tau_{xy=0}$, and resulted in no contribution on σ_{xy} stress profile.

At a depth of 256 μm below the contact surface which is the location of the maximum compensatory tensile stress for the 4A specimens as shown in Figure 19, the influence on stress profiles with different amount of stress relaxations is demonstrated in Figure 39. The maximum σ_{xx} increased from 626 MPa at $x/a_{Ruiz,max} = 1.6$ under 0% RS, to 676 MPa at the same $x/a_{Ruiz,max}$ location under 50%RS, to 726 MPa at the same $x/a_{Ruiz,max}$ location unchanged under 100%RS. Hertzian peak pressure also increased from -271 MPa at $x/a_{Ruiz,max} = -0.24$ under 0%RS, to -220 MPa at the same $x/a_{Ruiz,max}$ location under 50%RS, to -171 MPa at the same $x/a_{Ruiz,max}$ location under 100%RS. No effect on σ_{xy} stress profile from different relaxation rates was noticed just like the case observed along contact surface.

On comparison of stress profiles on the contact surface without residual stress 0%RS to those at a depth of 256 μm, maximum σ_{xx} reduced from 976 MPa to 627 MPa, see Figure 37(a) and Figure 38(a). Also, the gradient of σ_{xx} stress profile became flat with the increasing depth. On the other hand, comparing the stress profiles on the contact surface with 50%RS to those at a depth of 256 μm, maximum σ_{xx} increases from 611 MPa to 675 MPa but the difference is not significant; see Figure 37(a) and Figure 38(a). However, when taking stress profiles under 100%RS into account, maximum σ_{xx} raised from 234 MPa along contact surface to 725 MPa at the depth of 256 μm due to the residual compressive stress near the contact surface and tensile stress within the interior of the specimen. It is clear that different amount of stress relaxation changes the location

of the maximum value of σ_{xx}, and hence changing the crack initiation location. At 50%RS the possibility of crack initiation is nearly equal at or near contact surface and inside the specimen. As more and more relaxation occurs, the location of the crack initiation will move towards the contact surface.

6.3. MSSR

MSSR calculation was conducted in this study for all testes at surface and subsurface locations and the maximum MSSR for each test was then determined. The correlation between MSSR fretting fatigue life was investigated, and the effects from stress relaxations are also discussed. The effectiveness of MSSR was looked into in terms of fatigue life, crack initiation location and orientation.

6.3.1. Determination of the Maximum MSSR

The fatigue predictive parameter, MSSR, was defined in Equation (14), and a detailed discussion for MSSR is presented in Section 2.4.6. As mentioned in Section 5.1, the values of MSSR parameter were symmetric with respect to a full load cycle. In addition, two load steps were needed for the MSSR determination. In this study, the peak and valley of axial loads were sampled and numbered into discrete steps as shown in Figure 14. The stable steps 4-5 as shown earlier were chosen to determine the MSSR parameter in this study. Among them, the MSSR with the greatest value was chosen as the maximum MSSR of that test and is further summarized in Table 2.

6.3.2. MSSR under Residual Stress Relaxation

It should be mentioned that full relaxation is equivalent to 0% residual stress imposed, which defines a condition where no residual stress is imposed into stress and MSSR calculation, this will be referred to as 0%RS. The maximum MSSR with (0%RS)

had the highest value. Once residual stress other than 0% was imposed, which was 50% and 100% in this study, the MSSR parameter varied in depth. These will be referred to as 50%RS and 100%RS, respectively. Figure 40 (a and b) compares MSSR versus depth for 4A specimen tested at room temperature and 260 °C. In both cases once residual stress other than 0% was imposed, the maximum MSSR always occurred at the contact surface for both room temperature and 260 °C. Figure 41 (a and b) compares MSSR versus depth for 7A specimen tested at room temperature and 260 °C. In both cases once residual stress other than 0% was imposed, the maximum MSSR also occurred at the surface for both room temperature and 260° C [2]. Figure 42 (a and b) compares MSSR versus depth for 10A specimen tested at room temperature and 260 °C. It was noticed that at room temperature and with 100%RS imposed the maximum MSSR could either occur at the surface or at a depth of 306 μm. It was also noticed that at room temperature and with 50%RS imposed maximum MSSR always occurred at the surface. On the other hand, at 260 °C maximum MSSR for the 10A specimen always occurred on the surface for all cases.

6.3.3. Crack Initiation Details

All elevated temperature tests showed crack initiation at the surface experimentally for the 4A and 10A specimens from this study and the 7A specimen tested at 260 °C also showed surface crack initiation as reported from a previous study [2]. In a previous study at room temperature [3] the 4A and 10A specimens showed surface and subsurface initiation respectively and 7A specimen tested at room temperature showed surface crack initiation [2]. The maximum MSSR with different residual stress condition discussed in section 6.3.3. verifies experimental results. For the 4A specimen tested at

room and 260° C maximum MSSR and crack location occurred at the surface for all residual stress cases. For the 7A specimen tested at room and 260° C maximum MSSR and crack location occurs at the surface for all residual stress cases [2].

For the 10A specimen tested at room temperature maximum MSSR with 100%RS could occur either at the surface or at a depth of 306 μm, experiments showed subsurface crack initiation 200~300 μm. With 50%RS maximum MSSR occurred at the surface this implies that not enough residual stress relaxation occurred in the 10A specimen tested at room temperature to shift the crack initiation from subsurface to surface location. For the 10A specimen tested at 260° C maximum MSSR and crack location occurred at the surface for all residual stress cases.

MSSR predictions for crack initiation locations and orientations are summarized in Table 2. For example in Test 4 the maximum MSSR was found near the trailing edge at locations where $x/a_{Ruiz,max} = 0.92$, comparing that to experimental result $x/a_{Exp} = 0.83$ the values are close with 10% difference between them. Another example was MSSR prediction of crack orientation in Test 13 were the angel was 37.5˚ which is close to its experimental counterpart result $\theta = 35$˚ shown in Figure 31 with 2.5˚ difference between them. It can be seen that the MSSR parameter was good in predicting the crack initiation location, and orientation.

6.3.4. Fatigue Life

Figure 43 (a, b and c) shows a comparison between the MSSR versus fatigue life N_f relationships for 4A specimens at room temperature and 260° C with different residual stress percentages (0%RS, 50%RS and 100%RS). MSSR data collapsed into two separate curves clearly indicating a better fatigue life N_f from the room temperature condition.

Over all, MSSR data shown in Figure 42 for the three limiting cases on the MSSR parameter have an appropriate trend. Figure 43 (a, b and c) shows a comparison between the MSSR versus fatigue life N_f relationships for 7A specimens at room temperature and 260° C with different residual stress percentages (0%RS, 50%RS and 100%RS). MSSR data collapsed into two separate curves clearly indicating a better fatigue life N_f at the room temperature condition. Over all, MSSR data shown in Figure 43 for the three limiting cases on the MSSR parameter have an appropriate trend. Figure 44 (a, b and c) shows a comparison between the MSSR versus fatigue life N_f relationships for 10A specimens at room temperature and 260° C with different residual stress percentages (0%RS, 50%RS and 100%RS). MSSR data collapsed into two separate curves clearly indicating a better fatigue life N_f at the room temperature condition. Over all, MSSR data shown in Figure 44 for the three limiting cases on the MSSR parameter have an appropriate trend.

Figure 45 (a, b and c) shows a comparison between the MSSR versus fatigue life N_f relationships for 4A, 7A and 10A specimens at room temperature and 260° C with different residual stress percentages (0%RS, 50%RS and 100%RS). MSSR data collapsed into two separate curves clearly indicating a better fatigue life N_f at the room temperature condition. Over all, MSSR data shown in Figure 45 for the three limiting cases on the MSSR parameter have an appropriate trend. All MSSR data fell within a scatter in a behavior similar to experimental results with MSSR data collapsed well within the scatter band. It is clear that elevated temperature negated the effect of shot-preening for all three intensities. Further, all shot-preening intensity provided an improvement to life within the scatter band, with the 10A providing a slightly better fatigue life that 4A and 7A.

Figure 45 (e) shows a comparison between the MSSR versus fatigue life N_f relationships for 4A, 7A and 10A specimens at room temperature and 260° C with different residual stress percentages. Specimen tested at room temperature were imposed with 50%RS as a representation of relaxation at room temperature. Specimen tested at elevated temperature were imposed with 0%RS as a representation of full relaxation at 260° C. It is interesting to note that data fell within the scatter band indicating that MSSR is an effective predictive tool.

Investigating crack initiation under these conditions from Figures (40, 41 and 42) it was noticed for the 4A specimen tested at room temperature with 50%RS shown in Figure 40 and the 4A specimen tested at 260° C with 0%RS, maximum MSSR always occurred on the contact surface, which is in agreement with surface crack initiation found from experiments. For the 7A specimen tested at room temperature with 50%RS shown in Figure 41 and the 7A specimen tested at 260° C with 0%RS, maximum MSSR occurred on the contact surface, which is in agreement with surface crack initiation found from experiments. Investigating the 10A specimen tested at room temperature with 50%RS shown in Figure 42. Although maximum MSSR occurred at the contact surface with a value of 32 MPa^0.5, the MSSR value at 300 μm was 27MPA^0.5, the values are relatively close which makes the crack initiation possible at both these locations. Experiments showed subsurface crack initiation at a depth of 200~300 μm. For the 10A specimen tested at 260° C with 0%RS, maximum MSSR occurred at the contact surface, which is in agreement with surface crack initiation found from experiments.

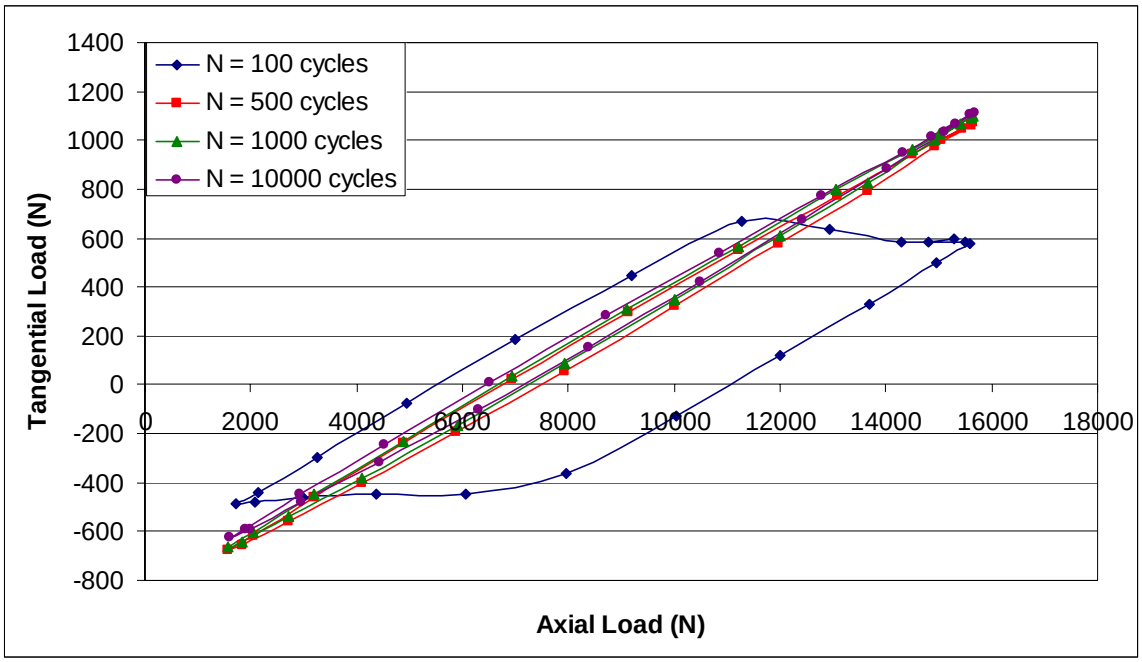

Figure 20. Typical Hysteresis Loop of Tangential Load vs. Axial Load (Test 4)

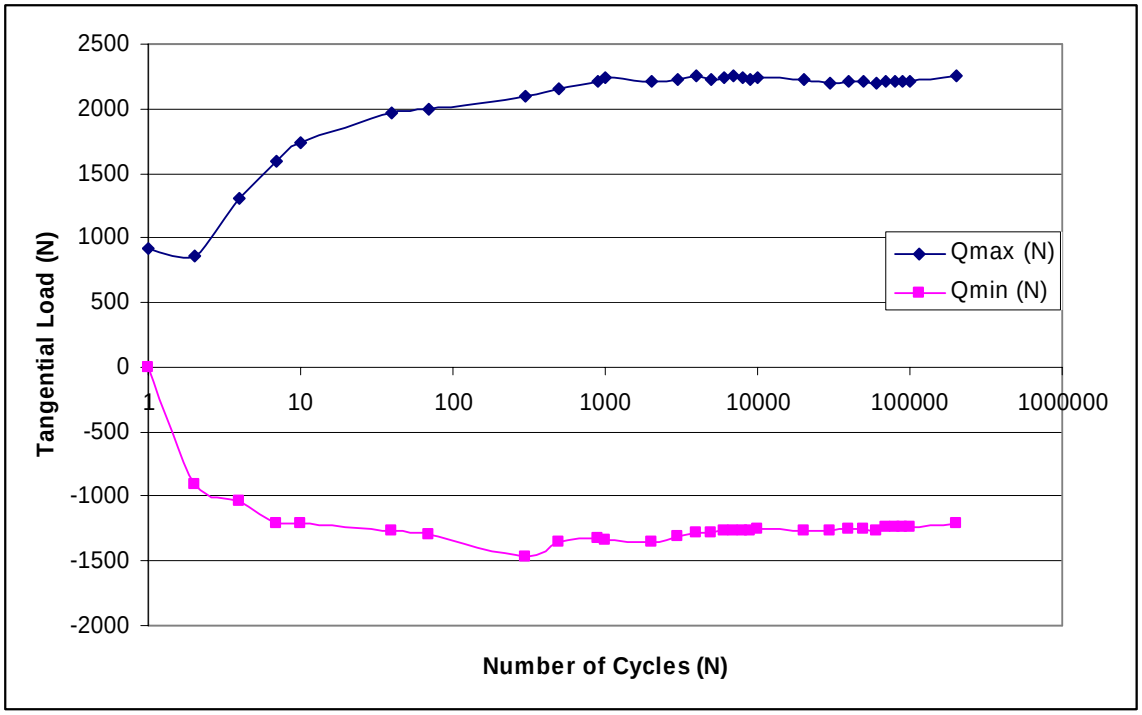

Figure 21. Qmax & Qmin vs. N (Number of Cycles)

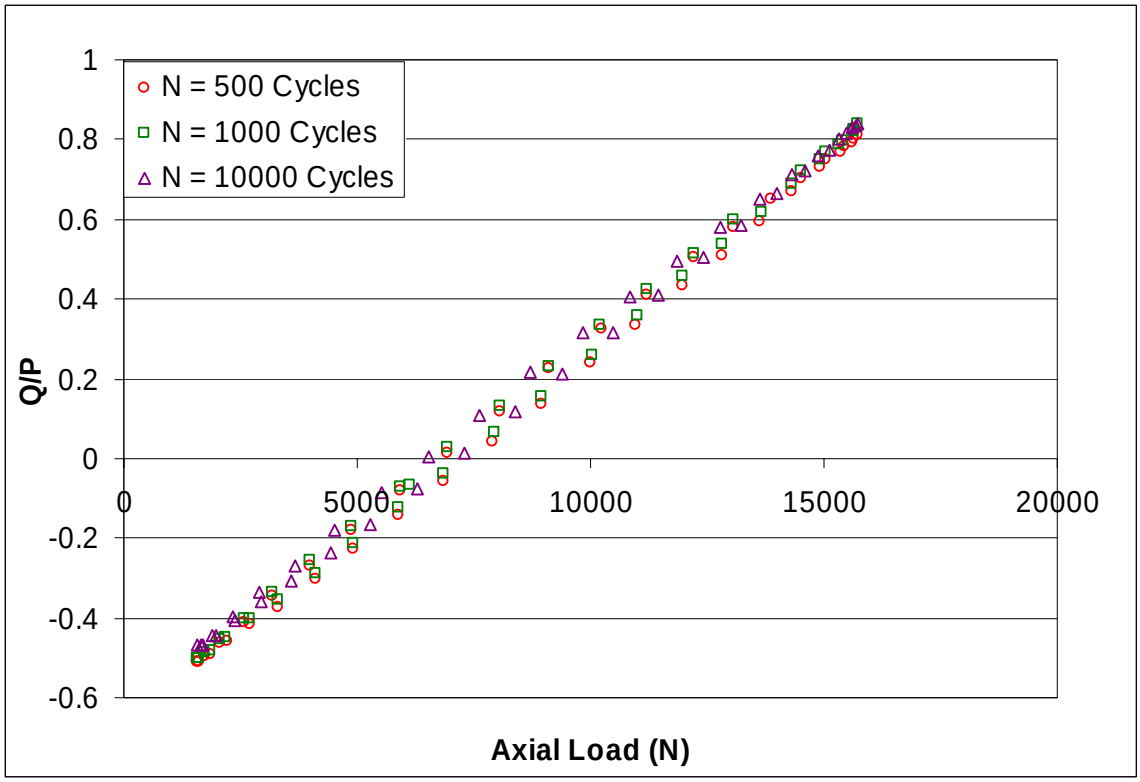

(a) Q/P vs. Axial Load

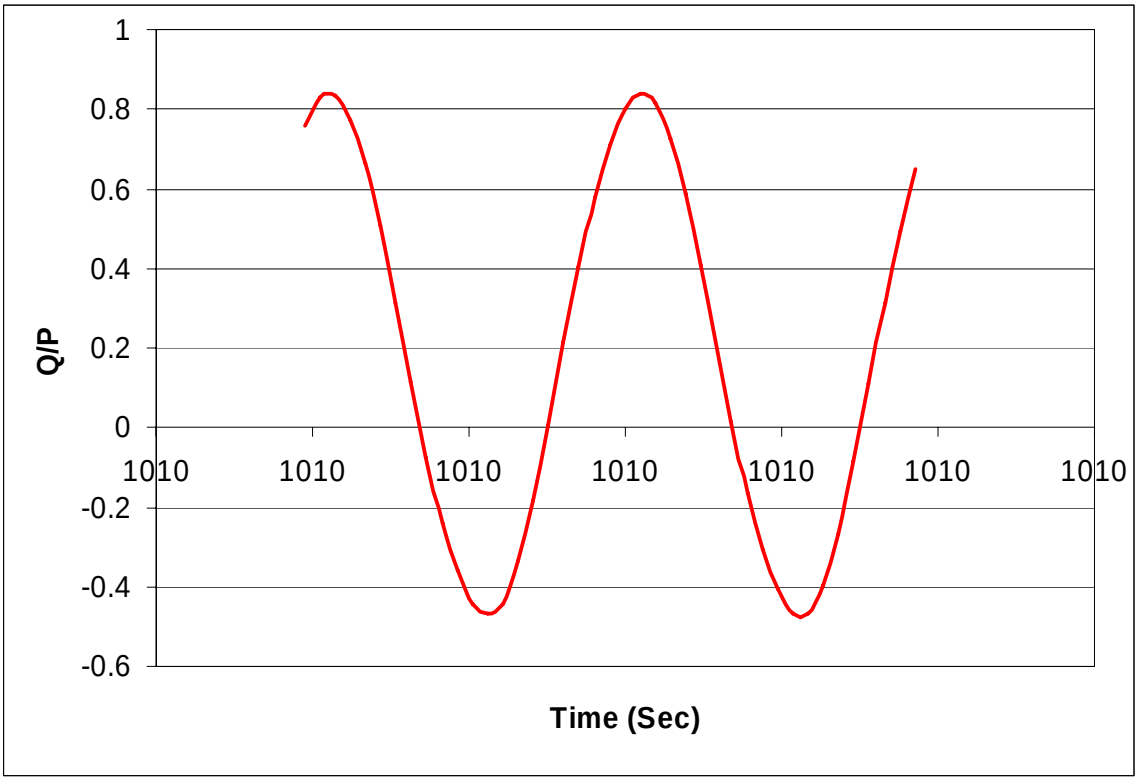

(b) Q/P vs. Time at 10,000th Cycle

Figure 22. Q/P Ratio for Test 4

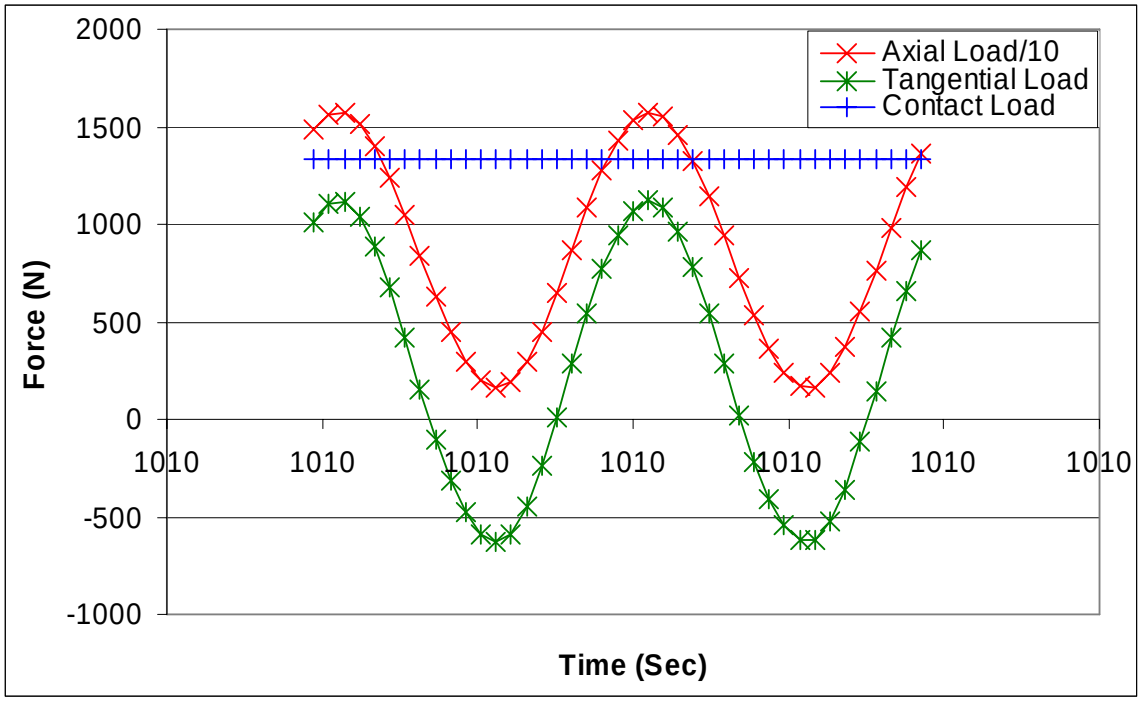

Figure 23. Relations among Axial Load, Contact Load, Tangential Load at 10,000th Cycles (Test 4)

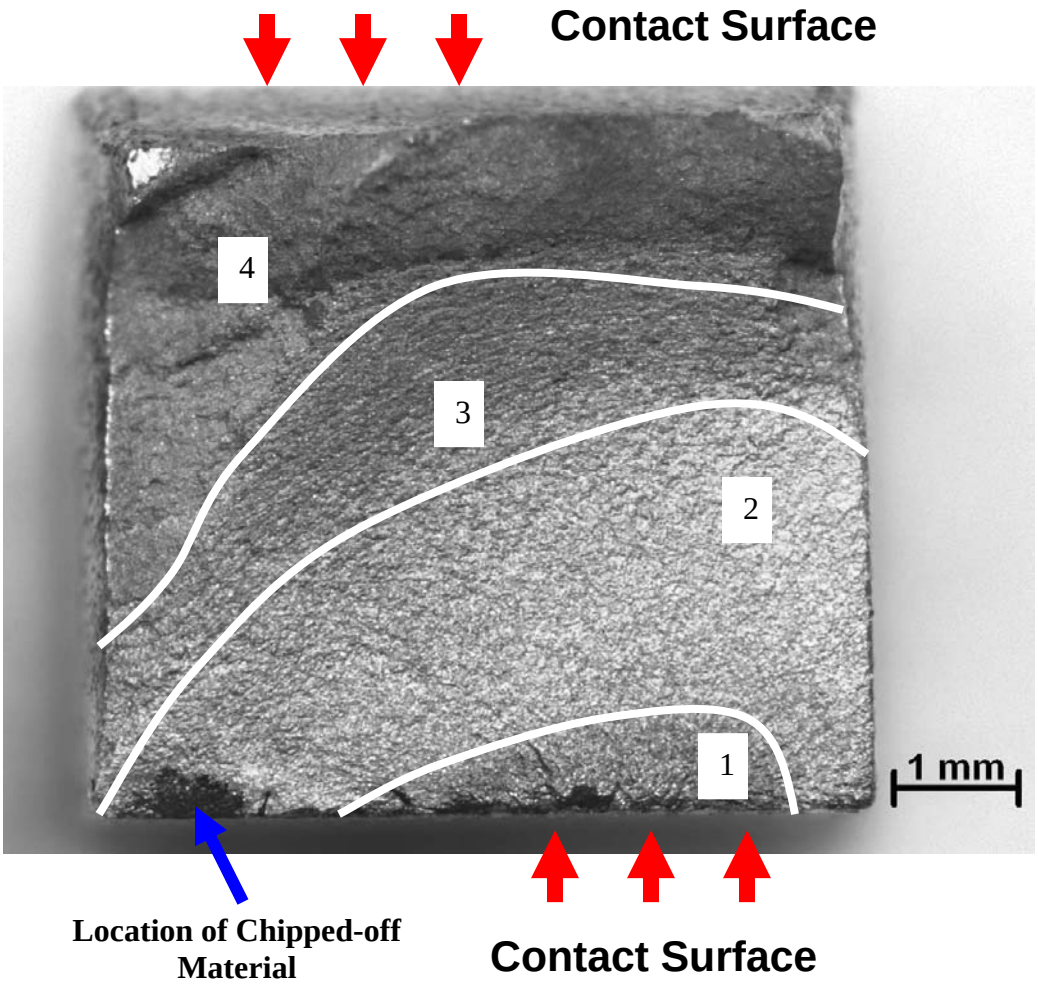

(a) Typical Fracture Surface with Four Distinguishable Regions

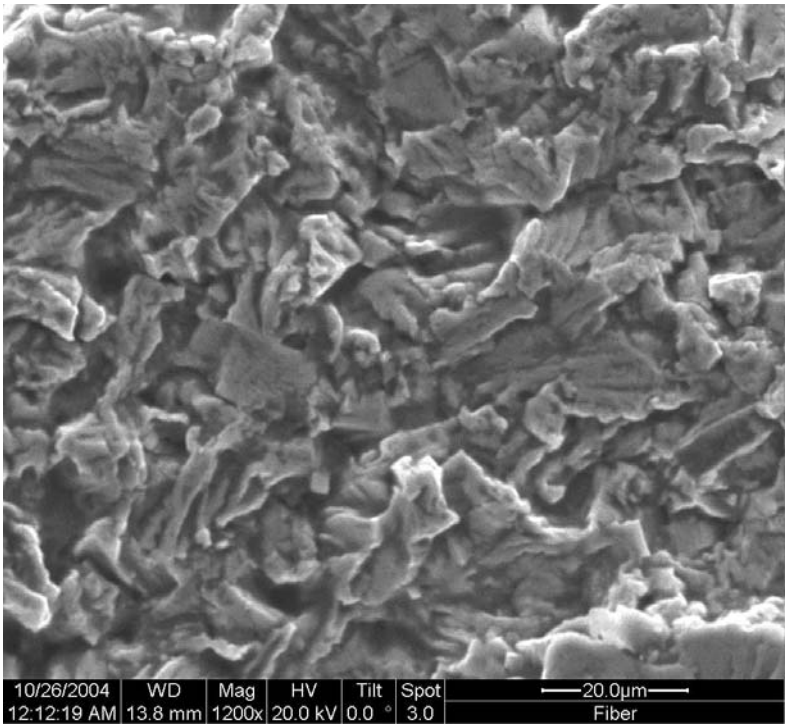

(b) Debris and Cleavage Facets at Region 1

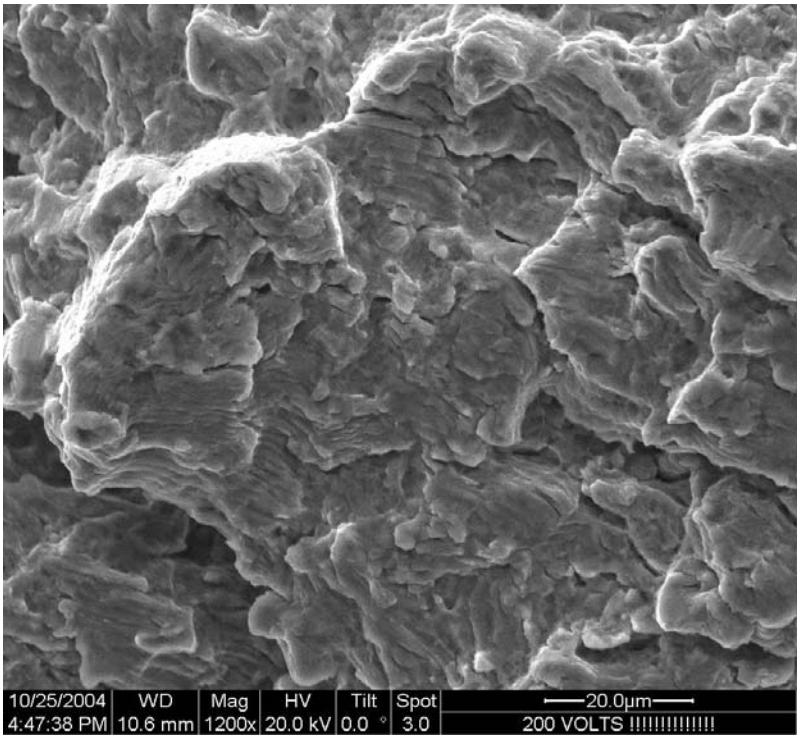

(c) Fine Striations at Region 2

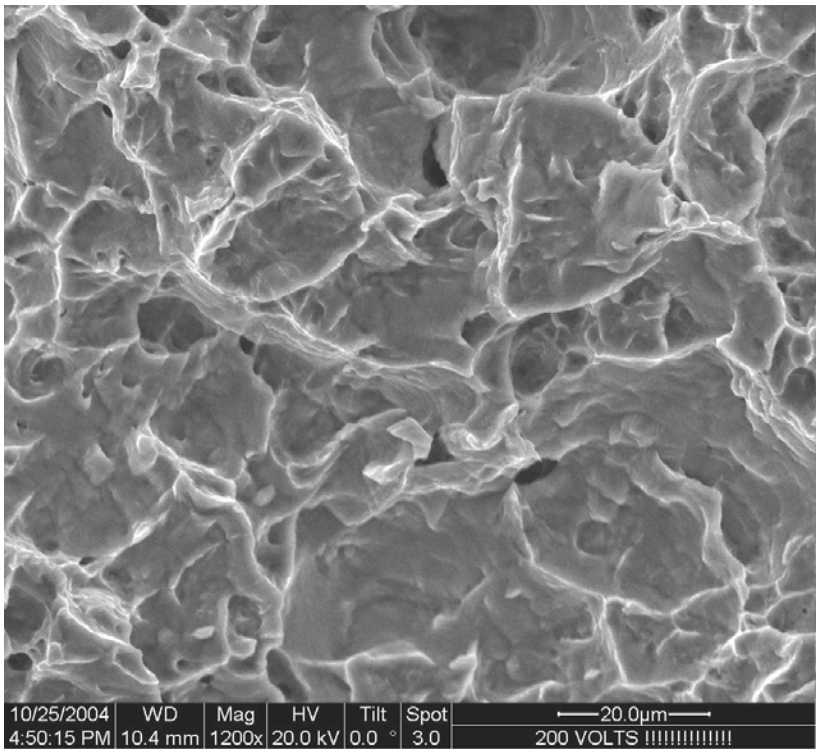

(d) Large Dimples at Region 3

Figure 24. Fracture Surface for Test 4

Load Condition: σ_{max} =390 MPa, σ_{min} =39 MPa

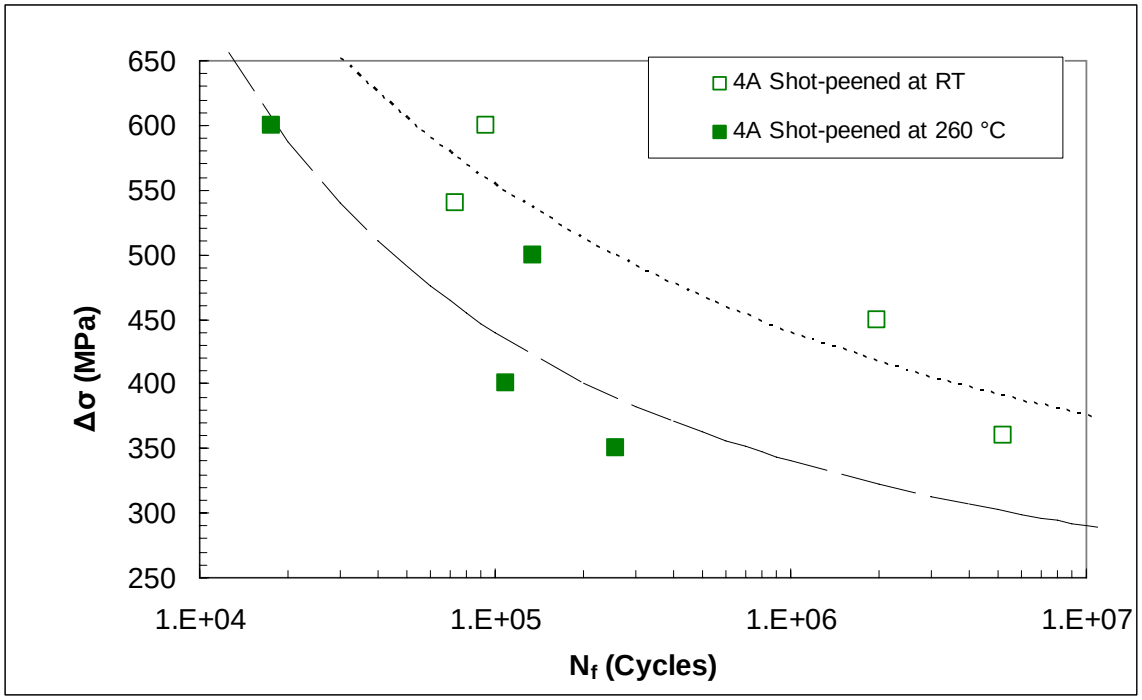

(a) Stress range versus Cycles to failure at 260 °C and room temperatures for 4A specimens.

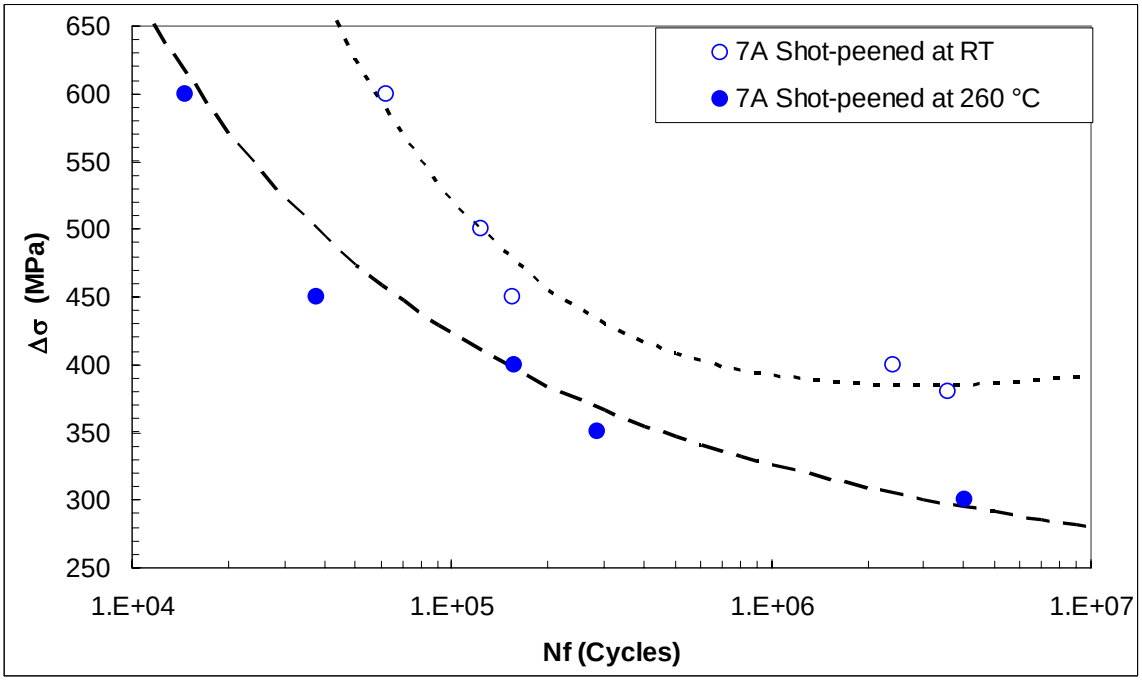

(b) Stress range versus Cycles to failure at 260 °C and room temperatures for 7A specimens from a previous study [2].

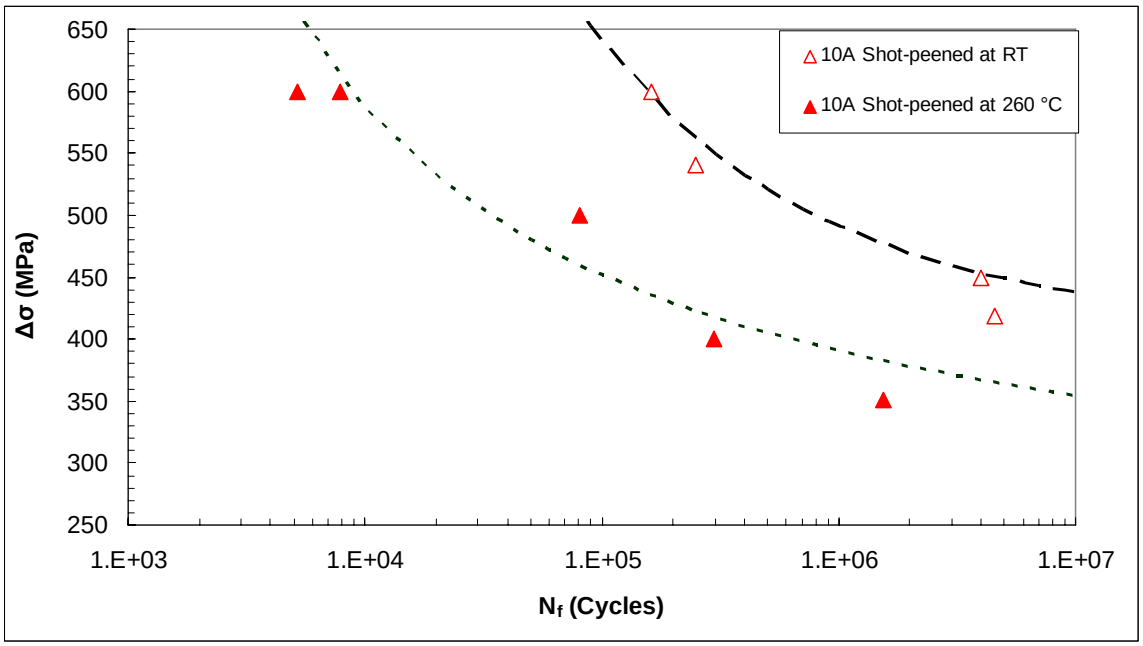

(c) Stress range versus Cycles to failure at 260 °C and room temperatures for 10A specimens.

Figure 25. Stress range versus Cycles to failure for various shot-peening intensities at 260 °C and room temperatures.

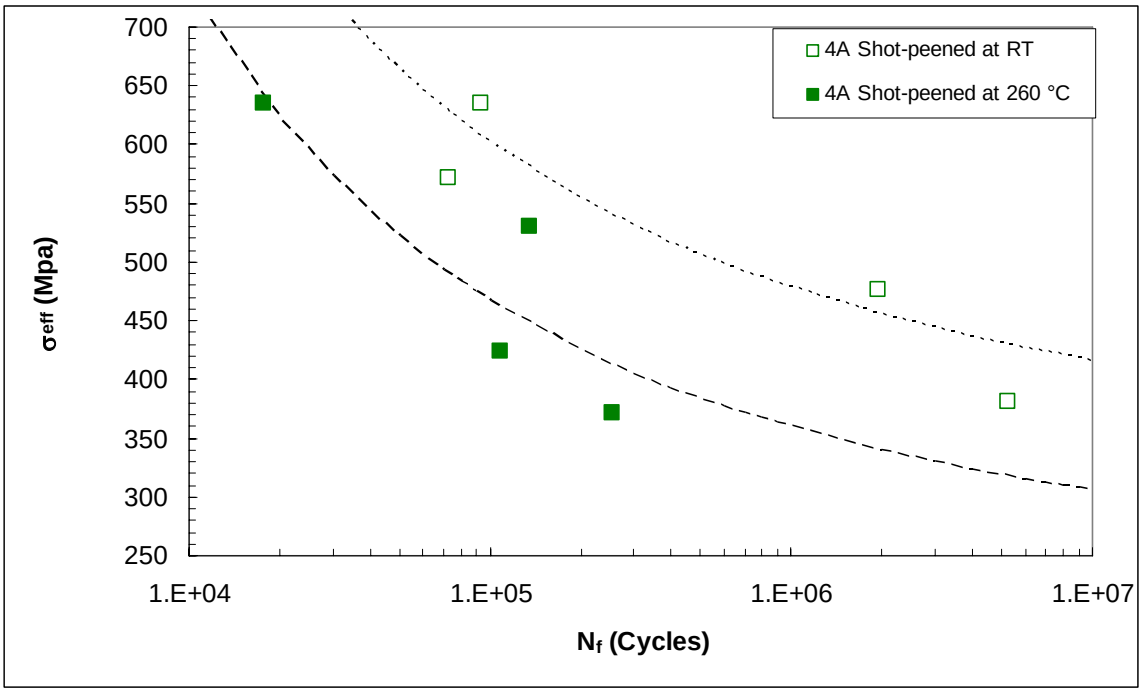

(a) Effective stress versus Cycles to failure at 260 °C and room temperatures for 4A specimens.

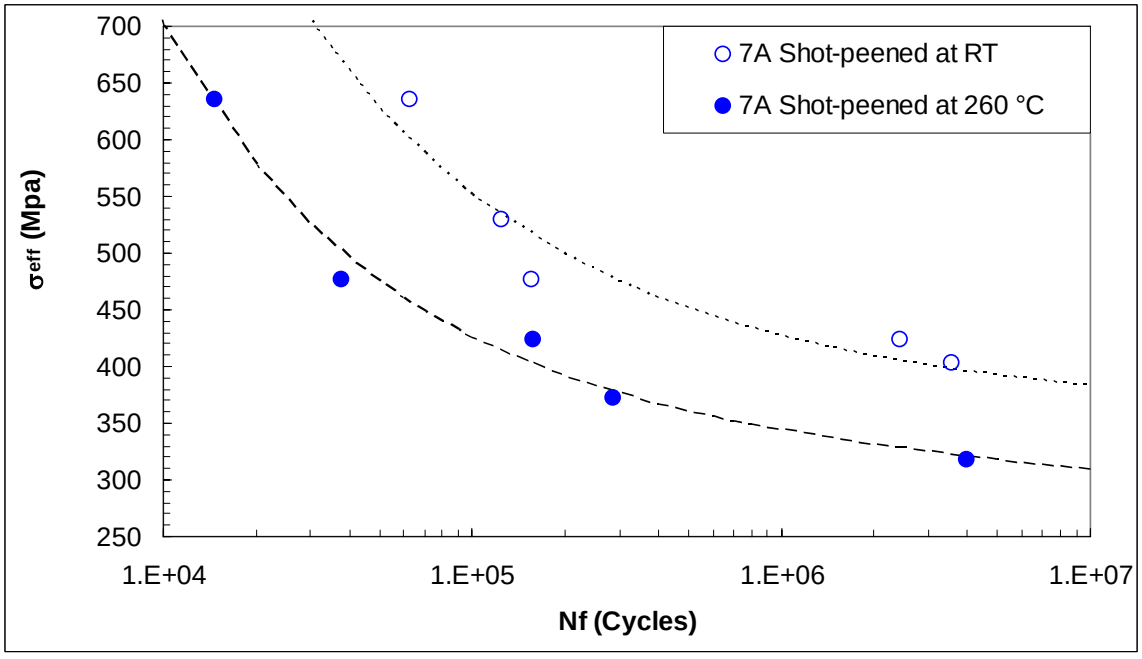

(b) Effective stress range versus Cycles to failure at 260 °C and room temperatures for 7A from specimens from a previous study [2].

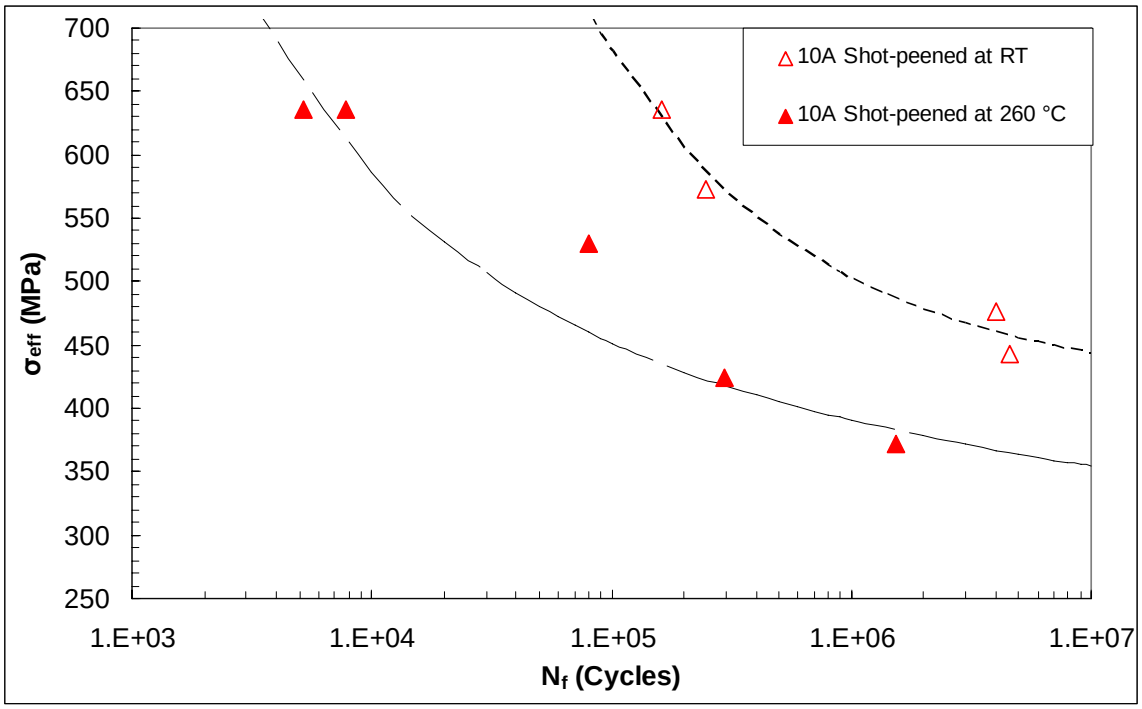

(c) Effective stress versus Cycles to failure at 260 °C and room temperatures for 4A specimens.

Figure 26. Effective stress range versus Cycles to failure for various shot-peening intensities tested at 260 °C and room temperatures.

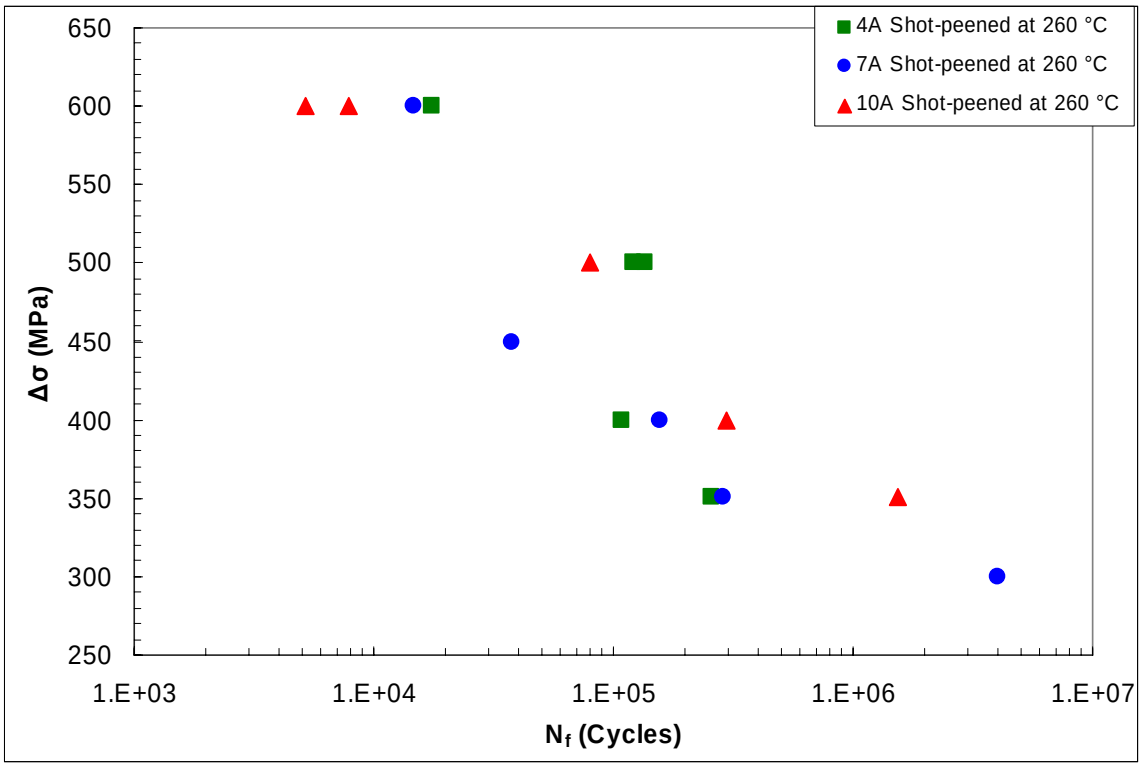

(a) $\Delta\sigma$-N_f for tests at elevated temperature 260° C

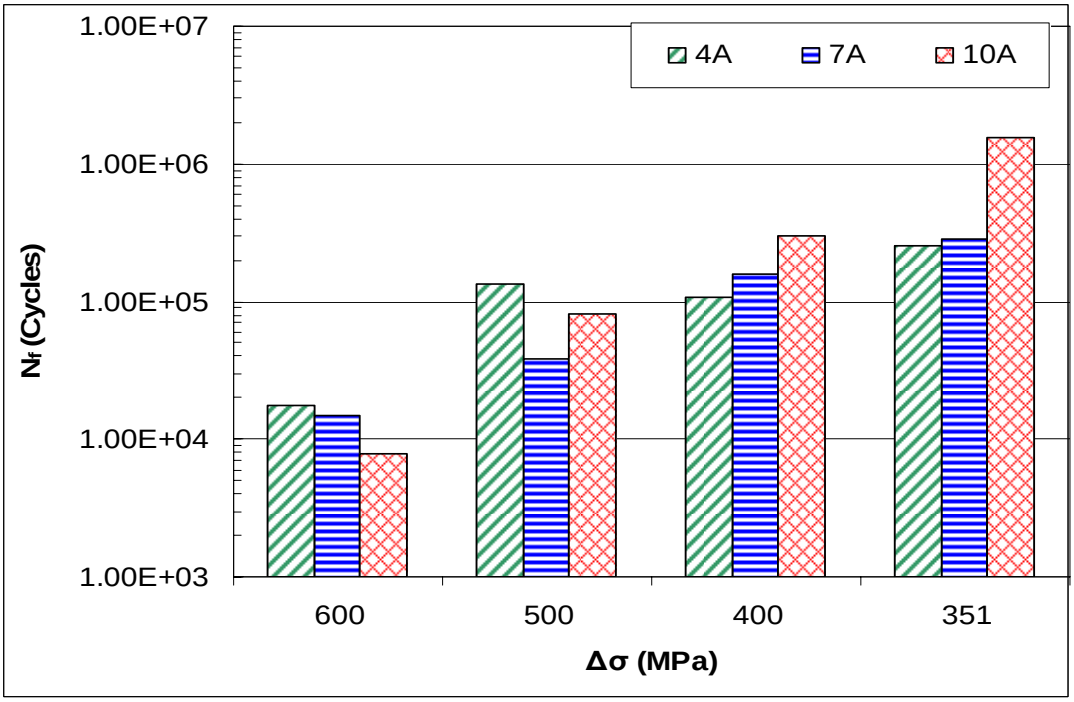

(b) Bar graph showing $\Delta\sigma$-N_f for elevated temperature testes for4A,7A and 10A

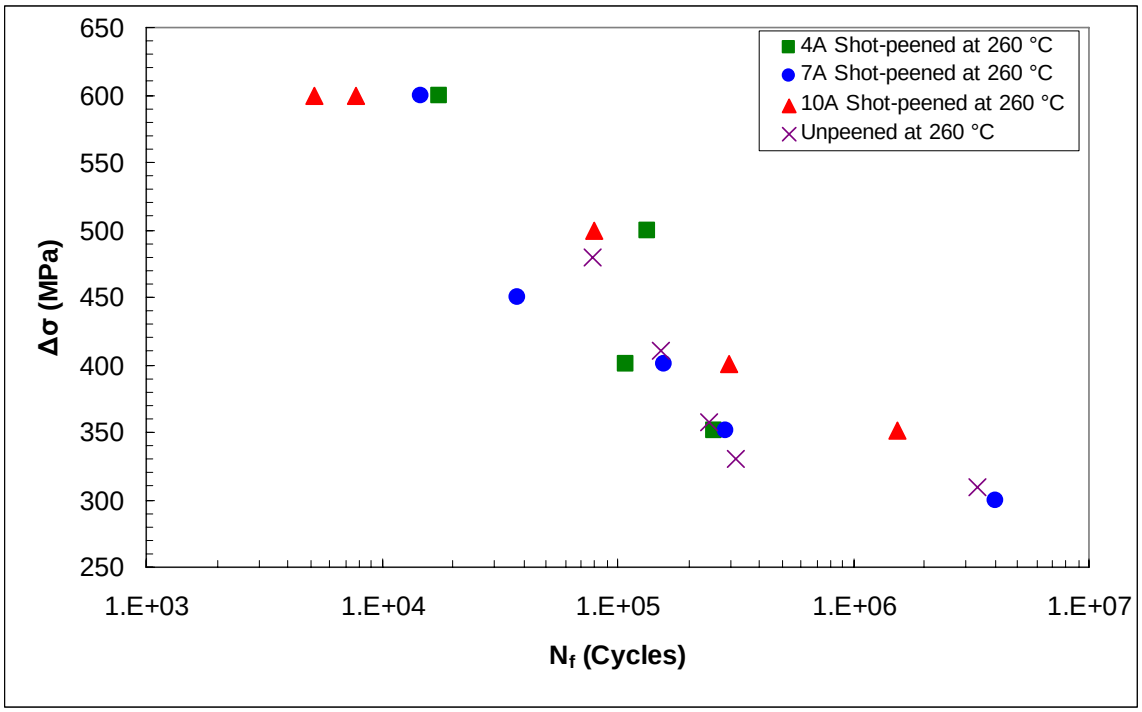

(c) Comparison of $\Delta\sigma$-N_f for peened and unpeened specimens tested at 260° C

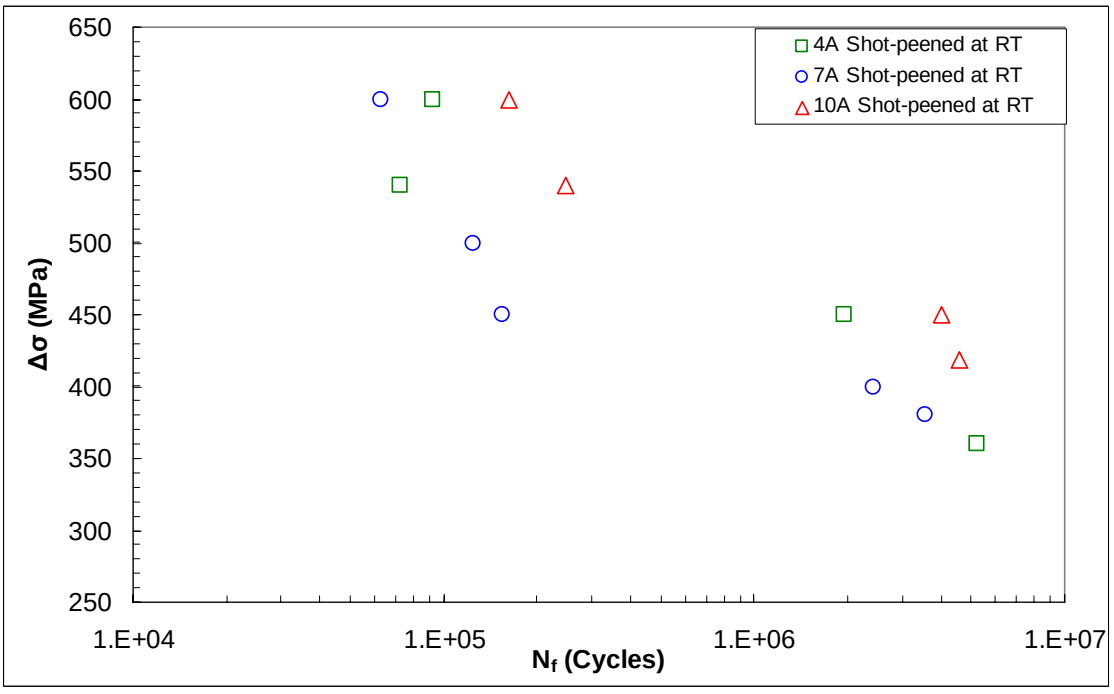

(d) $\Delta\sigma$-N_f for peened specimens at room temperature

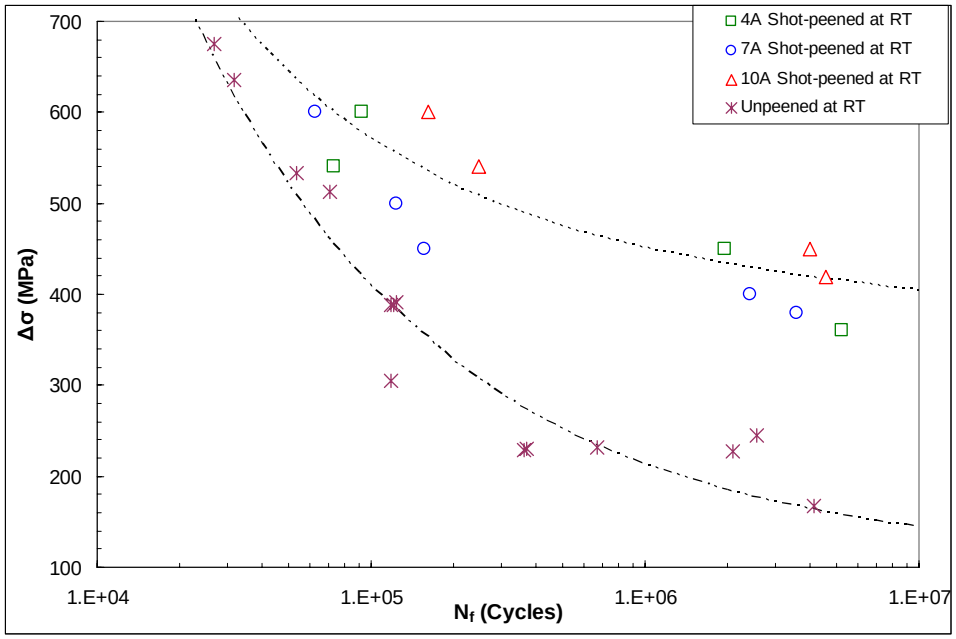

(e) Comparison of $\Delta\sigma$-N_f for peened and unpeened specimens tested at room temperature

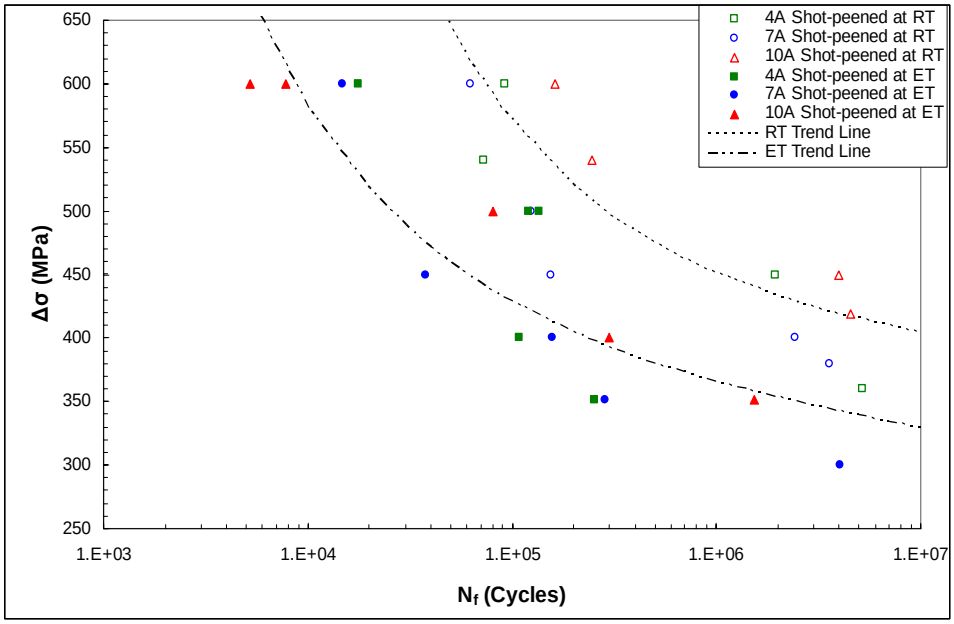

(f) Comparison of $\Delta\sigma$-N_f for peened specimens at both room and elevated temperature 260° C

Figure 27. $\Delta\sigma$ -N_f for unpeened, 4A, 7A and 10A specimens tested at room and elevate temperatures 260° C

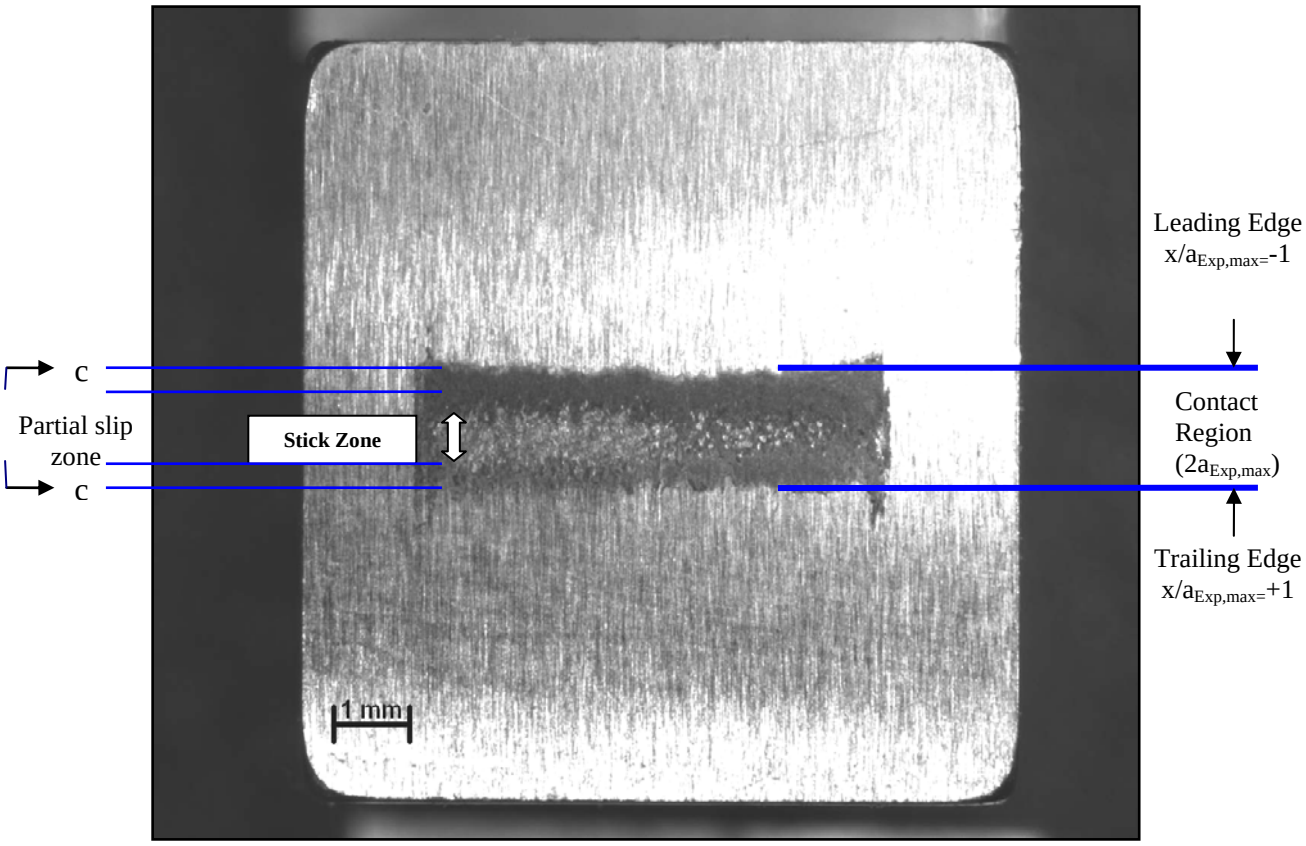

Figure 28. Scar Pattern from Test 2 specimen 4A tested at elevated temperature

Load Condition: σ_{max} =555 MPa, σ_{min} =55 MPa

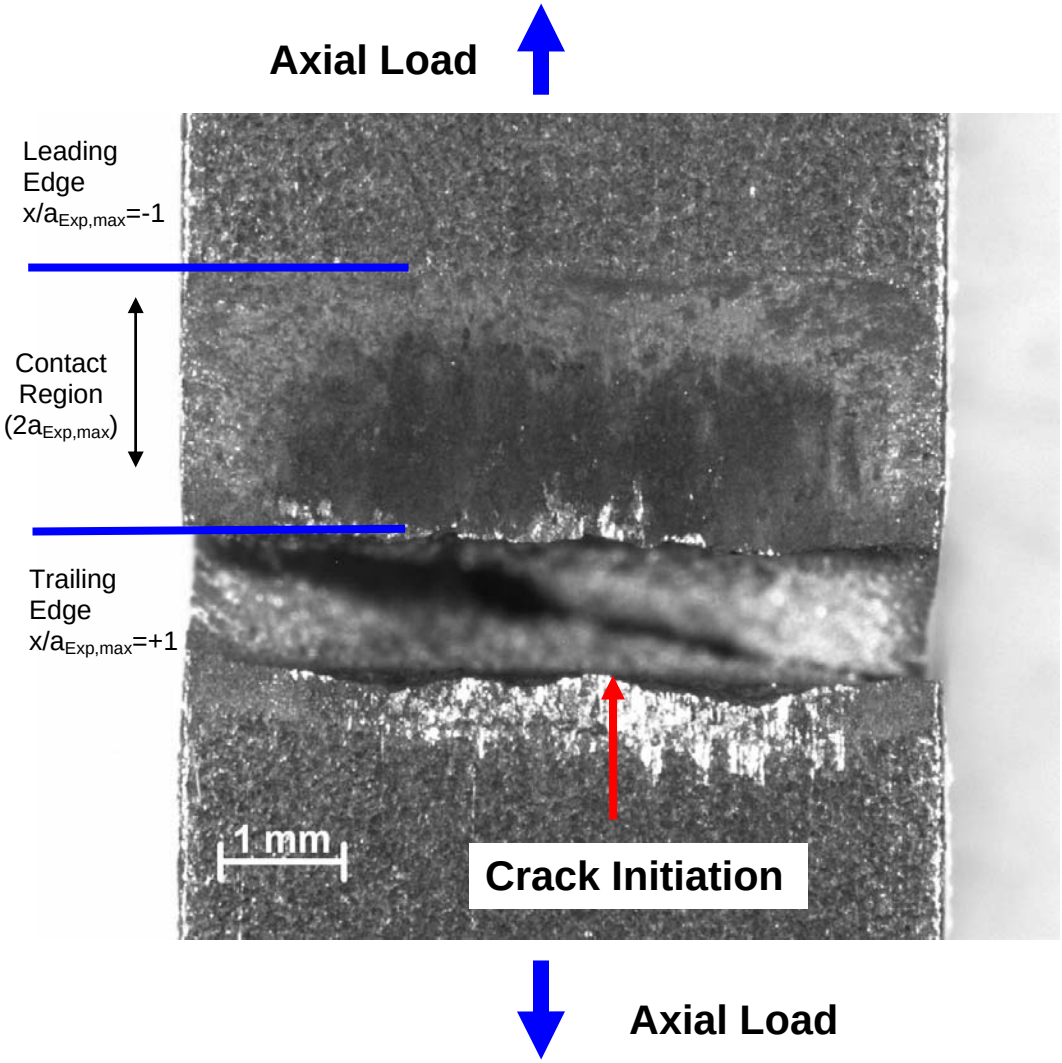

Figure 29. Crack Initiation Location

Crack Initiation at Location near $x/a_{Exp,max} = +1$ (Test 4)
4A specimen tested at elevated temperature, load condition: σ_{max} =390 MPa, σ_{min} =39 MPa

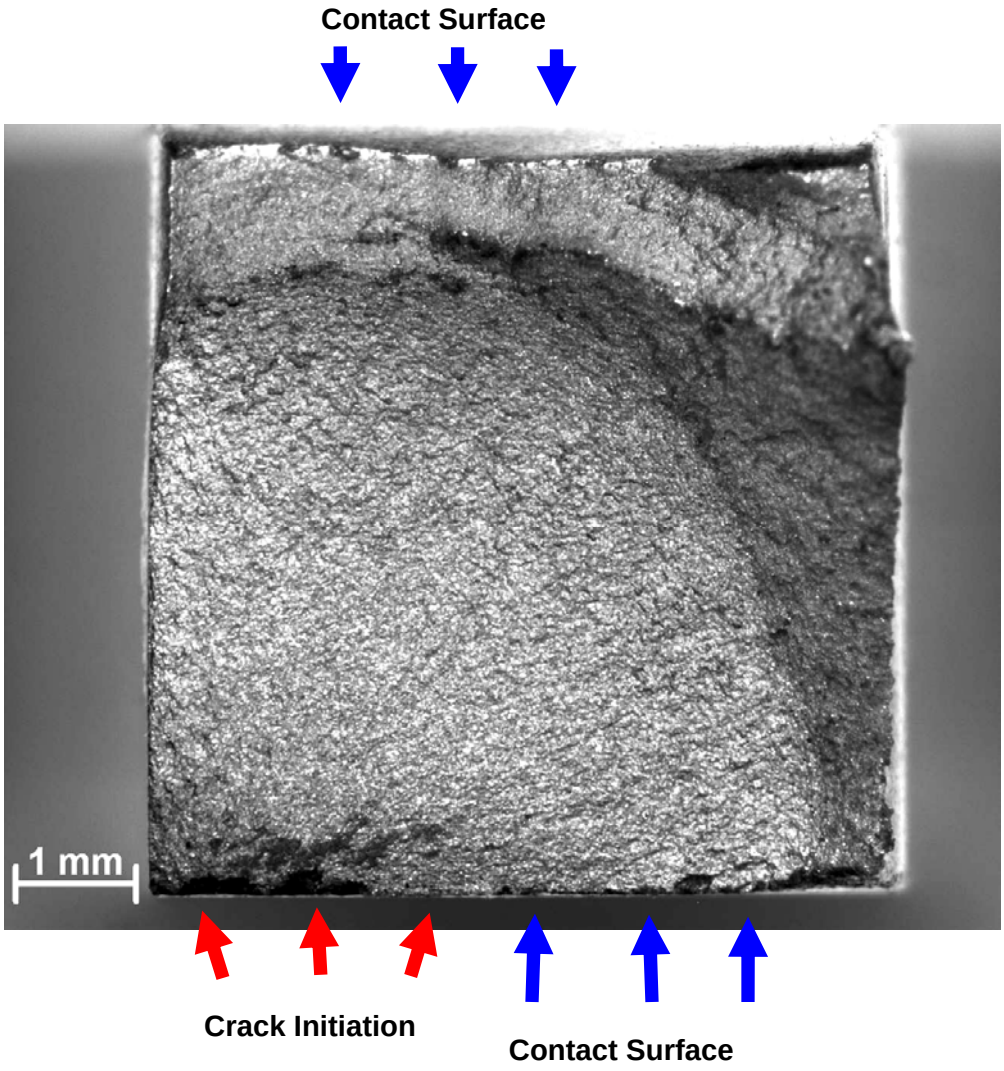

(a) Crack Initiation Observed on Contact Surface (under Lower Magnification)

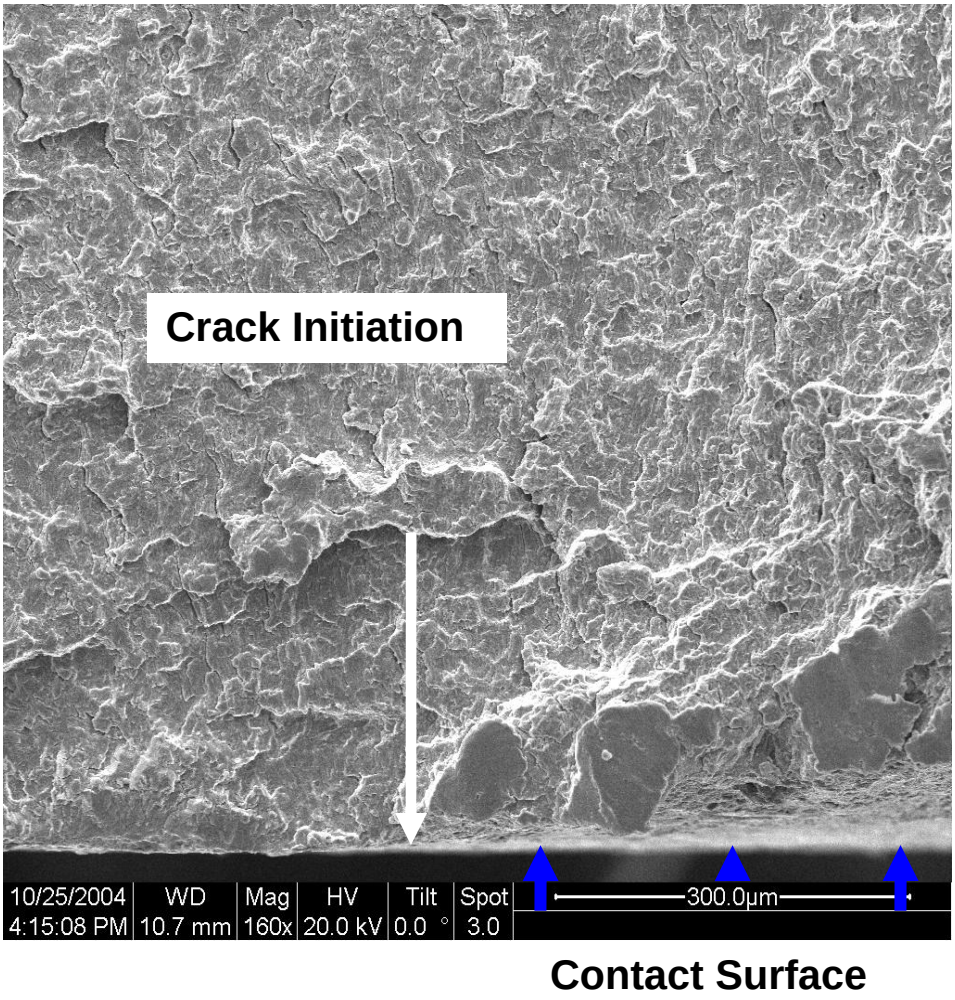

(a) Crack Initiation Observed on Contact Surface (under Higher Magnification) clue (river patterns)

Figure 30. Surface Crack Initiation for 4A Specimens tested at elevated temperature,

Test 4 load condition: σ_{max}=390 MPa, σ_{min}=39

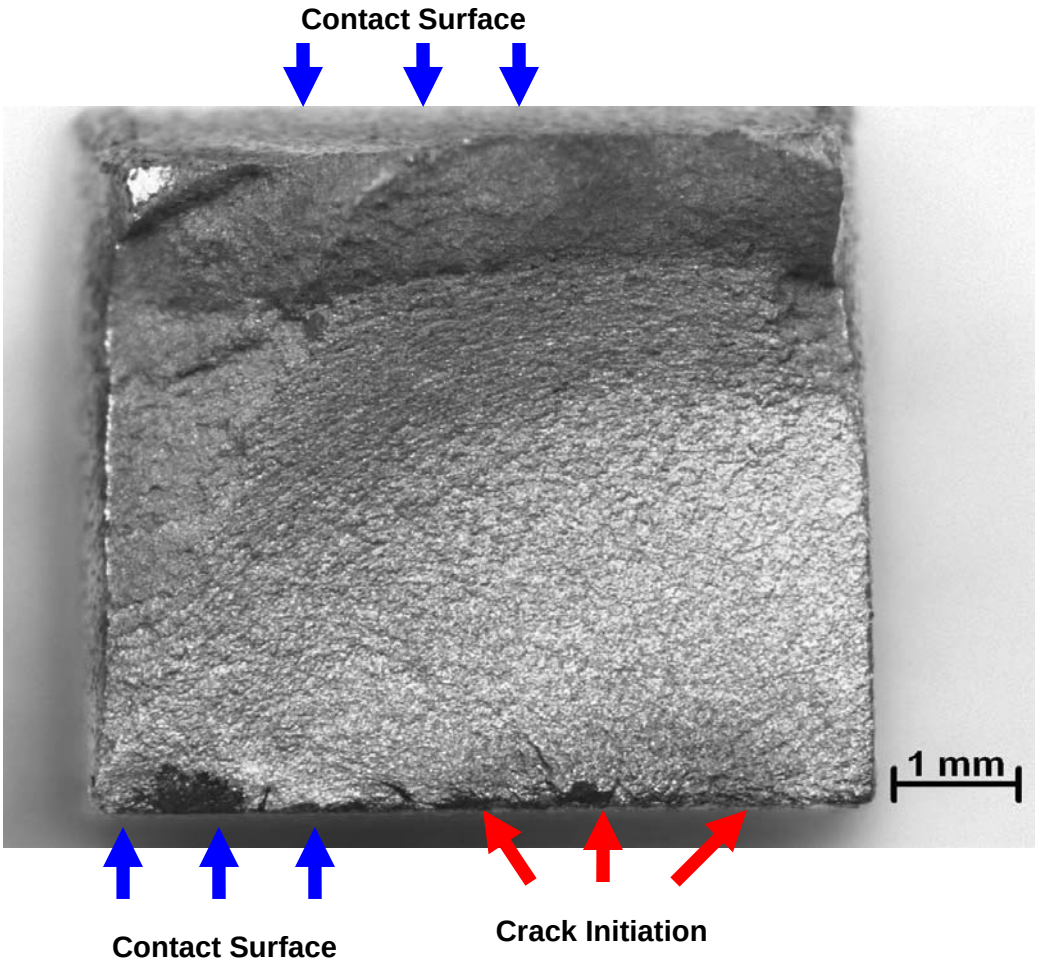

(a) Multiple crack initiation locations Observed on the surface of Specimen (under Lower Magnification)

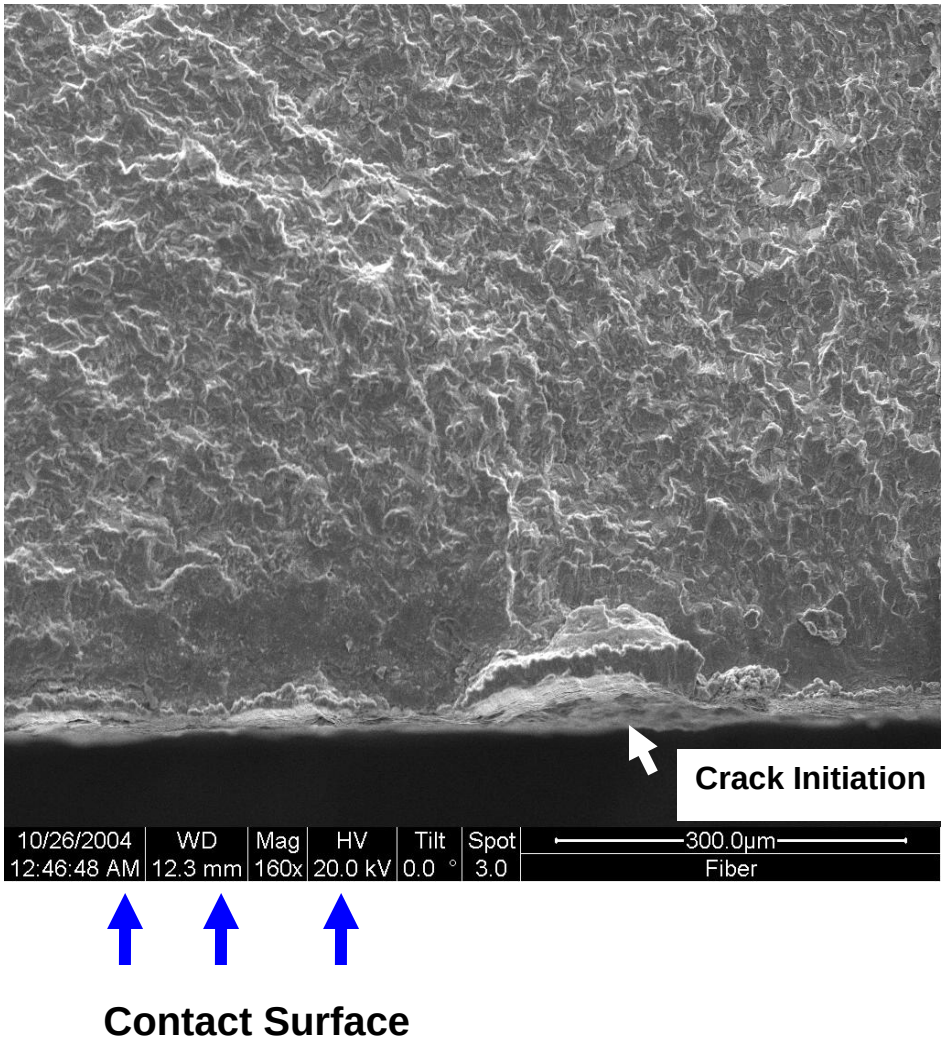

(b) Crack Initiation Observed in the Surface of Specimen (under Higher Magnification)

Figure 31. Surface Crack Initiation for 10A Shot-peened Specimens

Photo from an elevated temperature test, load condition: σ_{max} =444.4 MPa, σ_{min} =44.4 MPa

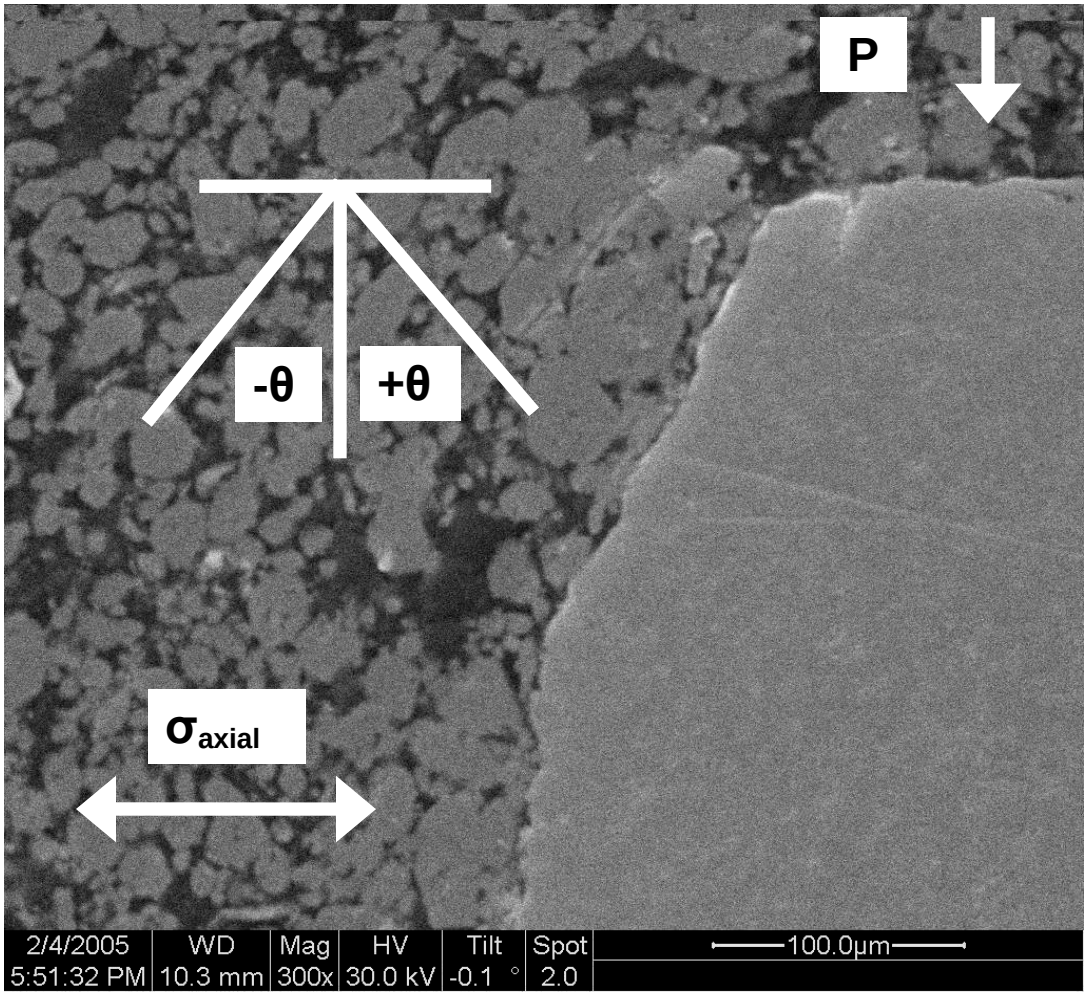

Figure 32. Crack Initiation Orientation for a 10A specimen, θ = -55˚

Photo Taken from Test 13, load condition: σ_{max}=444.44 MPa, σ_{min}=44.44 MPa (equivalent to θ = 35˚)

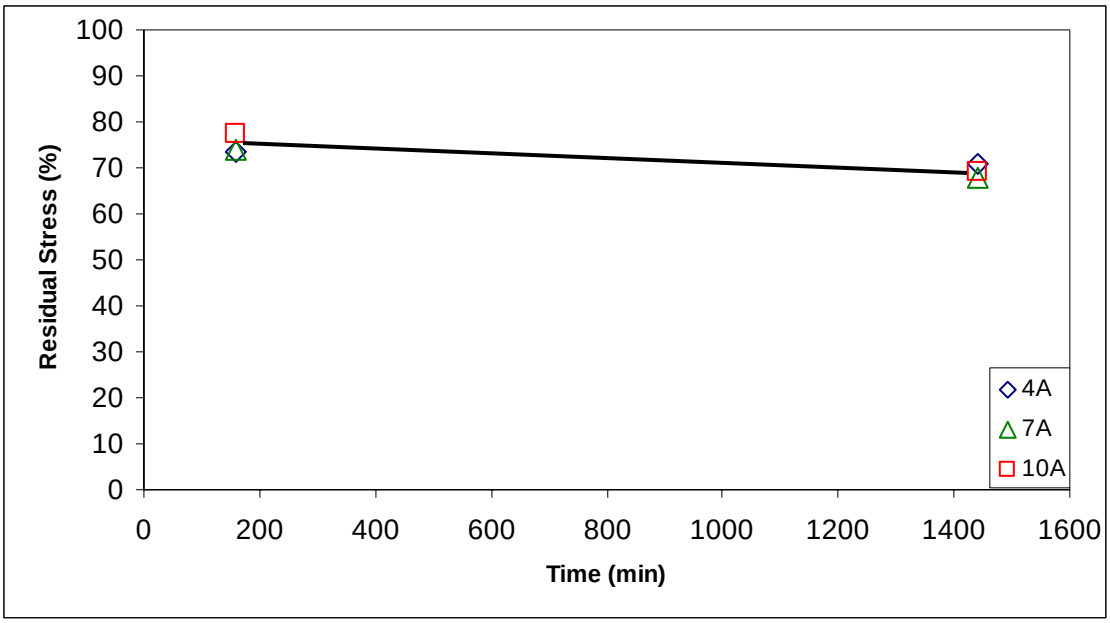

Figure 33. Effects of temperature exposure (260° C) and exposure time on the stress relaxation at the specimens' surface.

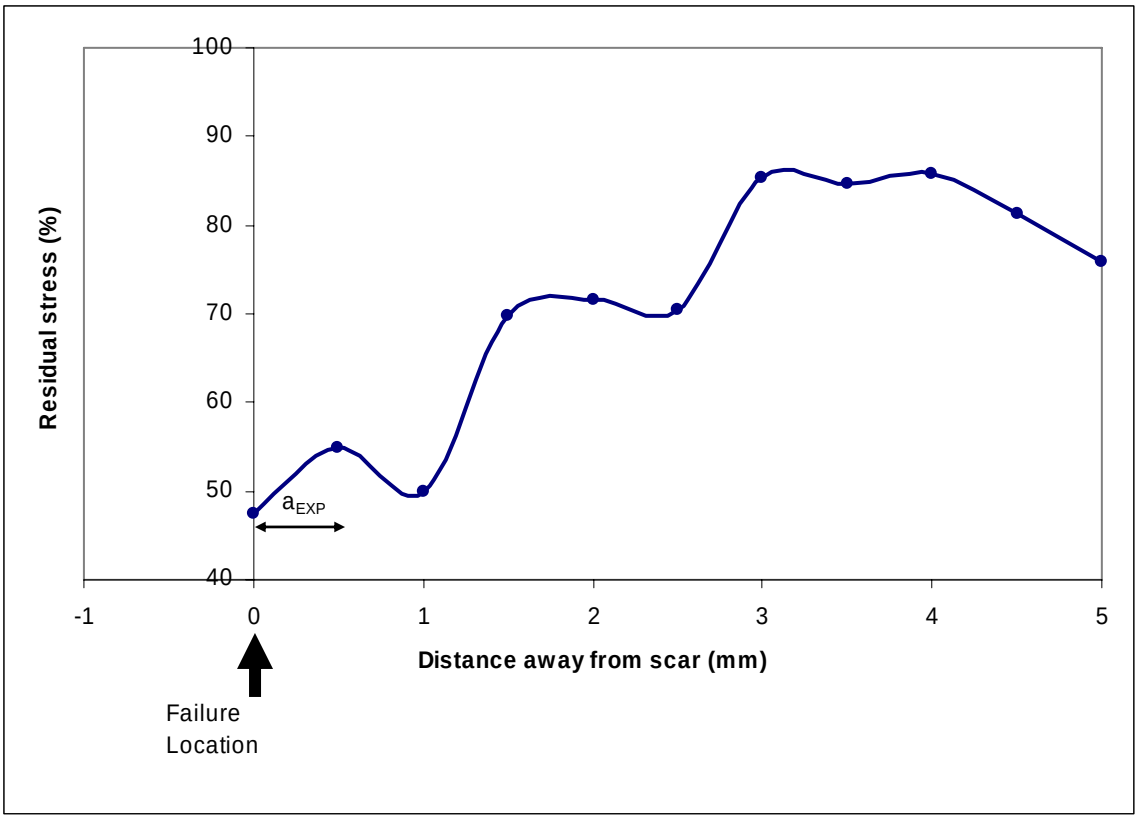

Figure 34. Residual stress profile along the surface of the top half of a failed 4A specimen fatigued at elevated temperature

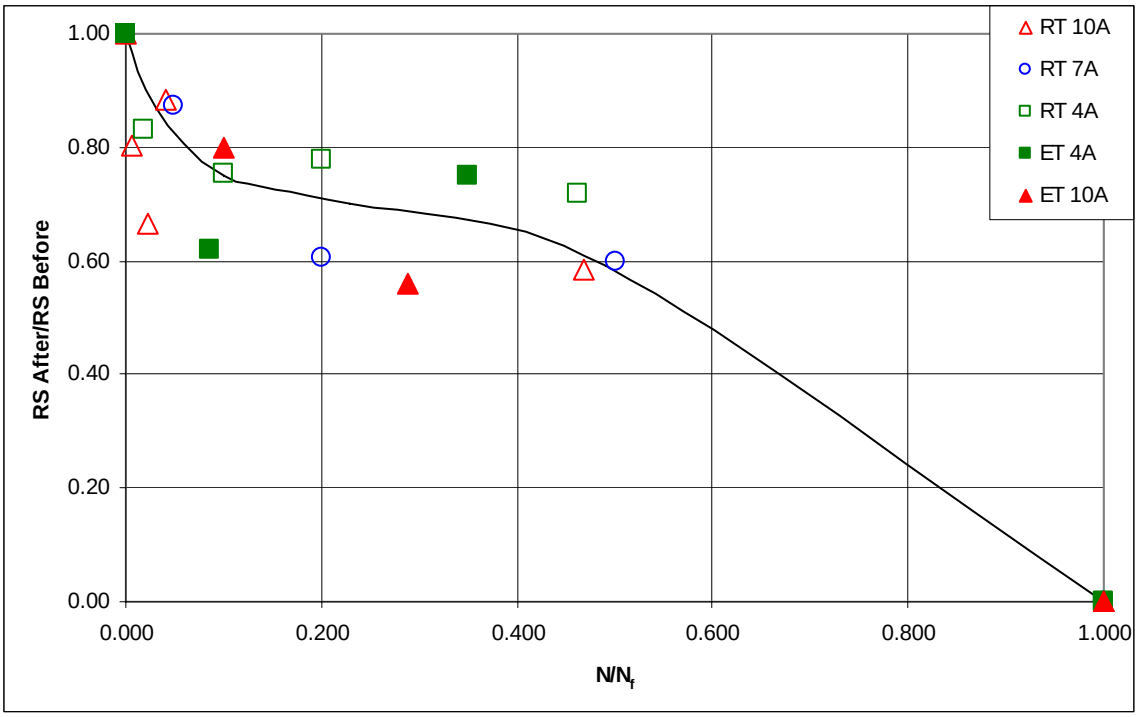

Figure 35. Normalized residual stresses (NRS) versus relative fretting fatigue cycle (N/N_f) for both room temperature and elevated temperature 260° C

Note:
The fitting curve shown in Figure 35 is used to approximately demonstrate the trend observed from (NRS).

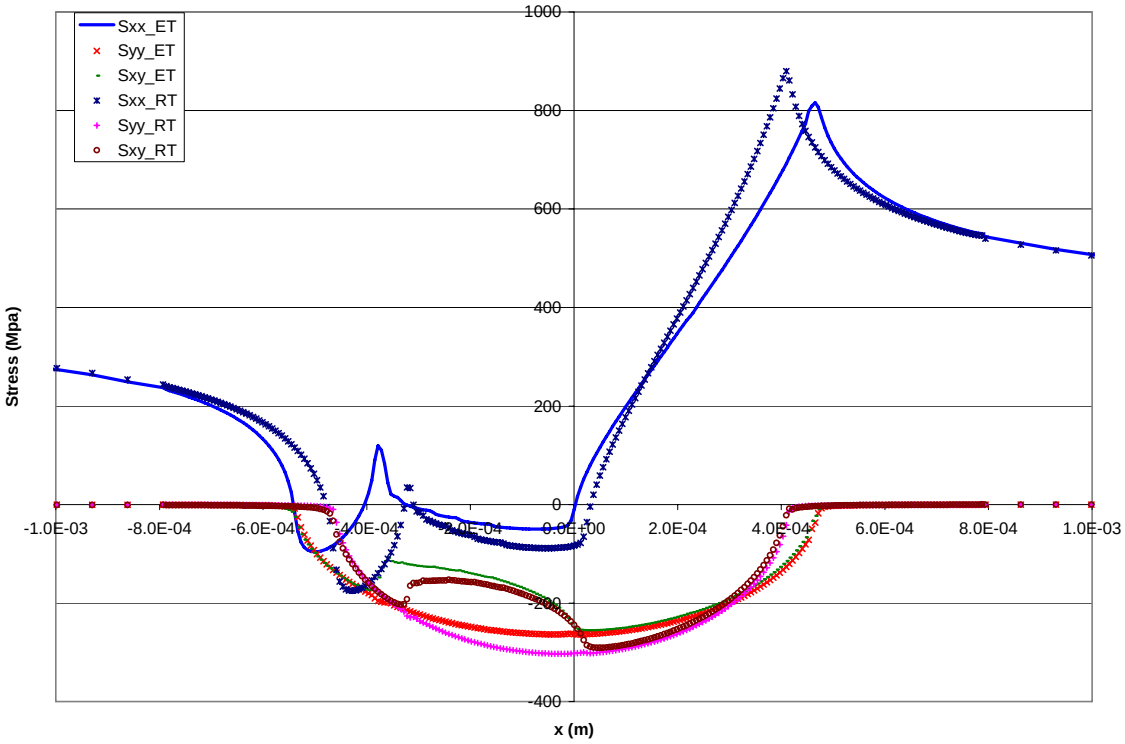

Figure 36 Variation of stress at the contact surface of the fretting specimen.

Note:
125 and 95 GPa of elastic moduli was used for the specimen fatigued at room temperature and 260˚ C, respectively. Load Condition: σ_{max} =390 MPa, σ_{min} =39 MPa

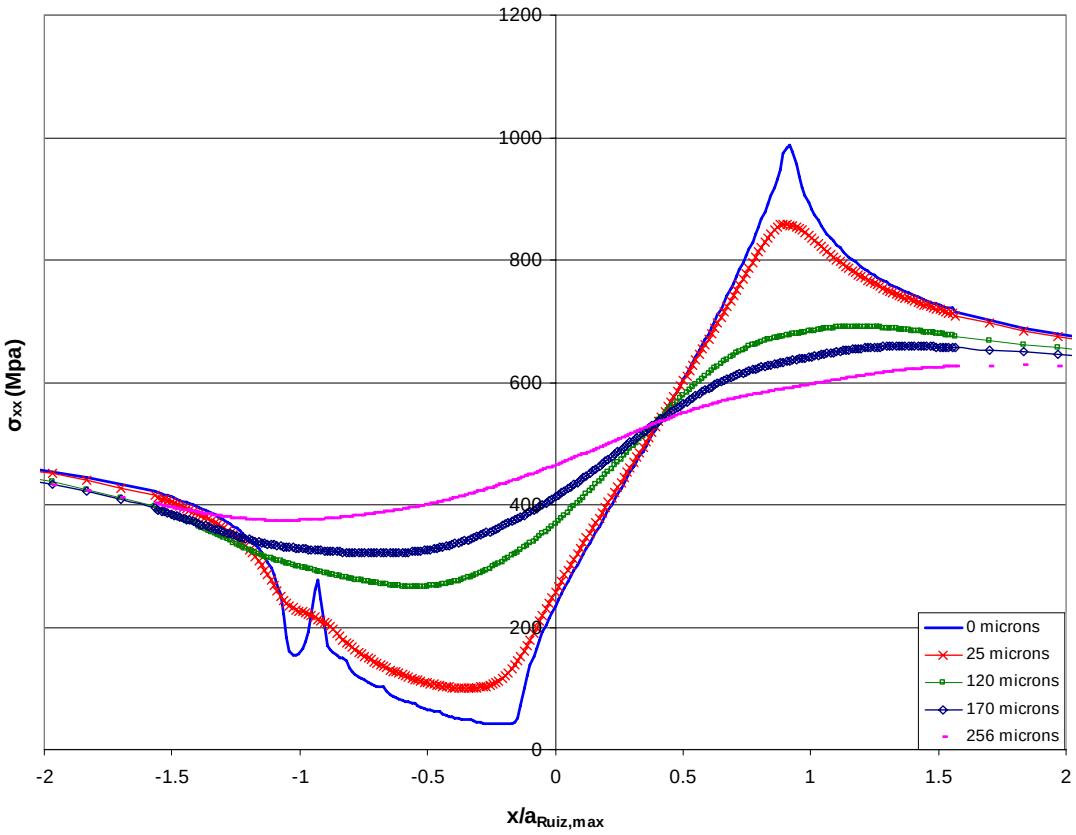

(a) σ_{xx} Stress Profile at Different Depths with 0% RS (Full relaxation)

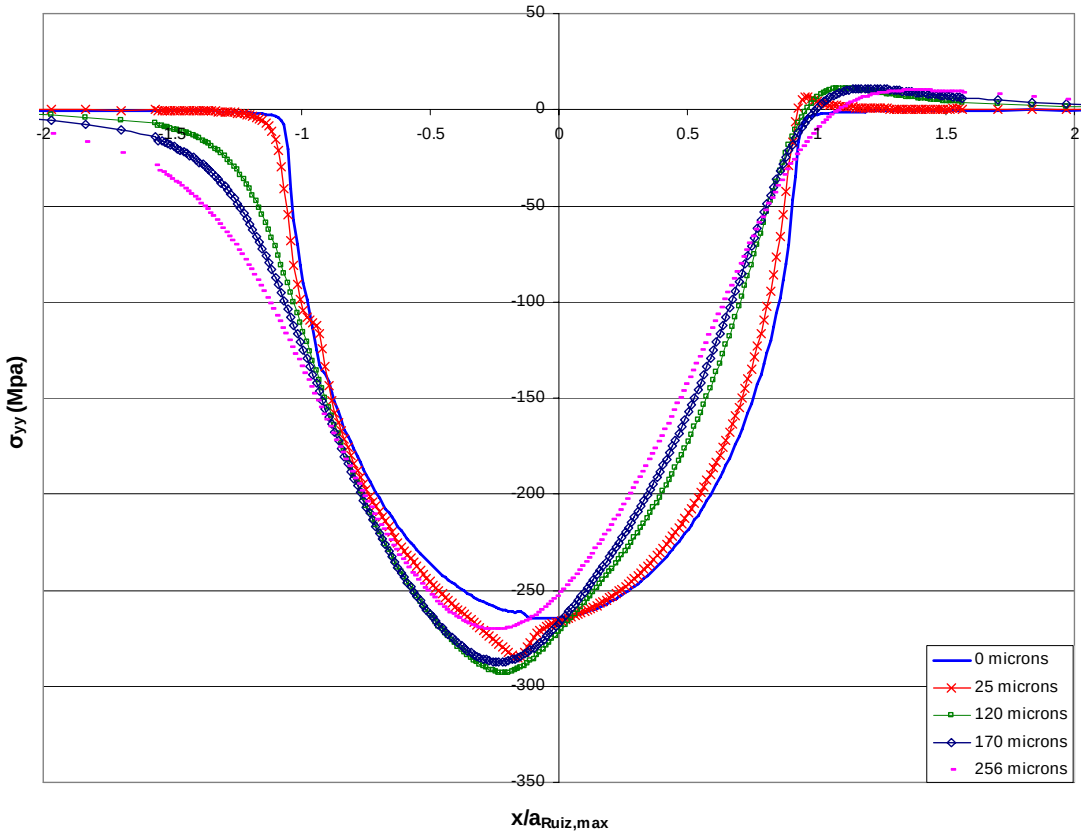

(b) σ_{yy} Stress Profile at Different Depths with 0% RS (Full relaxation)

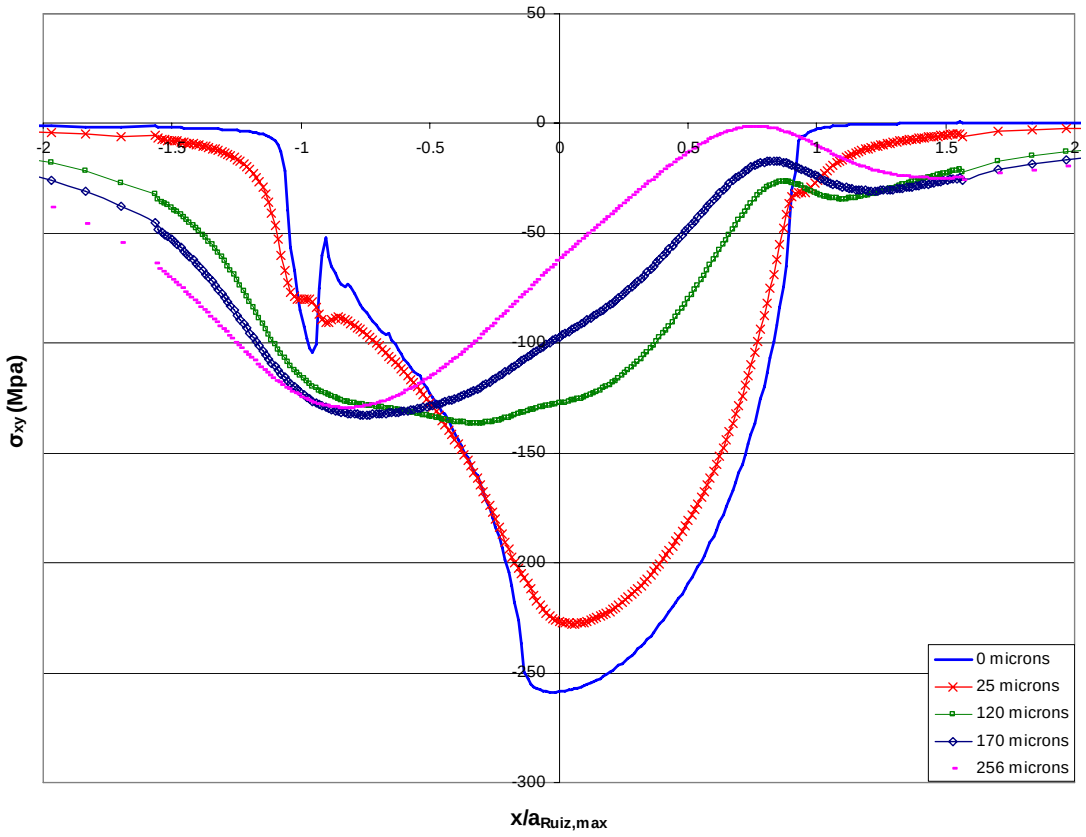

(c) σ_{xy} Stress Profile at Different Depths without 0% RS (Full relaxation)

Figure 37. Comparison of Stress Profile at Different Depths for Test 2, Step 4

Load Condition: σ_{max} =555 MPa, σ_{min} =55 MPa
4A specimen tested at 260° C

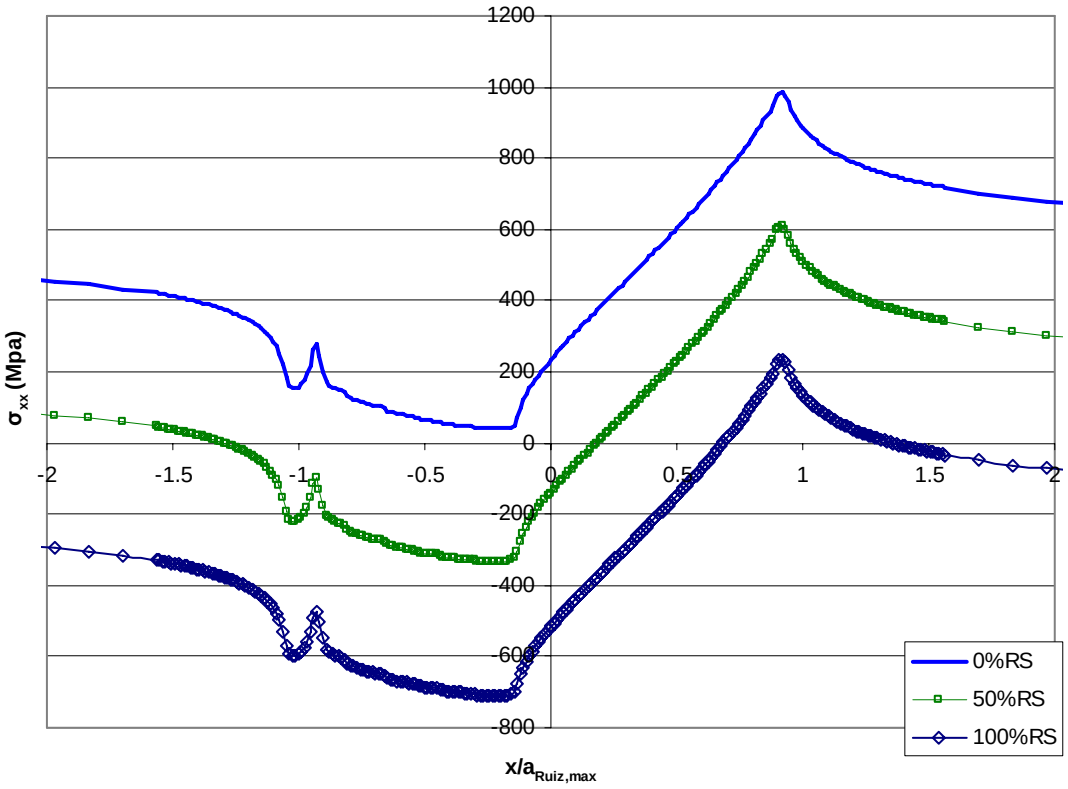

(a) σ_{xx} Stress Profile on Contact Surface with Different amount of Residual Stress

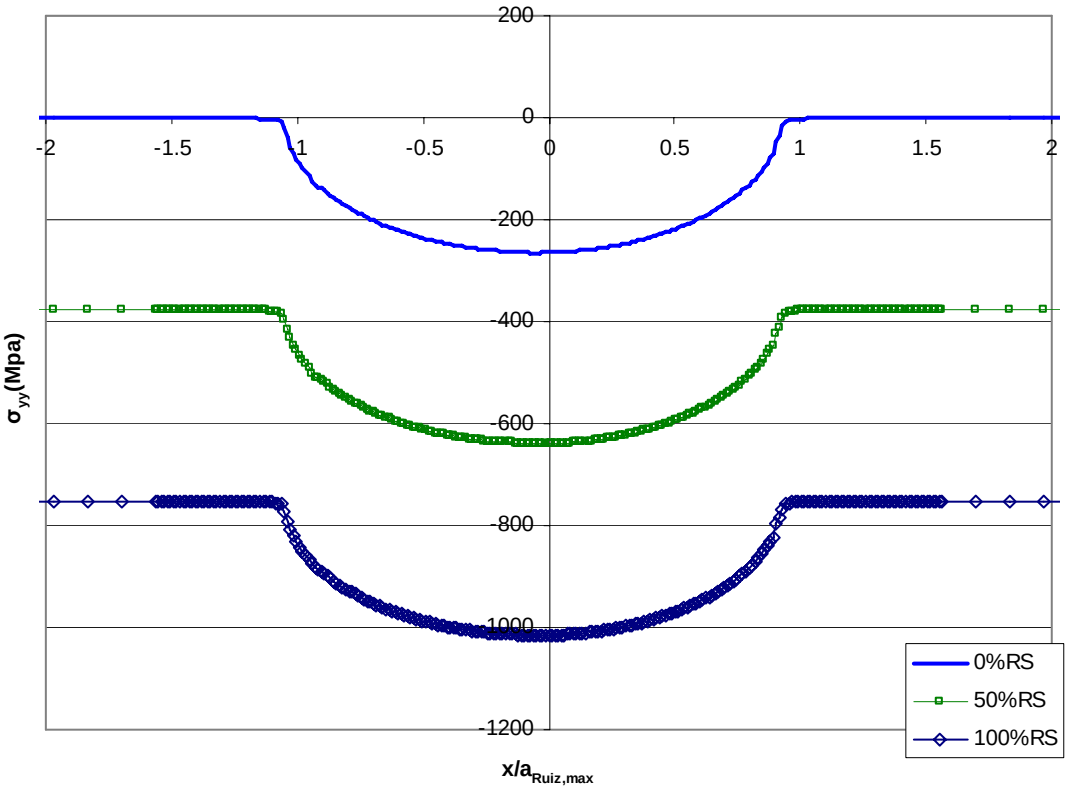

(b) σ_{yy} Profile on Contact Surface with Different amount of Residual Stress

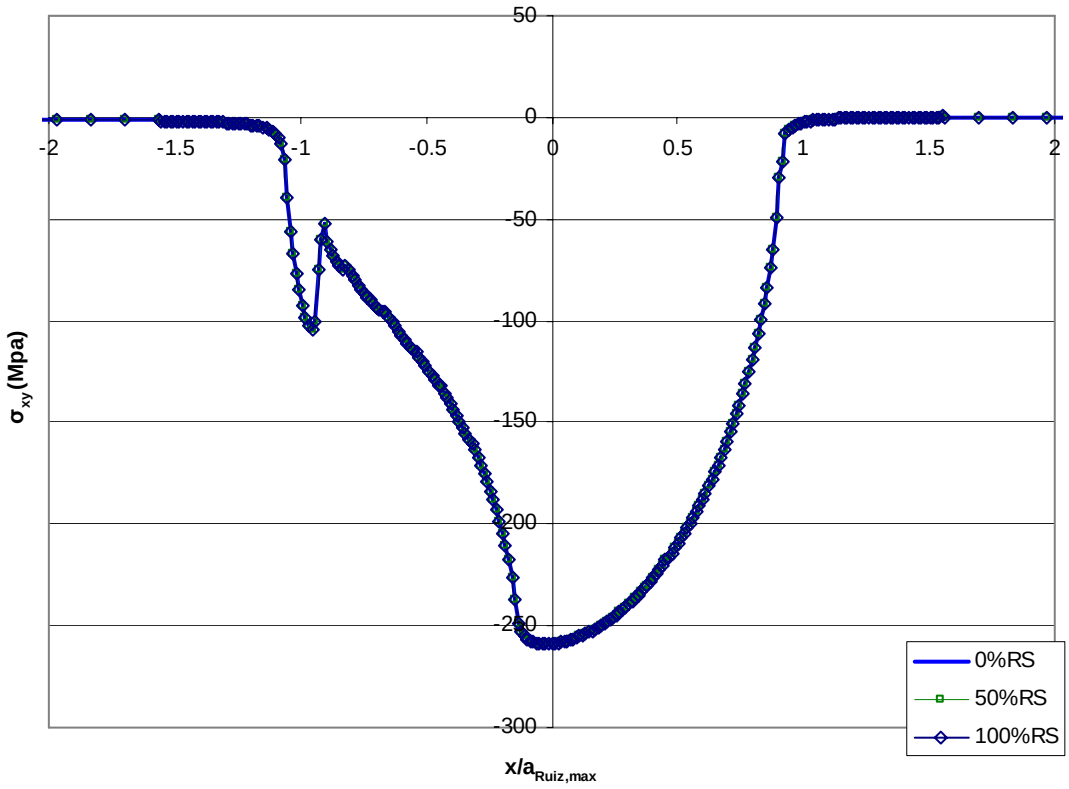

(c) σ_{xy} Profile on Contact Surface with Different amount of Residual Stress

Figure 38. Comparison of Stress Profile under the Influence Different amount of Stress Relaxation along Contact Surface for Test 2, Step 4

Load Condition: σ_{max} =555 MPa, σ_{min} =55 MPa
4A specimen tested at 260 ºC

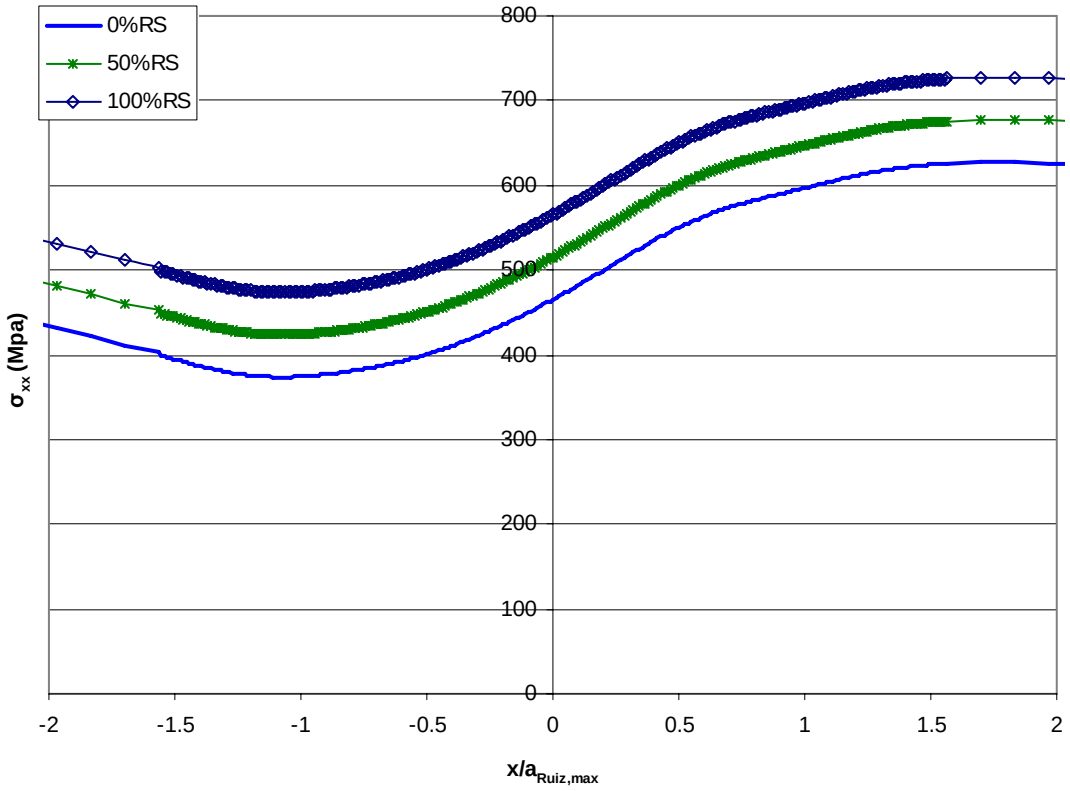

(a) σ_{xx} Stress Profile at a Depth of 256 μm with Different amount of Residual Stress

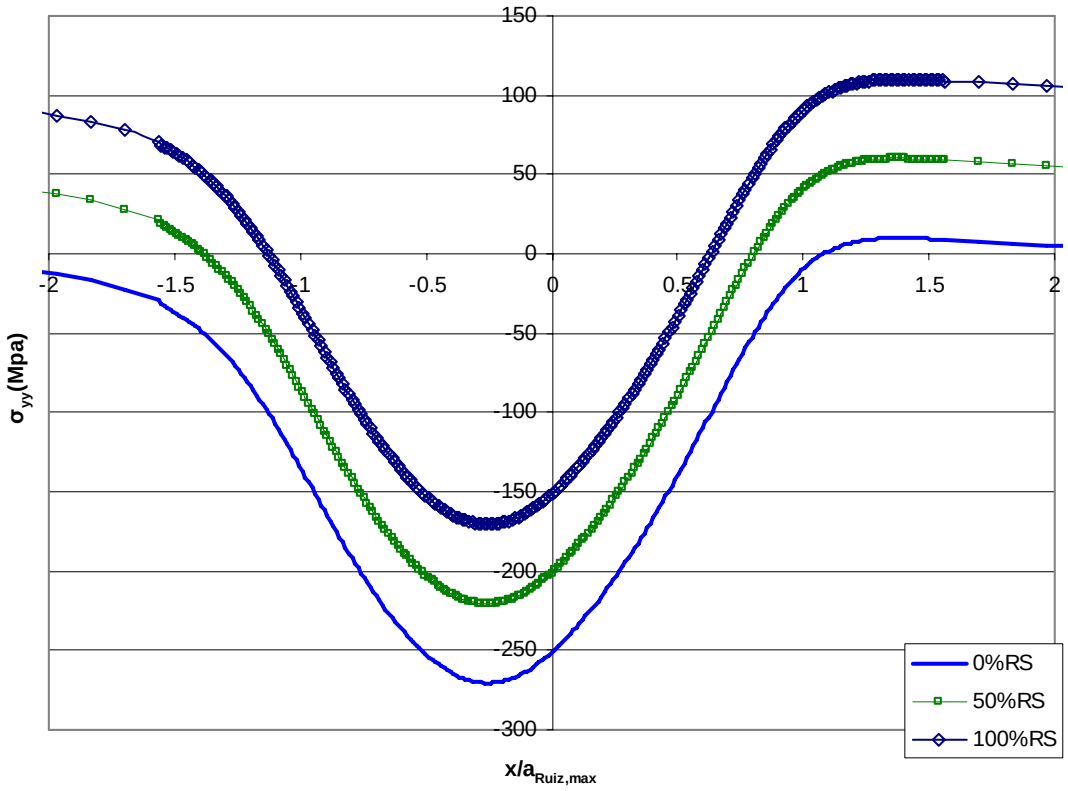

(b) σ_{yy} Stress Profile at Depth of 256 μm with Different amount of Residual Stress

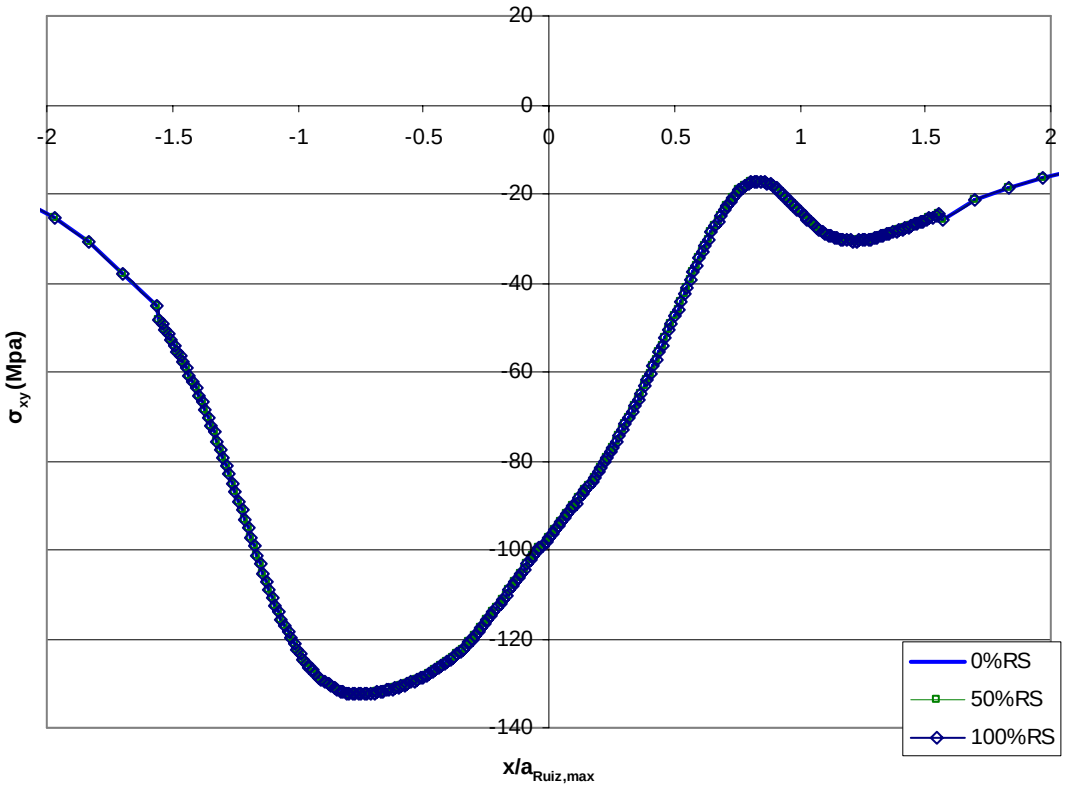

(c) σ_{xy} Stress Profile at a Depth of 256 μm with Different amount of Residual Stress

Figure 39. Comparison of Stress Profile under the Influence of Different amount of Stress Relaxation at 256 μm Depth for Test 2, Step 4

Load Condition: σ_{max} =555 MPa, σ_{min} =55 MPa
4A specimen tested at 260˚ C

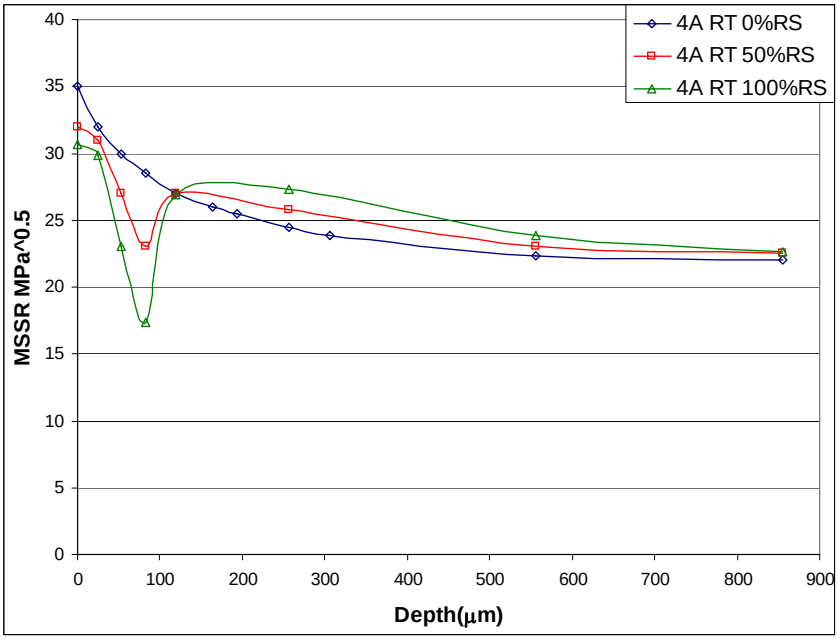

(a) MSSR under Influence of Residual Stress at Different Depths for 4A specimen tested at room temperature from a previous study [5]

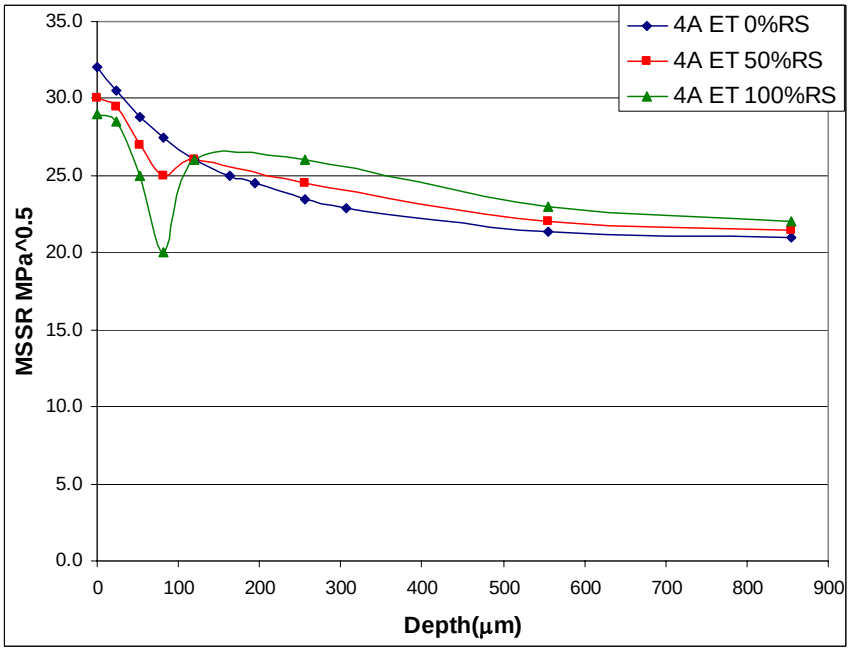

(b) MSSR under Influence of Residual Stress at Different Depths for 4A specimen tested at 260° C for Test 2

Figure 40. Comparison between MSSR under Influence of Residual Stress at Different Depths for 4A specimen at room temperature and 260° C

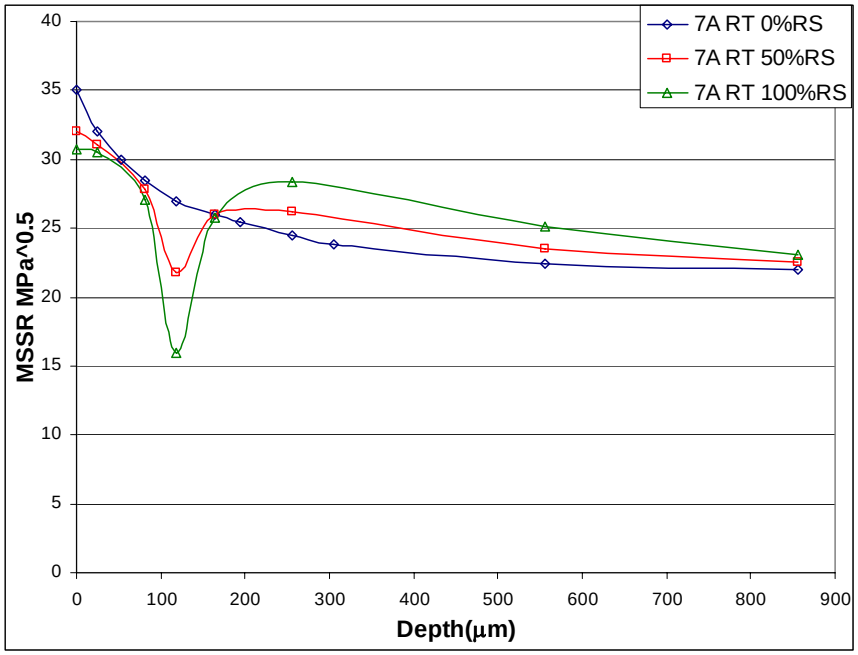

(a) MSSR under Influence of Residual Stress at Different Depths for 7A specimen tested at room temperature from a previous study [2]

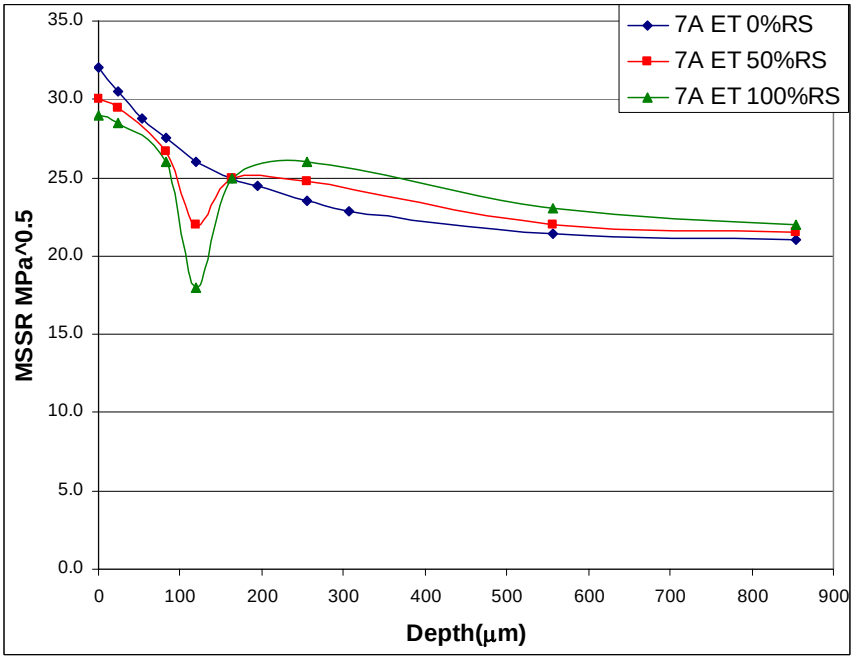

(b) MSSR under Influence of Residual Stress at Different Depths for 7A specimen tested at 260° C from a previous study [2]

Figure 41. Comparison between MSSR under Influence of Residual Stress at Different Depths for 7A specimen at room temperature and 260° C

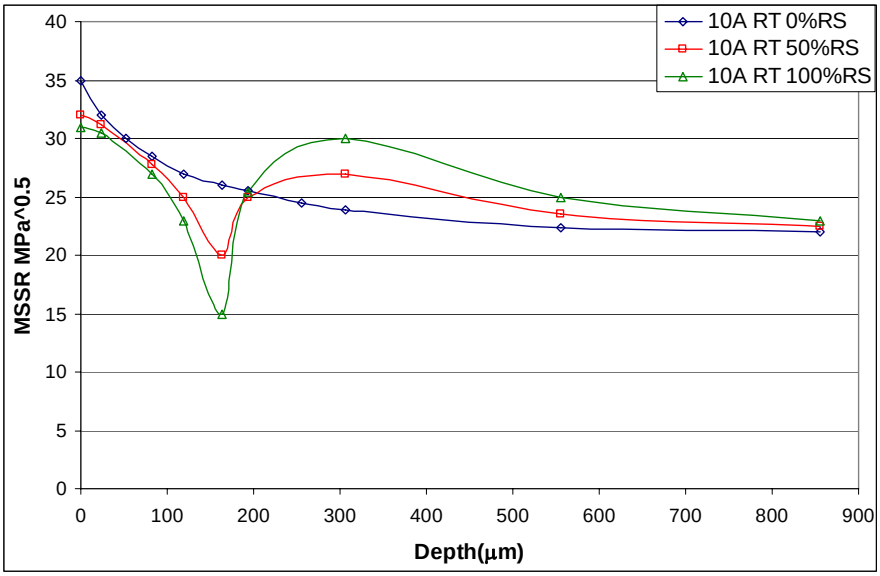

(a) MSSR under Influence of Residual Stress at Different Depths for 10A specimen tested at room temperature from a previous study [5]

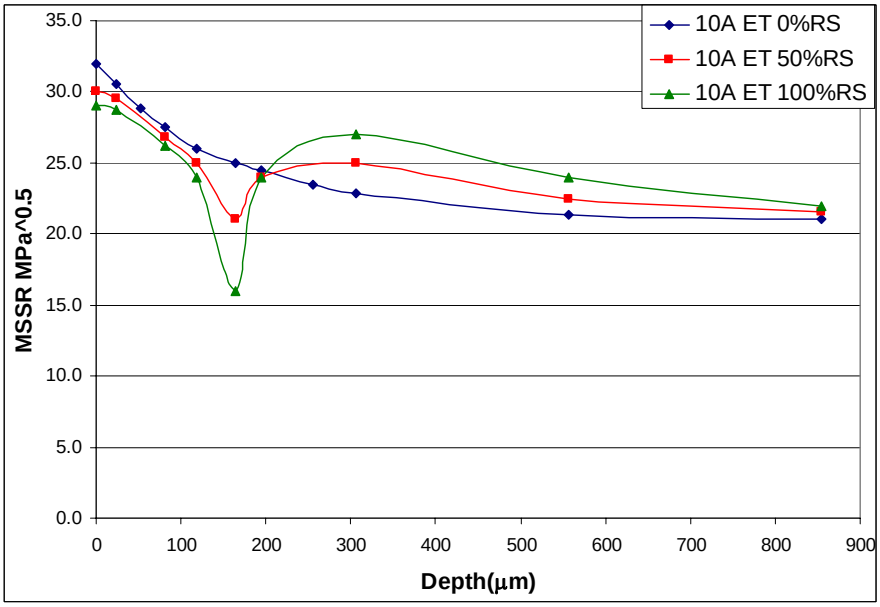

(b) MSSR under Influence of Residual Stress at Different Depths for 10A specimen tested at 260° C for Test 2

Figure 42. Comparison between MSSR under Influence of Residual Stress at Different Depths for 10A specimen at room temperature and 260° C

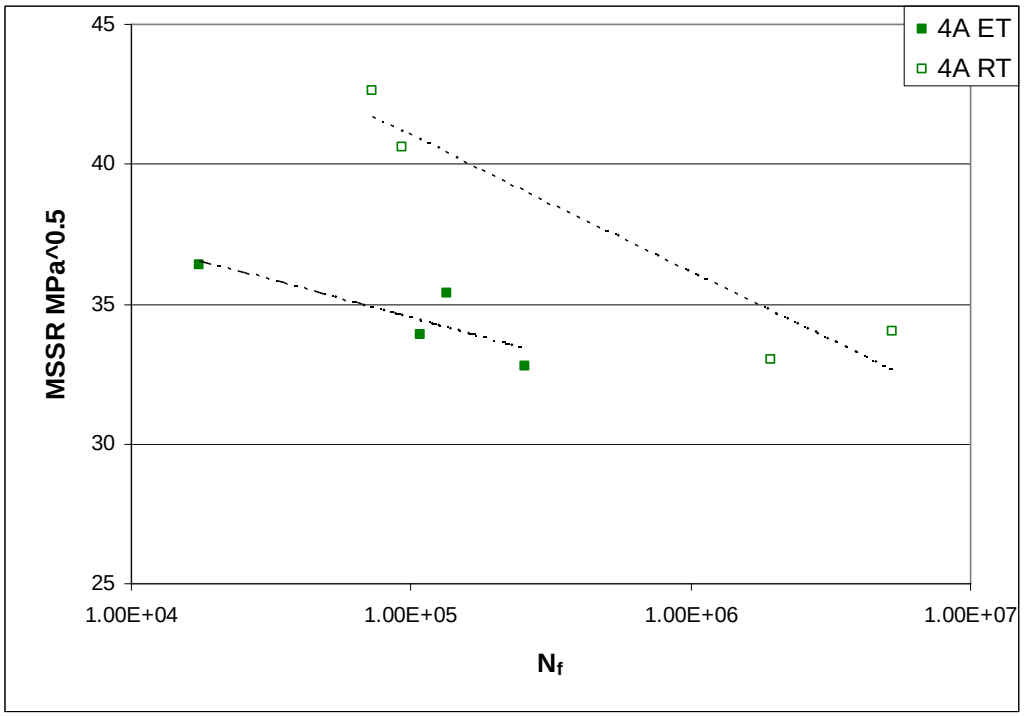

(a) MSSR –N_f for 4A Specimens with 0% Residual Stress

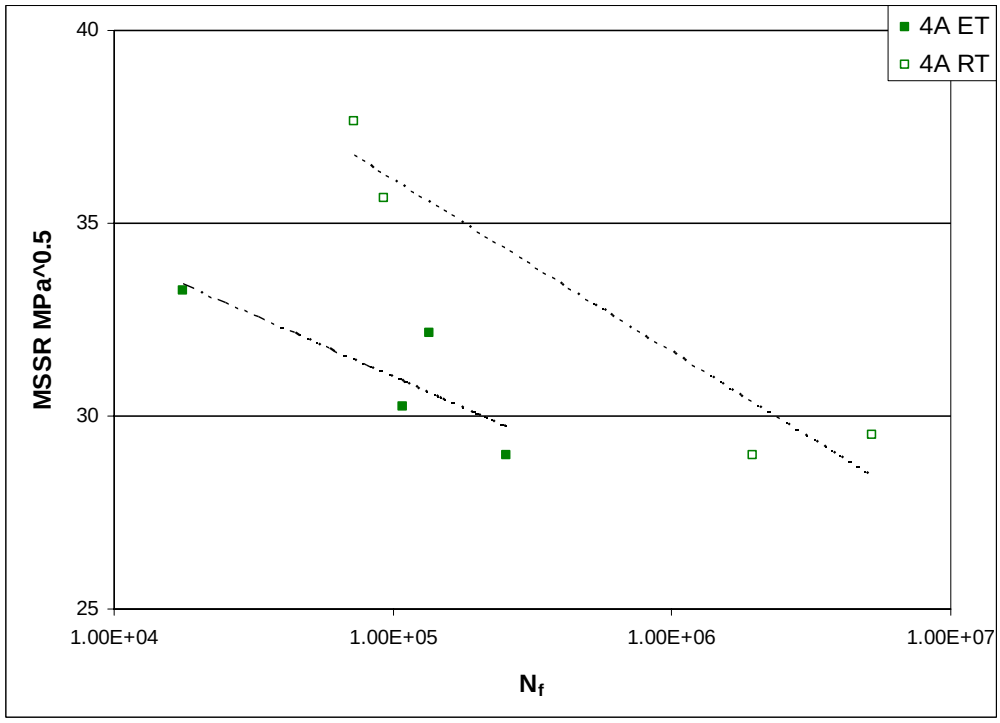

(b) MSSR –N_f for 4A Specimens with 50% Residual Stress

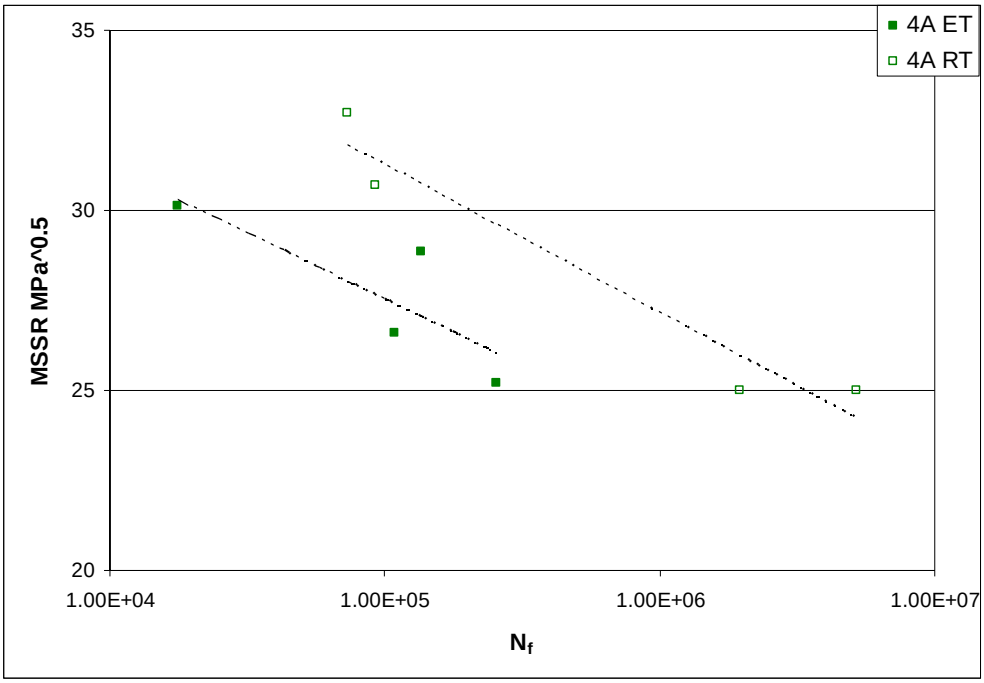

(c) MSSR –N_f for 4A Specimens with 100% Residual Stress

Figure 43. Comparison of MSSR-N_f for 4A Specimen tested at room temperature and 260° C with 0%, 50% and 100% Residual Stress

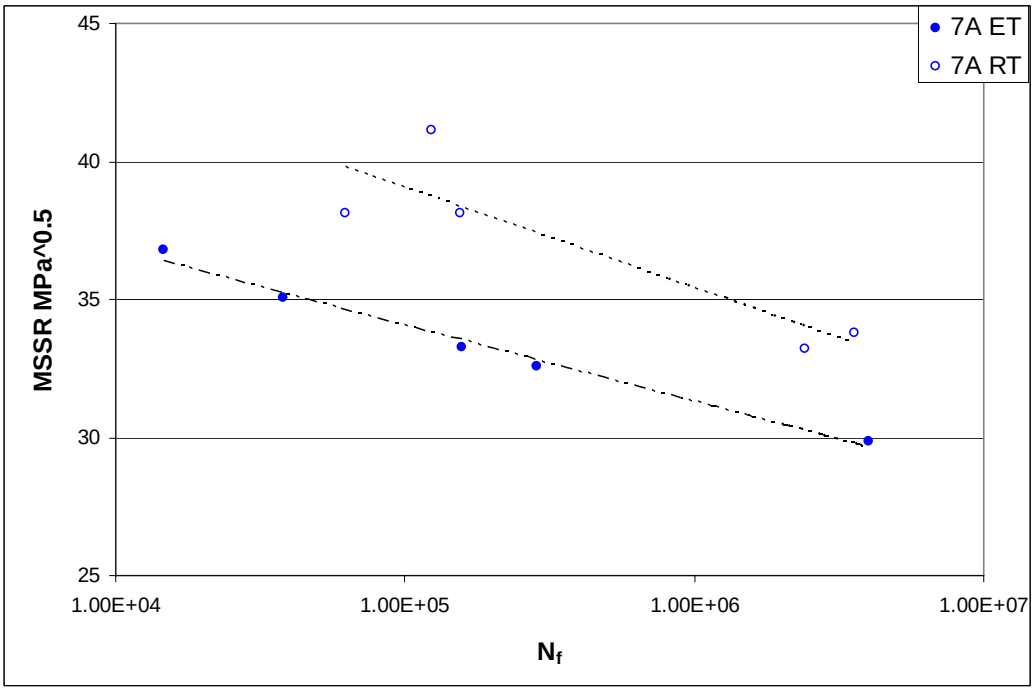

(a) MSSR –N_f for 7A Specimens with 0% Residual Stress

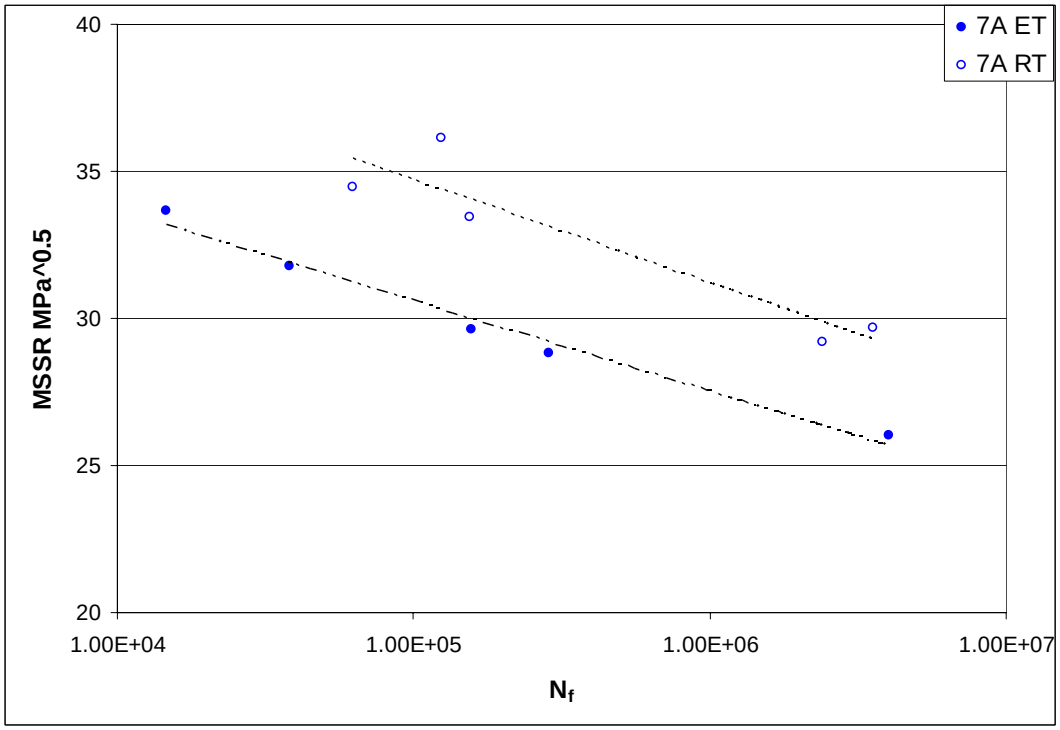

(b) MSSR –N_f for 7A Specimens at 50% Residual Stress

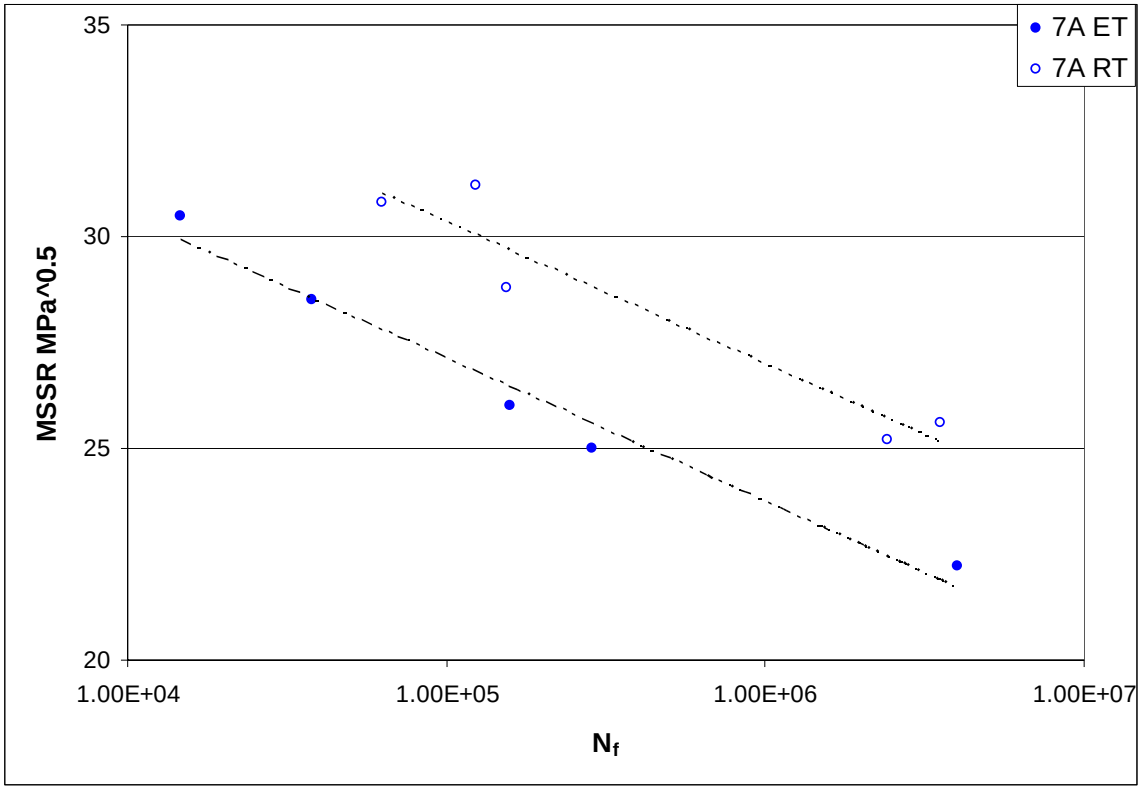

(c) MSSR –N_f for 7A Specimens at 100% Residual Stress

Figure 44. Comparison of MSSR-N_f for 7A Specimen tested at room temperature and 260° C with 0%, 50% and 100% Residual Stress

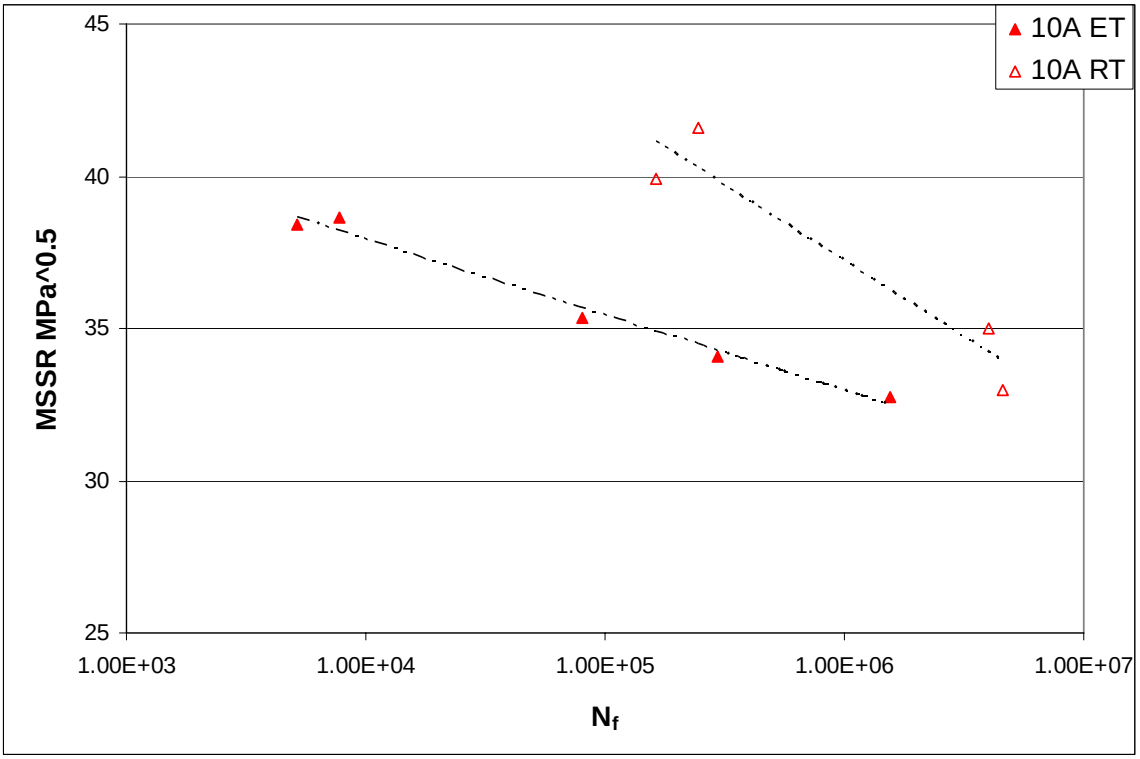

(a) MSSR –N_f for 10A Specimens at 0% Residual Stress

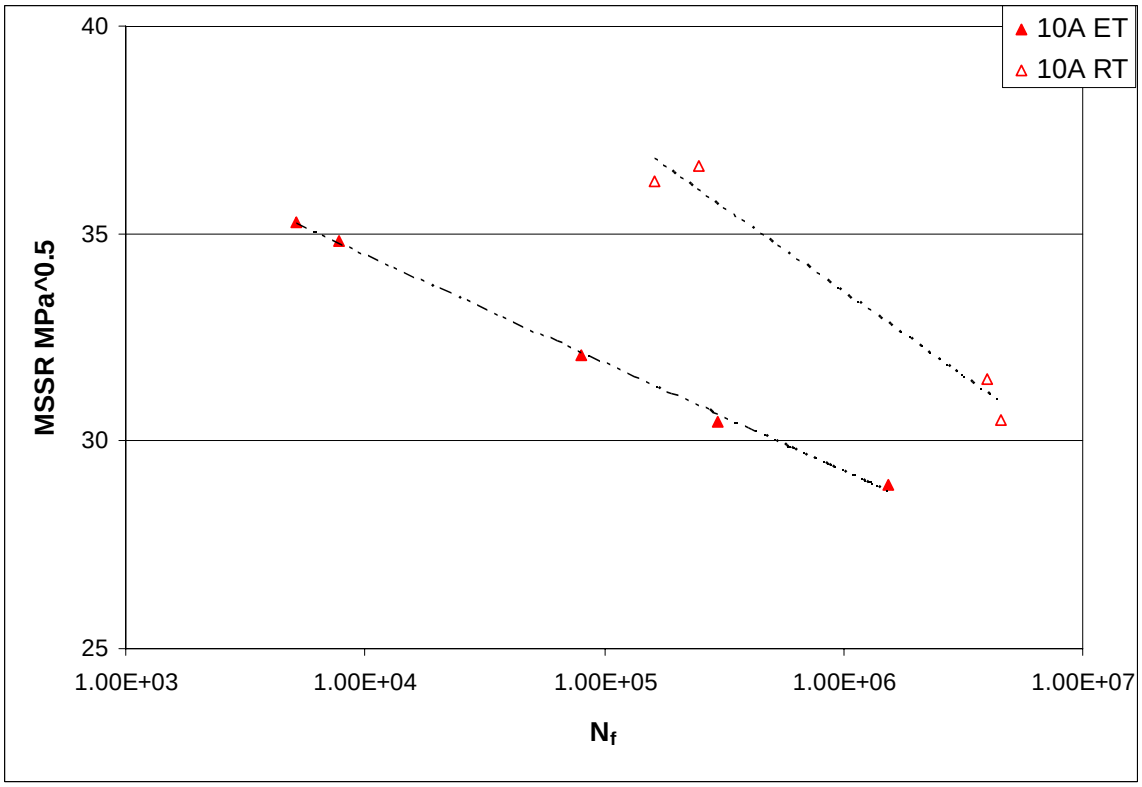

(b) MSSR –N_f for 10A Specimens at 50% Residual Stress

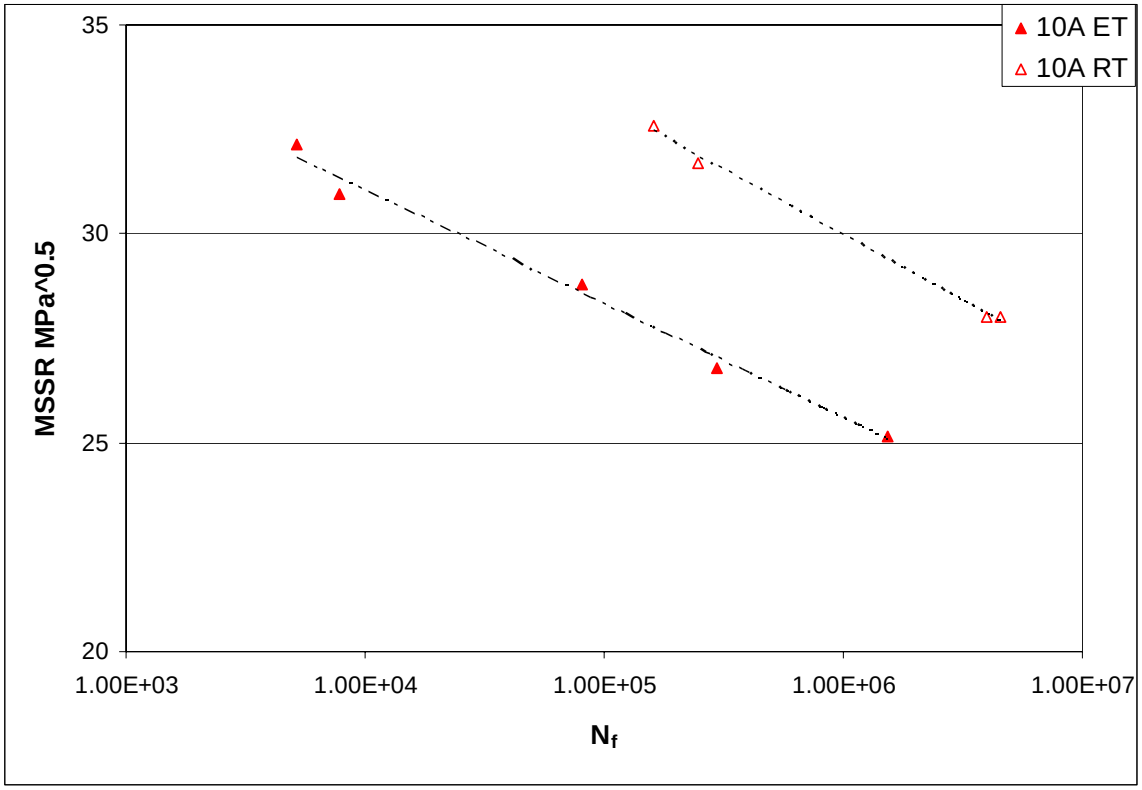

(c) MSSR –N_f for 10A Specimens at 100% Residual Stress

Figure 45. Comparison of MSSR-N_f for 10A Specimen tested at room temperature and 260° C with 0%, 50% and 100% Residual Stress

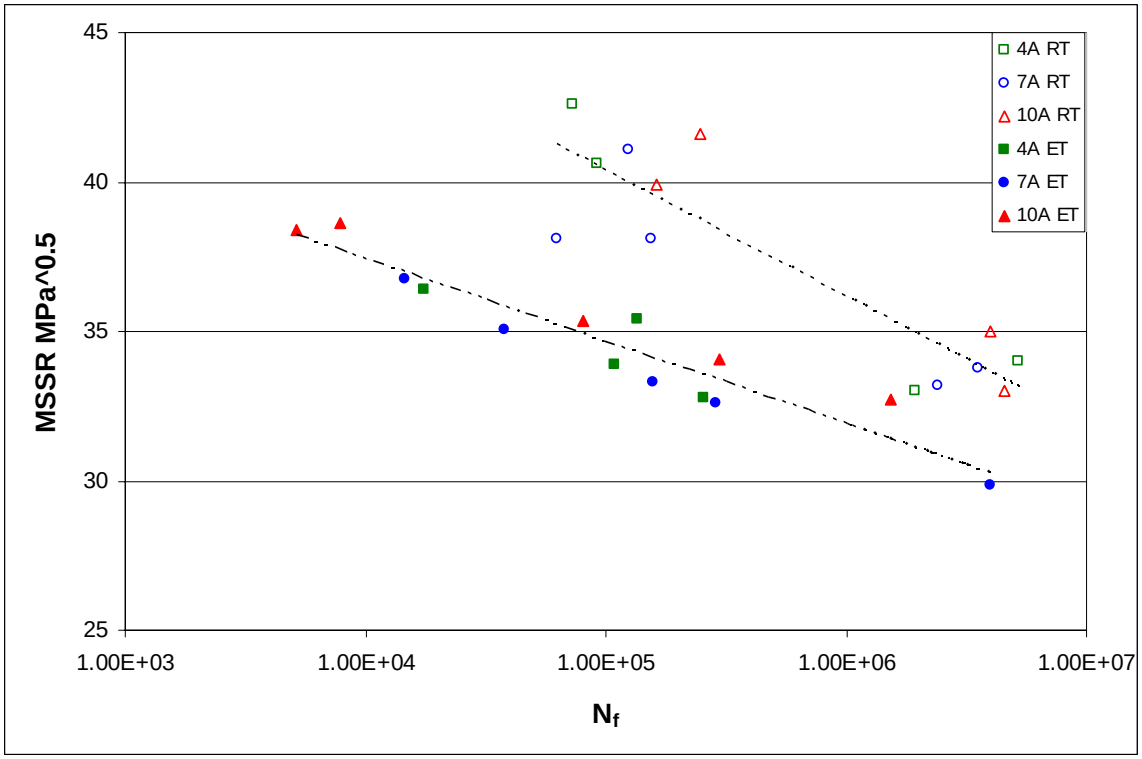

(a) MSSR –N_f for 4A, 7A and 10A Specimens at 0% Residual Stress

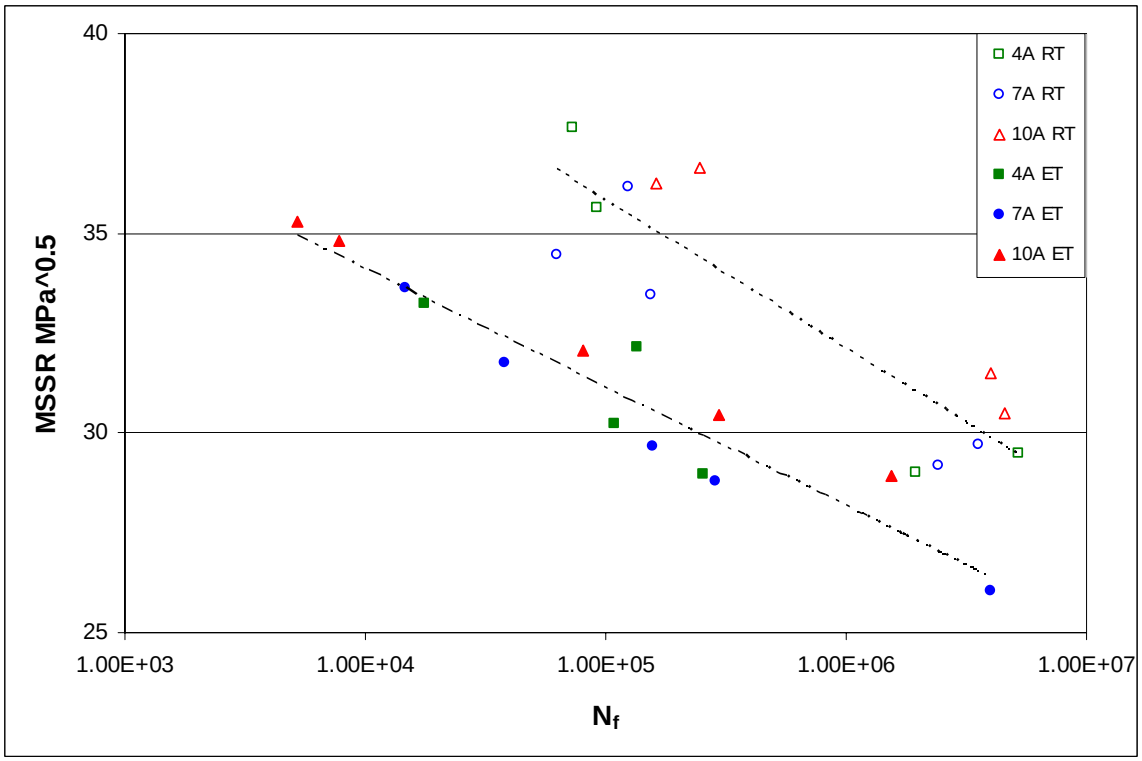

(b) MSSR –N_f for 4A, 7A and 10A Specimens at 50% Residual Stress

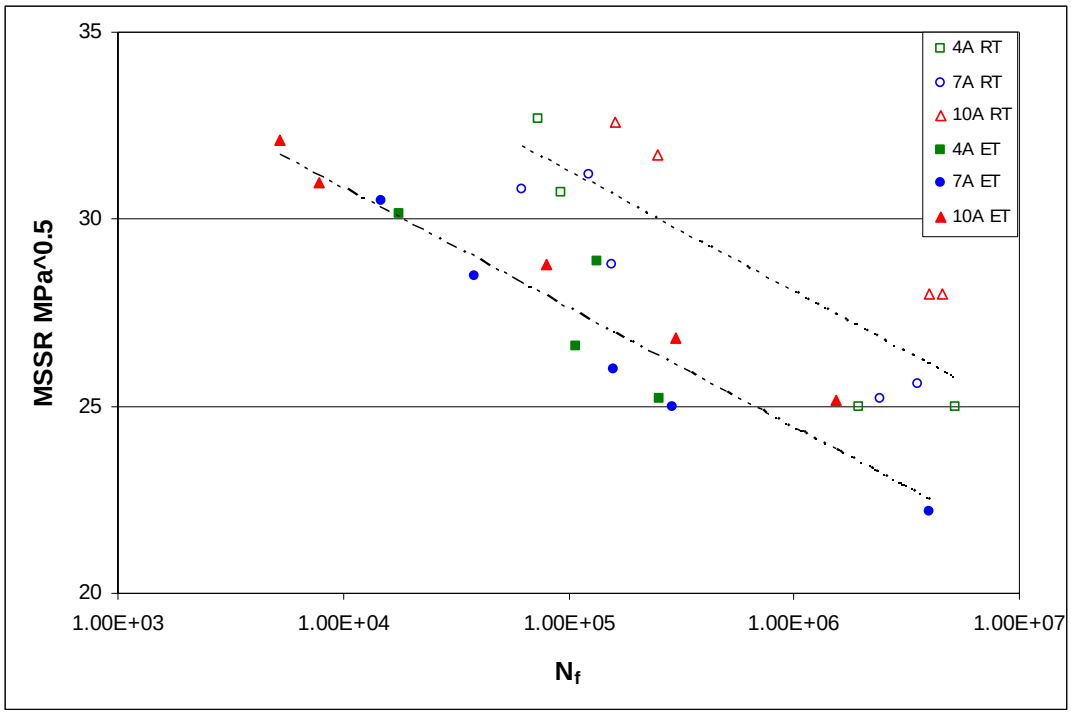

(c) MSSR –N_f for 4A, 7A and 10A Specimens at 100% Residual Stress

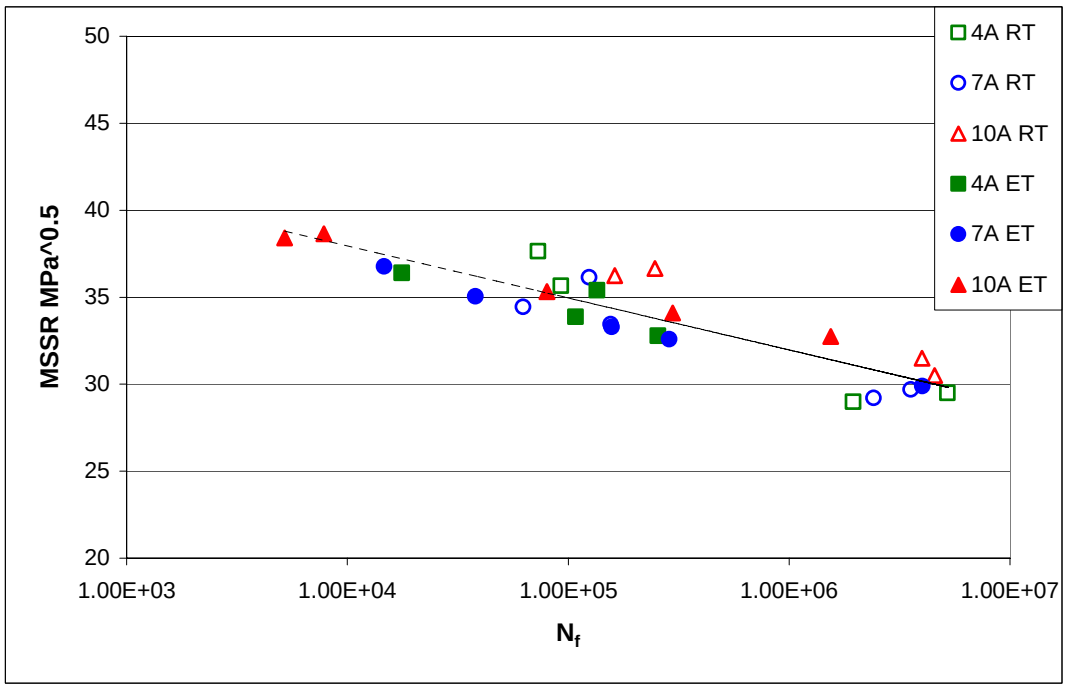

(d) Comparison between MSSR –N_f for 4A, 7A, 10A Specimens tested at RT with 50%RS and 4A,7A,10A Specimens tested at 260° C with 0% RS

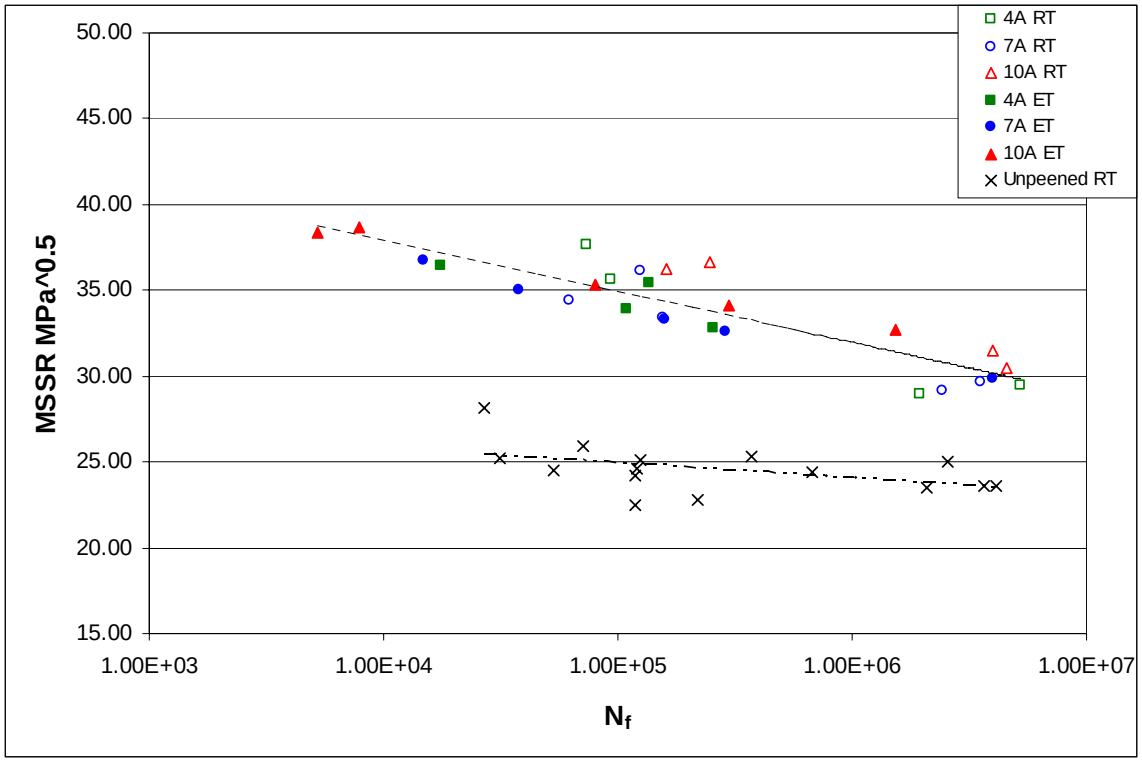

(e) Comparison between MSSR –N_f for 4A, 7A, 10A Specimens tested at RT with 50%RS, 4A,7A,10A Specimens tested at 260° C with 0% RS, and Unpeened specimens tested at RT

Figure 46. Comparison of MSSR-N_f for 4A, 7A and 10A Specimens tested at room temperature and 260° C with 0%, 50% and 100% Residual Stress

Table 1. Summary of Experimental Results

Test #	Temp.	Shot peened (Almen)	σ_{max} (MPa)	σ_{min} (MPa)	$\Delta\sigma$ (MPa)	σ_{eff} (MPa)	Q_{max} (N)	Q_{min} (N)	N_f (Cycles)	f_{FEA}
1	260°C	4A	666.66	66.66	600	635.8	722.99	-410.64	17625	1
2	260°C	4A	555	55	500	529.53	1072.41	-279.93	134935	1
3	260°C	4A	444.44	44.44	400	423.86	1153.08	-660.12	108065	1
4	260°C	4A	390	39	351	371.94	1111.08	-625.69	254929	1
5*	260°C	7A	666.66	66.66	600	635.8	843	-715	14682	1
6*	260°C	7A	555	55	500	476.85	1178	-452	37962	1
7*	260°C	7A	444.44	44.44	400	423.86	1139	-439	157554	1
8*	260°C	7A	390	39	351	371.94	1113	-567	286684	1
9*	260°C	7A	333.33	33.33	300	317.89	702	-412	4010000	1
10	260°C	10A	666.66	66.66	600	635.8	751.63	-290.97	5201	1
11	260°C	10A	555	55	500	529.54	978.16	-597.41	80161	1
12	260°C	10A	444.44	44.44	400	423.86	1242.5	-609.38	297463	1
13	260°C	10A	390	39	351	371.94	1114.15	-601.69	1541799	1
14	260°C	10A	666.66	66.66	600	635.79	1401.21	-540.39	7818	1.1
15	RT	4A	666.66	66.66	600	635.8	1489.76	-465.31	92650	1.2
16	RT	4A	500	50	450	476.85	1364	-666	1950000	1.1
17	RT	4A	400	40	360	381.48	1012.99	-662.62	5222001	1
18	RT	4A	600	60	540	572.22	1846.5	-639.88	73024	1.4
19**	RT	7A	666.66	66.66	600	635.8	1013.29	-583.06	62501	1
20**	RT	7A	555	55	500	529.54	1643.35	-793.07	124222	1.3
21**	RT	7A	500	50	450	476.85	1482.76	-741	155545	1.2
22**	RT	7A	444.44	44.44	400	423.86	631.99	-483.64	2415267	1
23**	RT	7A	422.22	42.22	380	402.67	916.52	-577.16	3562668	1
24	RT	10A	666.66	66.66	600	635.8	1953.19	-768.46	162154	1.5
25	RT	10A	600	60	540	572.22	1488.94	-614.54	247213	1.2
26***	RT	10A	500	50	450	476.85	1607	-440	3995527	1.3
27***	RT	10A	465	46.5	418.5	443.47	1278	-603	4561168	1

Note:
* Data from lee's tests [2]
** Data from Yuksel's tests [1]
*** Data from Martinez's tests [3]

Table 2. Summary of maximum MSSR from this Study with full relaxation (0%RS)

TEST #	$MSSR_{max}$ (MPa^0.5)	$\Delta\tau$ (MPa)	$\Delta\tau_{crit}$ (MPa)	θ (deg)	$R_{\Delta\tau}$	σ_{max} (MPa)	σ_{min} (MPa)	depth μm	x/a_{max}
1	36.40	648.6332	587.35	38.9	-0.20	590.44	-103.64	0	0.93
2	35.41	617.4917	554.25	38.2	-0.22	560.23	-102.83	0	0.91
3	33.88	595.8301	511.10	37.4	-0.32	509.07	-145.26	0	0.91
4	32.77	557.1208	475.45	37.5	-0.33	479.36	-144.11	0	0.92
10	38.41	634.192	578.32	40	-0.18	600.18	-93.70	0	0.94
11	35.32	622.3181	546.21	39.1	-0.27	563.04	-130.95	0	0.93
12	34.09	606.2007	523.00	36.6	-0.31	510.22	-142.02	0	0.89
13	32.73	554.7164	474.53	37.5	-0.33	477.89	-139.96	0	0.92
14	38.64	733.0206	650.34	38.1	-0.24	677.16	-123.78	0	0.89
15	40.60	833.2374	731.63	36.8	-0.27	734.22	-142.59	0	0.89
16	33.00	749.1522	650.92	36.9	-0.29	690.19	-126.26	0	0.88
17	34.00	622.9717	522.89	37.8	-0.37	508.01	-176.84	0	0.93
18	42.60	916.7398	781.84	36.5	-0.34	832.89	-154.56	0	0.89
24	39.90	981.8623	837.29	35	-0.34	856.19	-159.68	0	0.86
25	41.60	812.1402	701.14	37.6	-0.31	714.89	-163.35	0	0.91

VII. Summary, Conclusions, and Recommendations

7.1. Summary

Nearly all work accomplished to date has focused on only one fretting fatigue parameter at a time, and only little effort has been devoted to investigate the effects resulting from varying a combination of parameters. In reality, some mechanical components of a turbine engine are operated under high temperature environment, and shot-peening is one of the most comment surface treatments used to improve material strength under fatigue conditions. Therefore, a better understanding of how variation of shot-peening intensity under elevated temperature conditions affects the fretting fatigue behavior which in turn can help engineers to better account for its effects, and hence more explorations focusing on elevated temperature and shot-peening intensity effects are imperative. The main objective of this study was to investigate the effects of temperature and shot-peening intensity on fretting fatigue behavior.

Fifteen fretting fatigue tests on specimens shot-peened with 4A and 10A intensities were conducted, including nine elevated temperature tests and six room temperature tests. The thickness for all specimens was 6.35 mm. Also, four temperature exposure tests were conducted; the specimens were exposed to a temperature of 260 °C for 2 hrs and 24 hrs. X-ray diffraction method was used to measure residual stress values for both fretting fatigue tests and temperature exposure tests. Fretting fatigue tests were conducted over a wide range of maximum stresses σ_{max} = 333 to 666 MPa with stress ration of R = 0.1. These global loads were applied by a computer-controlled uniaxial servo-hydraulic test machine, using a peak valley compensator to reduce the variation

between control and feedback signals. Applied load outputs were monitored and recorded continuously until specimens fractured into two pieces, and induced tangential loads were determined as the half of difference between lower axial load and upper axial load. These experimental load outputs were then utilized as the load inputs for FEA modeling.

An optical and a scanning electron microscope were used to examine the fracture surfaces, crack initiation locations, and crack orientations. The determination of crack initiation location for the specimens was then utilized for superimposing of residual stress into MSSR calculation. Also, the crack initiation locations and orientations were used to verify the applicability of MSSR predictions on crack initiation mechanism.

Since the infinite half space assumption was violated in this study, analytical solutions were no longer valid, and FEA, a numerical method that doesn't require the infinite half-space assumption to be satisfied, was imperative. Also, the commercially available software, ABAQUS, was used for conducting FEA in this study. For all simulations, the experimental contact load was always applied initially as the first step to prevent the occurrence of gross slip conditions, followed by the measured maximum axial load as the second step. After step 2, the load sequence was applied based on the experimental peak/valley values and frequencies. For the experimental elevated temperature tests, since the specimens were heated till a stable temperature of 260 °C was reached before starting the fretting fatigue cycles, the FEA model simulation of elevated temperature was only applied through the material constant at that temperature. The static coefficient of friction was chosen as a constant, 1.0, for all tests except for those where maximum $Q/P < 1.0$ from experimental results was not satisfied. For these exceptions, the maximum Q/P from experimental observations was applied as the static coefficients

of friction instead. The validation of the FEA model was accomplished by comparing with the Ruiz solutions for contact half-width, stress profiles and Hertzian peak value. Effect of different variables such as the variation of $\sigma_{xx,}$ σ_{yy} and σ_{xy} and the steady state in FEA model were also conducted.

A shot-peening process introduced residual stresses into peened specimens, which was compressive near the peened surface and tensile after some depth within the interior. 4A and 10A specimen had relatively close compressive residual stress value at the surface, but location and value of the zero and maximum tensile residual stress was different, the 10A specimen had a zero residual stress at a greater depth location and a greater tensile residual stress than the 4A specimen. During fretting cycles, residual stress was subjected to relaxation, which was 0% before applying fretting fatigue cycles and 100% after a specimen broke into two pieces at failure location. This relaxation occurred uniformly throughout the specimen at all depths and elevated temperature fostered more relaxation. However, the correlation between relaxation rates and fretting fatigue life is still unclear. A residual stress relaxation rate hypothesis was postulated by the present author for room and elevated temperature 260 °C conditions which was based on experimental results of stress relaxation behavior under both room and elevated temperatures. This hypothesis assumed that the amount of stress relaxation was greater at elevated temperature conditions than that found in the room temperature condition. The corresponding stress relaxations to each case were superimposed into FEA stress solutions to investigate the performance of fatigue parameters in fretting fatigue mechanism prediction.

Three fatigue parameters: the stress range, effective stress, and MSSR were investigated for their effectiveness on predictions on fatigue life and crack initiation mechanisms. The stress range and the effective stress parameters were formulated based on global applied axial loads and didn't take into account residual stress as well as local stress distribution. The critical plane-based fatigue parameter, MSSR, incorporates the influence from residual stress and contact stress, which should be the case since fretting fatigue configuration introduced a non-uniform stress distribution near a contact region. MSSR was discussed about its fretting fatigue mechanism predictions including fatigue life, crack initiation location, and orientation.

7.2. Conclusions

1. Elevated temperature 260 °C negates the effect of shot-peening of 4A, 7A and 10A intensities. Elevated temperature condition fostered a greater residual stress relaxation than the room temperature condition.
2. 4A, 7A and 10A shot-peening intensities improved fatigue life under fretting fatigue conditions at room temperature. All shot-peening intensities provided an extension to fatigue life and the 10A shot-peening intensity provided the greatest extension to fatigue life.
3. Residual stress relaxation could be due to both thermal and mechanical effects. All 4A, 7A and 10A specimens relaxed by the same percentage under temperature exposure only. Thermal and mechanical loads are major contributors in residual stress relaxation phenomenon.
4. Based on the stress range for specimens tested at elevated temperature, fatigue life was significantly reduced for the 4A, 7A and 10A. On the other hand, at room

temperature the fatigue life was extended due to shot-peening of 4A, 7A and 10A intensities.

5. Based on the effective stress for specimens tested at elevated temperature, fatigue life was significantly reduced for the 4A, 7A and 10A. On the other hand, at room temperature the fatigue life was extended due to shot-peening of 4A, 7A and 10A intensities.
6. Cracks initiated near the trailing edge in all fretting fatigue tests. For all specimens tested at elevated temperature, cracks occurred on the contact surface.
7. Under fretting fatigue configuration with alternating axial loads applied, the maximum stress concentration for σ_{xx} was noticed to occur near the trailing edge, and the σ_{yy} stress distribution was no longer symmetric with respect to the center of a contact zone.
8. The MSSR parameter was effective to collapse fatigue life data into a single curve for specimens tested at elevated temperature 260 °C. Similar results were also observed for specimens tested at room temperature. When the different stress relaxation assumption was imposed into the 4A, 7A and 10A specimens, MSSR parameter is effective in collapsing fatigue data from both room and elevated temperature conditions within a scatter band.
9. The MSSR parameter was effective in predicting crack initiation location and crack initiation orientation for fretting fatigue behavior under both room and elevated temperature conditions.
10. When room temperature tests were represented by imposing 50%RS (i.e. half relaxation) and elevated temperature tests were represented by imposing 0%RS (i.e.

full relaxation) the MSSR parameter was most effective it collapsing fatigue life data into a single curve for all specimens tested at room temperature and 260° C. Also, under these conditions the MSSR was most effective in predicting crack initiation location and crack initiation orientation for fretting fatigue behavior under room and elevated temperature.

7.3. Recommendations for Future Work

This study performed fretting fatigue analysis on titanium alloy under both elevated 260 °C and room temperature 25˚ C conditions. Since elevated temperature was found to negate the effect of shot-peening in this study, further effort should be devoted to investigate different alloys that might have better performance under elevated temperature and fretting fatigue conditions. Also, other surface treatments which can produce different stress profile such as laser-peening should be investigated under elevated temperature conditions.

Surface treatments such as a shot-peening process produce residual stress distribution, and this residual stress is subjected to relaxation due to mechanical and thermal loads. Although residual stress would completely relax at failure location, the correlation between relaxation rate and fretting fatigue cycles is still a research issue. For future work it is recommended that theoretical approaches be developed for examining stress relaxation behavior.

Bibliography

1. H. I. Yuksel. “Effects of Shot-peening on High Cycle Fretting Fatigue Behavior of Ti-6Al-4V,” MS Thesis AFIT/GAE/ENY/02-12. Air Force Institute of Technology (AU), Wright-Patterson AFB OH, December 2002.
2. H. Lee, O. Jin, and S. Mall. “Fretting Fatigue Behavior of Shot-peened Ti-6Al-4V at Room and Elevated Temperature,” *Fatigue Fract Engng Master Struct*, 26: 1-12 (2003).
3. M. M. Hamdy and R. B. Waterhouse. “The fretting wear of Ti-6Al-4V and aged Inconel 718 at elevated temperatures,” *Wear* 71: 237-248 (1981).
4. M. M. Hamdy and R. B. Waterhouse. “The fretting fatigue behavior of Ti-6Al-4V at temperature up to 600° C,” *Wear* 45: 1-8 (1977).
5. Y. Kato, S. Takafuji and M. Kiriyama. “Effect of shot peening on fatigue strength of Ti-6Al-4V alloy at elevated temperature,” *f. Soc. Mater. Sci. fpn*. 45: 43-47 (1996).
6. O. Sahan. “Fretting Fatigue Behavior of Titanium Alloy Ti-6Al-4V at Elevated Temperature,” M.S. Thesis, Air Force Institute of Technology, Dayton, OH, (2002).
7. H. Lee, S. Mall. “Stress Relaxation Behavior of Shot-peened Ti-6Al-4V under Fretting Fatigue at Elevated Temperature,” *Materials Science and Engineering* A366: 412-420 (2004).
8. M. H. Wharton and R. B. Waterhouse. “Environmental Effects in the Fretting Fatigue of Ti-6Al-4V,” *Wear*, 62:287-297 (1980).
9. W. Y. Allen. “Fretting Fatigue Behavior of Shot-peened Titanium Alloy Ti-6Al-4V under Seawater Conditions,” Master’s thesis, AFIT/GAE/ENY/04-J01, Air Force Institute of Technology, Wright-Patterson Air Force Base, Ohio.
10. S. A. Martinez. “Quantitative Characterization of Fretting Fatigue Damage in Shot-peened Ti-6Al-4V,” Thesis, University of Dayton, Dayton, Ohio (August 2004).
11. V. Sabelkin, S. A. Martinez, S. Mall, S. Sathish, and M. P. Blodgett. “Effects of Shot peening Intensity on Fretting Fatigue Crack Initiation Behavior of Ti-6Al-4V,” Department of Aeronautics and Astronautics, Air Force Institute of Technology, Wright Pattern Air Force Base, Ohio, in press.
12. C. Lee. “Effects of Variable Contact Load on Fretting Fatigue Behavior of Shot-peened and Un-peened Titanium Alloy,” MS Thesis AFIT/GAE/ENY/04-D01. Air Force Institute of Technology, Wright-Patterson AFB OH, December 2004.
13. R. B. Waterhouse. “Fretting Fatigue,” *International Materials review*, 37: 77-97 (1992).

14. S. A. Martinez, S. Sathish, M. P. Blodgett, S. Namjoshi and S. Mall. “Residual Stress Relaxation due to Fretting Fatigue in Shot-peened Surfaces of Ti-6Al-4V,” *American Institute of Physics*, 1531-1537 (2003).

15. S. Namjoshi, V. K. Jain, S. Mall. “Effects of Shot-peening on Fretting Fatigue Behavior of Ti-6Al-4V,” *Transactions of the ASME*, 124: 222-228 (April 2002).

16. V. Sabelkin, S. A. Martinez, S. Mall, S. Sathish, and M. P. Blodgett. “Effects of Shot peening Intensity on Fretting Fatigue Crack Initiation Behavior of Ti-6Al-4V,” Department of Aeronautics and Astronautics, Air Force Institute of Technology, Wright Patterson Air Force Base, Ohio, in press.

17. C. D. Lykins, S. Mall, and Douglas. “An Investigation of Fretting Fatigue Crack Initiation Behavior of the Titanium Alloy Ti-6Al-4V,” PhD. dissertation, University of Dayton, December 1999.

18. A. J. Jutte. ”Effect of a Variable Contact Load on Fretting Fatigue Behavior of Ti-6Al-4V,” Thesis, Air Force Institute of Technology, Wright-Patterson Air Force Base, Ohio, 2004.

19. K. Iyer. “Peak Contact Pressure, Cyclic Stress Amplitudes, Contact Semi-width and Slip Amplitude: Relative Effects on Fretting Fatigue Life,” *International Journal of Fatigue*, 23:193-206 (2001).

20. K. Walker. “The Effect of Stress Relation during Crack Propagation and Fatigue for 2024-T3 and 7075-T6 Aluminum,” Presented to subcommittee E-9V Winter Meeting (Feb 1969).

21. S. Mall, V. K. Jain, S. Namjoshi, and C.D. Lykins. ”Fretting Fatigue Crack Initiation Behavior of Ti-6Al-4V,” *Standard Technical publication 1425*, ASTM International (2003).

22. S. A. Namjoshi, S. Mall, V. K. Jain, and O. Jin. “Fretting Fatigue Crack Initiation Mechanism in Ti-6Al-4V,” *Fatigue Fract Engng Master Struct*, 25: 955-964 (2002).

23. K. Smith, P. Watson, and T. Toper. “A Stress Strain Function for the Fatigue of Metals,” *Journal of Materials*, JMLSA, 5, No. 4: 767-778 (1970).

24. M. Szolwinski, and T. Farris. “Mechanics of Fretting Fatigue Crack Formation”, *Wear*, 93-107 (1996).

25. R. Neu, J. Pape, and D. Swalla-Michaud. “Methodologies for Linking Nucleation and Propagation Approaches for Predicting Life under Fretting Fatigue”, Fretting Fatigue: Current Technology and Practices, ASTM 1367, D. Hoeppner, V. Chandrasekaran and C. Elliot, Eds. American Society for Testing and Materials.

26. K. Walker. “The Effective Stress Ratio during Crack Propagation and Fatigue for 2024-T3 and 7075-T6 Aluminum,” In: Effects on Environment and Complex Load History on Fatigue Life. Philadelphia (PA): *American Society for Testing and Materials*, 1-14 (1970).

27. C. D. Lykins, S. Mall, and V. K. Jain. “An Evaluation of Parameters for Predicting Fretting Fatigue Initiation,” *Int J fatigue*, 22: 703-16 (2000).

28. W. N. Findley. ”Fatigue of Metals under Combination of Stresses,” *Trans ASME*, 79: 1337-48 (1975).

29. S. A. Namjoshi, S. Mall, V.K. Jain, and O. Jain. “Effects of Process Variables on Fretting Fatigue Crack Initiation in Ti-6Al-4V,” *Journal of Strain Analysis*, 37, No.6: 535-542 (2002).

30. D. Hills and D. Nowell. *Mechanics of Fretting Fatigue*, Kluwer Academic Publishers, Netherlands, 1994.

31. L. Fellows, D. Nowell, and D. Hills. “Contact Stresses in a Moderately Thin Strip,” *Wear*, 185: 235-238 (1995).

32. K. Iyer and S. Mall. “Effects of Cyclic Frequency and Contact Pressure on Fretting Fatigue under Two-level Block Loading,” *Fatigue Fract. Engng. Mater. Struct*., 23: 335-346 (2000).

33. K. Chan and Y. Lee. *Ruiz Program*, South West Research Institute, Personal Communication, 1998.

34. L. J. Fellows, D. Nowell, D.A. Hills. *Wear* 185: 235-8 (1995).

35. D. A. Hills and D. Nowell. “A Discussion of: Peak Contact Pressure, Cyclic Stress Amplitude, Contact Semi-width and Slip Amplitude: Relative Effects on Fatigue Life”, *International Journal of Fatigue*, 23: 747-748 (2001).

36. K. Iyer and S. Mall. “Analysis of Contact Pressure and Stress Amplitude Effects on Fretting Fatigue Life,” *Journal of Engineering Materials and Technology*, 123:85-93 (January 2001).

Vita

1LT Salman Albinali graduated from Ahmed Alomran High School in Manama City, Kingdome of Bahrain. He attended Embry-Riddle Aeronautical University in Florida, USA, for his undergraduate studies where he graduated with a Bachelor of Science degree in Aerospace Engineering in 1998.

His first assignment was at the fighter wing maintenance squadron at Shaikh Isa Air Base, Kingdome of Bahrain, as a maintenance officer in the Engine Shop. In 1999 he attended the Air Force Maintenance Officer Course AMOC at Sheppard Air Base in Texas, USA. In 2000, he became the Engine Flight Commander and worked in this position for three years. In September 2003, he entered the Graduate school of Engineering and Management, Air Force Institute of Technology. Upon Graduating with a Master of Science degree in Aeronautical Engineering, he will be assigned back to Shaikh Isa Air Base to resume his job as the Engine Flight Commander.

REPORT DOCUMENTATION PAGE

Form Approved
OMB No. 074-0188

1. REPORT DATE *(DD-MM-YYYY)*	**2. REPORT TYPE**	**3. DATES COVERED** *(From – To)*
21-03--2005	**Master's Thesis**	September 2003 – March 2005

4. TITLE AND SUBTITLE

Effects of temperature and shot-peening intensity on fretting fatigue behavior of Titanium Alloy Ti-6Al-4A

5a. CONTRACT NUMBER

5b. GRANT NUMBER

5c. PROGRAM ELEMENT NUMBER

6. AUTHOR(S)

Salman Albinali, 1LT, RBAF

5d. PROJECT NUMBER

5e. TASK NUMBER

5f. WORK UNIT NUMBER

7. PERFORMING ORGANIZATION NAMES(S) AND ADDRESS(S)
Air Force Institute of Technology
Graduate School of Engineering and Management (AFIT/EN)
2950 Hobson Way, Building 641
WPAFB OH 45433-7765

8. PERFORMING ORGANIZATION REPORT NUMBER

AFIT/GAE/ENY/05-M25

9. SPONSORING/MONITORING AGENCY NAME(S) AND ADDRESS(ES)
AFRL/MLLP
Attn: Dr. Mark Blodgett
2230 Tenth Street, Suite 1
WPAFB OH 45433-7817 DSN: 789-9799 e-mail: Mark.Boldgett@wpafb.af.mil

10. SPONSOR/MONITOR'S ACRONYM(S)

11. SPONSOR/MONITOR'S REPORT NUMBER(S)

12. DISTRIBUTION/AVAILABILITY STATEMENT
APPROVED FOR PUBLIC RELEASE; DISTRIBUTION UNLIMITED.

13. SUPPLEMENTARY NOTES

14. ABSTRACT

Effects of temperature and shot-peening intensity on fretting fatigue behavior of Ti-6Al-4A were investigated in this study. S-N curves were obtained for both room and elevated temperatures (260 °C) for two different shot-peened intensities (4A and 10A). Stress relaxation behavior under both fretting fatigue at elevated temperature and temperature exposure only were also investigated after their measurements were calculated using X-ray diffraction method. The crack initiation location and the crack angle orientation along the surface were determined using optical and scanning electron microscopy (SEM). Cracks initiated near the trailing edge of the tested specimens. Cracks initiated on the contact surface for both specimens with 4A and 10A shot-peened intensities at elevated temperature. Finite element analysis was preformed by commercially available software, ABAQUS, to obtain contact region state variables such as stress, strain and displacement. Those state variables were needed for the computation of fretting fatigue parameters. Fatigue parameters, such as stress range, effective stress and modified shear stress range (MSSR), were analyzed. It was found that there was relaxation of residual compressive stress during fretting fatigue at room and elevated temperature, greater stress relaxation occurred when higher temperature was applied. Also, both 4A and 10A specimens had the same percentage of residual stress relaxation due to temperature exposure only. Further, elevated temperature conditions negate the effect of shot-peening, thereby providing no improvement in fatigue life. On the other hand shot-peening at room temperature conditions improved fatigue life due to shot-peening. Both shot-peening intensities at room temperature provided an improvement to fatigue life with the 10A providing the greatest extension to fatigue life. Also, the (MSSR) parameter was effective in characterizing the fretting fatigue behavior in terms of fatigue life, crack initiation location and orientation.

15. SUBJECT TERMS
Fretting, Fatigue, Titanium Alloys, Elevated Temperature, Shot-peening

16. SECURITY CLASSIFICATION OF:			**17. LIMITATION OF ABSTRACT**	**18. NUMBER OF PAGES**	**19a. NAME OF RESPONSIBLE PERSON**
REPORT	**ABSTRACT**	**c. THIS PAGE**			Dr. Shankar Mall, AFIT/ENY
U	**U**	**U**	**UU**	154	**19b. TELEPHONE NUMBER** *(Include area code)* (937) 255-3636X4587; e-mail: shankar.mall @afit.edu

Standard Form 298 (Rev: 8-98)
Prescribed by ANSI Std. Z39-18